Università degli Studi di Udine
Dottorato di Ricerca in Tecnologie Chimiche ed Energetiche
CICLO XXVI
ANNO ACCADEMICO 2013/2014

Analysis and optimization of PCM enhanced storage tanks for Solar Domestic Hot Water systems

Roberta PADOVAN

COMMISSIONE

Senior Lecturer Nicolas KELLY	Revisore
Prof. Maurizio SASSO	Revisore
Prof. Piero PINAMONTI	Commissario
Prof. Sergio CAVALIERI	Commissario
Prof. Giulio LORENZINI	Commissario
Prof. Marco MANZAN	Supervisore
Prof. Alfredo SOLDATI	Coordinatore del Dottorato

Author's e-mail: rpadovan@units.it

Author's address:

Engineering and Architecture Department
University of Trieste
Via A. Valerio, 10
34127 Trieste - Italy
tel. +39 040 5583817

Abstract

The enhancement of a system efficiency is a crucial issue in the engineering design.
The aim of the thesis was to describe a possible strategy for the rational use of energy in the building and industrial sector. A storage device is a fundamental component in the domestic plants. Since the use of renewable sources is imposed by low, the possibility of enhancing the tanks storage efficiency had been investigated testing this device in the typical Solar Domestic Hot Water (DHW) systems. A crucial aspect in the building design, in terms of internal spaces composition, is the volume occupied by the tank, thus the objective of reducing the occupied volume becomes a design target, in order to reduce the primary energy consumed. Phase Change Material (PCM) had been inserted into the tank with the aim of enhancing the storage capacity. The latent heat may be an exploitable contribution to maintain the stored water at the set-point temperature. If it happens, it is possible to reduce the energy deriving from the non renewable sources or, on the other side, the amount of water needed as storage.
The obtained results derived from the ESP-r simulation software. The existing stratified tank plant components with 1 and 2 coils had been improved with the possibility to include PCM modules. The new components have been validated with experimental data reported in the literature. A typical SDHW system including the new component had been simulated and than optimized, tacking into account the two objectives designs listed before. For the PCM modules, a cylindrical geometry - axisymmetric scheme - had been chosen; a finite volume approach with an uniform discretization in both the radial and axial direction had been used. The enthalpic method for the heat transfer with phase change had been implemented, the convection had been modeled through correlations that modify the conductivity of the liquid phase. The outcomes shows that it is possible to reduce both the primary energy consumption and the volume of the tank, but the improvements are not dramatic.

Acknowledgments

I would like to express my sincere gratitude to Professor Marco Manzan for the education and aid that he has constantly given to me and for the strong motivation and encouragement he has always instilled in me.

I am grateful to the thermodynamic, heat transfer and computational fluid dynamics staff of my department: Professor Enrico Nobile for the support and the guidance in the computational fluid dynamics, Professor Ezio Zandegiacomo de Zorzi for the help in the comprehension of the thermodynamic and heat transfer problems, Walter Moze for the aid in the practical problems, Ph.D. Paola Ranut and Ph.D. Mitja Morgut for the disparate advice they provided to me. Their precious help was indispensable for this work. I also thank them for the involvement in a pleasant working atmosphere.

I sincerely thank Professor Joe Clarke, who guided and supported me for all my stay at the ESRU. I thank all the ESRU staff for the help in my work and the kind hospitality, in particular I would like to thank Jon Hand for the help with the code, Aizaz Samuel for the support in the modelization and Nick Kelly for the interest he demonstrated in my work.

This work has been supported by Ministero Sviluppo Economico with Project PIACE [Grant No. 00024EE01]: I thank Andrea Frazzica and Salvatore Santamaria from the Consiglio Nazionale delle Ricerche (CNR), Istituto di Tecnologie Avanzate per l'Energia "Nicola Giordano" (ITAE), for providing me with the experimental tests results they have carried out on several storage tanks. I thank the Riello company, and in particular Giuseppe Toniato, for the willingness in providing me with technical data of the storage tank.

I hold in high regard to thank many ESRU Ph.D. students. In particular I thank Filippo for his friendship and for the many exchanges of views about my research: I am grateful to him, I will never forget the time spent together. I thank Eric for his kindness and hospitality. Than I thank Asma, Gavin, John and Tom for the comfortable atmosphere that I had the pleasure to be surrounded.

I thank my parents who gave me the opportunity to study and Giulia for her constant helpfulness.

Finally I thank my personal energy source, Jean, for his support, and Gaia and Emy, who gave me their affection, a precious help to write my "book" in a cheerful atmosphere.

Contents

Preface iii

Introduction v

1 State of the art 1

2 Conduction problem with phase change 11
2.1 The analytical solution . . . 11
2.2 The numerical problem . . . 13
2.2.1 The enthalpic method . . . 13
2.2.2 A further approach to the phase change study . . . 15
2.2.3 The Euler Explicit method . . . 16
2.2.4 Time-Temperature graph . . . 19
2.2.5 The Euler Implicit method . . . 20
2.2.6 Method remarks and observations . . . 24
2.3 The convection effect . . . 25

3 PCM module 27
3.1 The geometry . . . 27
3.1.1 Axi-symmetric problem . . . 27
3.1.2 The adopted PCM grid . . . 27
3.1.3 Discretization correspondence among PCM cells and water layers . . . 29
3.1.4 The border condition - water side . . . 30
3.1.5 The border condition - PCM side . . . 31
3.1.6 An alternative grid for the PCM . . . 31
3.1.7 Sensitivity analysis . . . 32
3.1.8 CPU calculation time . . . 34
3.2 The PCM enhanced tank feasibility . . . 34

4 Simulated SDHW systems 37
4.1 The simulation code . . . 37
4.1.1 The subversion system . . . 37
4.1.2 An integrated system . . . 38
4.2 The plant . . . 42
4.2.1 The tank . . . 44
4.2.2 The implementation of the PCM modules in the tank component . . . 46
4.2.3 An alternative approach to model the tank component . . . 48
4.2.4 The solar collector . . . 52

4.2.5 The boiler . . . 54
4.2.6 The by-pass . . . 55
4.2.7 The user side: the DHW demand . . . 55
4.2.8 The controls . . . 56
4.2.9 The primary energy consumed . . . 57
4.3 The climatic data . . . 57

5 Optimization problem **59**
5.1 The optimization analysis . . . 59
5.1.1 Mono-objective optimization . . . 59
5.1.2 Multi-objective optimization . . . 60
5.1.3 Optimization algorithms . . . 60
5.1.4 Genetic algorithms . . . 61
5.1.5 The performed optimization . . . 64

6 Tank preliminary analysis **65**
6.1 Analysis on a traditional tank . . . 65
6.1.1 The cooling-down test . . . 66
6.1.2 A calibration test . . . 68
6.2 The PCM tank validation . . . 75
6.3 Calibration of a PCM tank modeled through building elements . . . 79

7 Simulations results **87**
7.1 The PCM tank initial simulations . . . 87
7.2 The tank optimizations . . . 91
7.2.1 The base case and the variation range of the variables . . . 92
7.2.2 The optimized traditional tanks . . . 94
7.2.3 The optimized PCM tanks . . . 95

Review and concluding remarks **107**

Appendix **109**

Glossary **113**

Bibliography **117**

Preface

The concept of technology became conscious after the lessons of Johann Beckmann. In 1777 he stated the necessity of giving a "systemic order" to the technical developments, such that a unique *techne* concept should ground and join together different human activities, as architecture, chemist's, manufacture. He not only recognized a common origin in the human activities, but also affirmed that the technology is the product of the continuous improvements of different existing developments that can be differently arranged together. After these technical developments, different for complexity and refinement, are arranged together, they may produce technologies whose worthiness and usefulness go beyond the sum of each distinct technology [1].

Almost all the new technologies derive from separated ideas, that are jointed together later. Often separated parts convey in a highly integrated system of a more evolute design. This combination of ideas may be compared to the Darwinian evolution, since the improvements, also the minimal ones, are compensated by their replications, so that the innovations constantly spread themselves among the population. The old ideas are mixed to the new and an evolutionary scenario is then generated. The evolution of the science and the technology is similar to the nature evolution [1].

The technological progress and the respect for the environment and the society coexist in the general concept of "sustainability": a "Sustainable development is development that meets the needs of the present without compromising the ability of future generations to meet their own needs." [2]

The climate change that is affecting the world in the last few centuries is often object of debates and controversy in many branches of the social, economical and industrial policy, both in the local and global scale. The global warming scenarios depicted by the Intergovernmental Panel on Climate Change (IPCC)[1] describe the next world climate evolution due to different evolution scenarios. One of the issues illustrated in the scenarios is to point out the level of the anthropogenic Greenhouse Gases (GHGs) in the atmosphere. The emissions source depends, among all, on the population increase, on the economic growth, on the land and labor productivity growth, on the technological options and on the resource endowment. Socioeconomic and technological models of the GHGs emissions are integrated with models regarding the response of the natural science of Earth system, including the atmosphere, oceans, and terrestrial biosphere. Several different scenarios are then predicted. In the stabilization scenarios, a transformation of the global energy system is needed to reduce the GHG emissions, and it should include reductions in the energy demand (compared to the reference scenarios) and changes in the combination of energy technologies and fuels [3], [4]. These considerations imply that linking the concept of energy efficiency to the only technological aspect seem to be reductive and simplistic:

[1]The IPCC is an intergovernmental body for the assessment of climate change, that provide the scientific knowledge in climate change and its potential environmental and socio-economical impacts.

the necessity of policy measures that promote the consumes reduction and improve the impact to the environment is due to the dichotomy between the boundedness of the fossil fuel sources on one side and the growth of the population on the other side, together with the demand of maintaining a high standard of life.

The energy efficiency is "the ratio of output of performance, service, goods or energy, to input of energy" [5]: rising up the efficiency of a system means reducing the amount of energy to obtain the same performance from a system. In the civil and industrial sector, like in the rest of the social-economical activities, it represents a synthesis of the exploitation of the fossil fuel and a rational use of the renewable source of energy [2] .

In the UE the 40% of total energy consumption is attributed to the building sector and this scenario is assumed to be in expansion. Thus, the construction branch offers a big cost-effective opportunity both to reduce the energy consumption (rising up the system efficiency) and reduce the GHG emissions (shifting the energy source from fossil to renewable) [6].

[2]The efficiency improvements can be modified by global and local policy by imposing an emission permit price (carbon tax) and investments in energy efficiency can be made only if the apparent average pay-back-time is reasonable.

Introduction

The aim of this thesis is to examine a technology that recently started to be investigated. This technology regards the enhancement of the efficiency of a solar domestic plant to produce hot water. It is supposed that exploiting the phase change phenomenon of some materials it is possible to reach some efficiency improvements. The studies concerning it analyze the possibility of reducing the consumption of fossil fuel by exploiting and optimizing the thermal storage of a water tank by means of additive PCM modules in the water. These materials are thought to be placed in one of the components of such plants in order to store and release the energy when it is available or when it is needed. The effect of the phase change phenomenon can be simulated together with the performance of a storage tank and those of the plant and building it belongs to: the system has to be modeled throughout a dynamic building-plant integrated simulation code.

The accuracy in modeling SDHW systems plays a prominent role in high performance building design, that are supposed to be the next future dwellings, since the energy demand for space heating is almost null (net-zero energy buildings) and most of the energy is used to warm the domestic water. For this reason, enhancing the storage efficiency of a Domestic Hot Water (DHW) plant is even more important. Moreover, the more sophisticate the model, the more details and control system have to be considered: this is why becomes necessary the use of a dynamic code.

In a DHW system a storage device is fundamental not only for a general energy supply, depending on the water mass flow and the temperature, but also for the energy consumption reduction, since it balances the demand and the availability of the hot water. For a solar system the requirement of an efficient storage tank is even more important, because free energy can be gathered and saved for the day periods when it is needed by the users: a storage tank is essential to compensate the delay between the moment when the energy is needed to warm up the water and when it is available for free. In other words it means to face the juxtaposition between the users need of hot water and the variable irradiation of the sun. In such way the operating times for auxiliary heating devices can be lengthened, their efficiency increased and their startup-shutdown emissions reduced.

The study and the modelization of a traditional short-term water storage tank, used as component in a SDHW system, is a quite complex fluid-dynamic issue. The problem, in fact, has to consider two different loads: those relative to the solar panel and those coming from the boiler. The heat flux from the boiler depends on the variable temperature of the tank water and the temperature of the water flowing through the coil; on the other side the temperature of the solar panel can vary in a much bigger interval, depending on the climatic conditions and the setting controls, thus the heat flux coming from the solar panel has to be controlled more carefully. Moreover the stored water is renewed on the basis of the user behavior: the hot water demand drives a variable flow of cold water

entering in the tank.

A lot of works in the literature report that a storage device can improve its performances through the thermal stratification. The thermal stratification is the phenomenon triggered by the progressive density reduction caused by the heating of the water. If the water tank volume dimension is calculated on the basis of the water need of the users, referred to a day-period, and if the temperature range that characterizes the stored water in the tank is wide, over 20 K, the benefit obtained by stratification is sensible [7]. In a solar system the thermal stratification reduces the period of operation of the auxiliary energy supply, therefore an increment of efficiency does not regard the only tank, but also the rest of the system. The performances of a fully stratified water tank can be 6% better than those of a fully mixed water tank; when a stratified tank is employed in a solar plant, the system can rise up to 20% its efficiency [8].

Because of the high specific heat of the water, the bigger the size of a traditional storage tank, the more the water can be maintained around the set-point temperature. In the small dwellings design the contrasting issue of enhancing the efficiency of the storage and the necessity of reducing the space occupied by the tank may get crucial.

A lot of tests and numerical predictions have been carried on in the literature about the PCM and its performances on some plants. More specifically, these works deal with the performance of the PCM in its melting and solidification process (f.e. focusing on the shape during the process), on the impact of it on various systems (f.e. Combined Heat and Power (CHP), Photovoltaic (PV), but also as micro-spheres in building construction elements), on the released heat into the water of a storage tank assumed linked to a solar panel (f.e. cooling down, reheat).

The efficiency of a PCM enhanced SDHW system is performed by mean of the simulating tool Environmental Systems Performance - research (ESP-r); this code is developed and distributed by the Energy Systems Research Unit (ESRU) of the University of Strathclyde - Glasgow - and Natural Resources Canada (NRCan), in collaboration with researchers and practitioners that would like to contribute to it. Since it is an open source code, any algorithm, like the phase change one, could be implemented and linked with previously existing ones to study the performance of the new model. This thesis deals on the implementation of a phase change model for the simulation of PCM modules in stratified tank components. The research, moreover, evaluates if such enhanced device may be useful for the improvement of the storage efficiency and finds out the designs performing the best simulated results.

ESP-r considers the plant and the building where it is located, as well as the flow networks that may be included, an integrated system. The modifications added to the plant components to model the PCM modules are strictly related to the engaged components; an additive thermal flux for the tank water, that depends on the temperature difference between the water and the PCM and the convection coefficient at the PCM module border, is straightforward calculated [9].

In a simple simulation of a storage tank, that could be for example a cooling-down test, choosing the PCM geometry and technical data is not a crucial point: these parameters are quite arbitrary since the simulation ends when all the PCM amount has changed

phase [3] . If a PCM tank is a component of a SDHW plant, these parameters are decisive for the tank performance, because it is necessary that all the PCM amount change its phase in the day cycle or in a fraction of it, in order to maximize the advantage carried on by the PCM. After the simulation of such tank has been performed, an optimization analysis can identify its correct design, that is the design able to maximize the plant efficiency and minimize the tank volume.

[3] In other words the cooling-down simulation can't demonstrate the efficiency of such a system for a SDHW plant, but only the PCM effectiveness and the time needed to freeze.

1

State of the art

The idea of dealing with the design of a PCM enhanced storage tank came out from the need of rising up the efficiency of the water stratification inside a traditional tank. The literature collects a lot of studies about this topic, starting by descriptions of what the PCM is and what are its peculiarity.

A bibliographic research was carried on the documentation covering both the storage tanks and the PCM. In particular the following topics have been investigated.

A thermally stratified storage tank

For a traditional tank the storage efficiency depends on many factors, that can be summarized in the operating conditions and the design parameters. These factors, enlighten in many numerical and experimental studies [10], [11], [12], are essentially the tank geometry (f.i. the inlet and outlet position and geometry), the water velocity and temperature at the inlet [13]. The stratification effect can be related to an extraction efficiency, intended as the velocity at which the initial difference between the inlet and the outlet temperature drops to a fixed value, for a fixed water flow rate ($\eta = \frac{\dot{m} \cdot t}{V}$). The stratification is inversely proportional to the distance between the inlet port and the tank bottom. It increases with the tank height/diameter ratio, with the inlet and outlet diameters, and decreases if the flow rate rises up. The suggested value for the height/diameter ratio is 3-4, taking into account a cost-performance analysis [10]. In other terms the stratification depends on the design and the charging parameters: since it is a consequence of the flow and the heat transfer characteristics, the stratification effect is strictly related to the Richardson and Peclet numbers, that stand for the coupled effect of the charging velocity and temperature difference. The Richardson number is a dimensionless number used in the fluid dynamics that indicates the ratio of the potential energy to the kinetic one:

$$Ri = \frac{gh}{u^2}$$

where g is the gravity acceleration, h a representative vertical length-scale, and u the velocity component in the vertical direction. The Peclet number

$$Pe = \frac{\rho c_p L}{k} = Re\, Pr$$

is a dimensionless number that indicates the ratio of the thermal flux transferred by convection to those transferred by conduction in a fluid. Re is the Reynolds number, Pr is the Prandtl number, ρ is the fluid density, c_p is its specific heat capacity, L is the characteristic length of the geometry and k is the fluid conductivity. The storage efficiency improves with the increasing of these numbers [11].

As reported in Bony et al. [14], the stratification permits the optimization of the storage and the limitation of the heat losses. It can't be taken for granted that a good stratification is simple to maintain in a plant like the system described in Chapter 4, since it depends on a variable that changes a lot, that is the DHW demand together with the collector flow rate[1].

The PCM

The first technological application of the PCM has been carried out by the NASA: such materials have been employed in aerospace engineering devices[2]. In the 70's, in conjunction with the petrol crisis, the increased interest in these products opened new perspectives for their use. Depending on their properties, the PCM can currently be used in several applications as thermal energy storage and waste heat recovering device, for example they can be used for solar installations. The phases from which the PCM switches for the application described in this thesis are the solid and the liquid.

The PCM are accumulators of heat that exploit the physical phenomenon of the phase transition: when a heat flux is provided or subtracted from the PCM, it stores/releases energy in the form of latent heat through an isothermal transformation until all the material has changed phase. During the solidification, at the phase change temperature, they store the heat which is subtracted from the ambient where they are located; vice versa, during the melting, the material maintain the temperature, releasing the same heat. Such transformations are cyclical and it is trivial noting that the more these materials are capable of storing heat, the more heat is subtracted or provided to the system in which they are inserted and the more benefices can be achieved.

The chemical compositions of the PCM are organic - Paraffins (C_nH_{2n+2}) and fatty acids ($CH_3(CH_2)_{2n}COOH$) and inorganic - salts hydrates (M_nH_2O), citing the sodium sulfate decahydrate, also known as Glauber's salt ($Na_2SO_4 \cdot 10H_2O$) and eutectic, that refer to a mixture of substances whose melting/solidification point is lower than those of any possible mixture of the same components. The PCM having an organic origin can have a wide phase change temperature range; solidify without presenting an excessive sub-cooling[3]; possess good ability to nucleation[4], have a high latent heat per unit volume;

[1] Even if this is controlled by a thermostat.

[2] D.V. Hale, M.J. Hover, M. J. O'Neill, Phase Change Materials Handbook, NASA Contractor Report NASA CR-61363, NASA Marshall Space Flight Center, Alabama, 1971

[3] The sub-cooling is the process of cooling of a liquid to the below its solidification temperature, without actually takes place the solidification do the same. This phenomenon is mostly observed in pure liquids and perfect stillness. If, however, shake the liquid, or you enter a foreign body, it causes its immediate solidification and its temperature rises to the point of solidification.

[4] The process of nucleation is the mechanism of transformation from one state of matter another, the formation of the first seed. In general, the beginning of a new phase (the formation of micro-crystals or droplets) is unstable due to thermal agitation.

are compatible with conventional construction materials; are are chemically stable, safe and non-reactive; are recyclable. The main disadvantages are that they show a sensible volume change in the phase change and a low thermal conductivity in their solid state; are very flammable and expensive The inorganic PCM have a lower price and are easly employable; do not vary a lot its volume during the phase change; possess greater storage thermal capacity and higher density than those of the paraffin; they are highly conductive, thermal stable, inflammable, but need nucleating agents. From the thermodynamic point of view it is desirable that these materials liquefy in the range of desired temperature, have a high latent heat per unit volume, as well as an high density, specific heat and conductivity; a reduced volume variation in the phase change, a good nucleation (in order to reduce or avoid the sub-cooling effect). They should be stable, not corrosive, non-toxic, non-explosive, cheap, inflammable and change phase through completely reversible cycles.

They can be enthalted in vessels or encapsulated (micro or macro capsules, for example acrylate films are used).

Stratified border condition for the PCM

A stratified temperature border condition for PCM has been analyzed by Farid and Hussian [15]. They study the implications of the stratified temperature of the air in a heat exchanger: the PCM is placed in vertical plates and the air flows upwards. The analysis of heat transfer air-PCM depends on the air flow; the air flows along the heat exchanger surface, so its temperature increases flowing upwards. To model the transient stratification the Latent Heat Storage Unit (LHSU) has been divided into several sections in the vertical direction. The heat calculation has been based on the inlet and outlet temperatures average and the air temperature calculated at the outlet of the lower section has been used as inlet condition for the boundary upper section. The authors underline that the adopted scheme is not suitable for long term simulations.

In other works the temperature of the PCM is constrained not to vary, so a mono-dimensional problem has been studied in spite of a bi-dimensional one. Vice-versa Zivkovic and Fujii [16] state that the PCM melting in the cylindrical containers is generally multi-dimensional (both radial and axial direction must be taken into account in the conduction) and the natural convection in the melted PCM has to be considered as well. The enthalpic model they use neglects the natural convection within the melt material, so they performed an experiment to understand the discrepancy between their simplified numerical model and the real model. The Zivkovic and Fujii [16] outcomes underline that the more mass of PCM fills the container, for example with increasing the thickness of the rectangular plane container and the diameter of the cylindrical one, the difference in the melting time of the two geometries increases sensibly: the rectangular container shows a much shorter melting time if equal volumes and heat transfer areas are considered. The experimental results confirm the numerical tests: the melting time for the cylinder is nearly twice that of the rectangular container, with a nearly linear correlation between the melting time and the mass of the PCM.

Modelization of a PCM enhanced tank in ESP-r

A dynamic code can simulate the performance of a building/plant system in the course of time.

At the present time a PCM tank, that is the object of the present study, could be modeled in ESP-r either by enhancing a traditional tank model or creating a specific suitable design that discretizes in an amount of finite volumes the tank envelope and the contained water. With the latter method (that will be here identified as "zonal approach") each predicted water layer should be modeled as a different zone and the construction structure forming the tank envelope should be modeled through building, or rather construction, elements. In this thesis, as reported in Subsection 1, the first method had been analyzed and is deeply described in the next Sections.

For a general plant component, the more details are needed to be included into a model, the more worth is choosing the zonal approach in spite of analyzing it through a pre-modeled component, since the problem can be described by more nodes and each node can be qualified by specific characteristics. For example, modeling the PCM tank through thermal zones and constructions permit to boost the description of the tank envelope, since the U-value changes for the different positions of the surfaces (tank top, bottom and lateral surface). Moreover a zonal approach allows to analyze the cycling charging and discharging, as well as the heating and cooling down of the tank through a water flow network.

Since several ESP-r routines contain algorithms modeling the PCM with the convection and the sub-cooling effect, a zonal approach may be chosen to compare results and model phenomena that are neglected or treated in a different way in other modelizations. A comparison about a PCM tank cooling-down test performed with both techniques is reported in [17] (see Subsection 4.2.3 and 6.3). A similar approach to model a non homogeneous temperature profile has been adopted by [18] to simulate the stratification of the air in a room. In the case of the tank, the clustered water zones are in contact each other through an imaginary separation layer, that is a fictitious construction. The geometry has to be simplified and the appropriate characteristics have to be assigned to the constructions and to the fluid surrounding the PCM. In ESP-r exist some routines that describe phase change characteristics for the construction layers: the code permit to assign "active material" quality to some nodes chosen by the user. Some of them are held in the current ESP-r development version[5], for example those referring to Hoffmann's thesis [19] and a new model, that include the modelization of the convection, has been implemented in a recent version of the software (Hasem's thesis [20]). Moreover, by proceeding in this way, it is possible not only to change the geometry of the model (PCM modules dimension, shape, collocation), but also to choose different PCM types for the same tank or assign PCM characteristics to different construction elements (such as the wrapper). The zonal approach results and those obtained for the tank plant component are comparable; their comparison shows that the convection effect in the liquid phase is not sensible for the chosen tanks.

[5] The structure of the ESP-r code will be discussed in Chapter 4.1.

The phase change problem

The analytical solution of the phase change problem, introduced by Neumann (1835-1840) [21], is very complex and in the literature has been used as a comparison term for the first numerical results [22] (see 2.2.4). It has been studied since the XIX century, and the name "Stefan problem" comes from the Slovene physicist Jozef Stefan, who started studying the general class of such problems. The existence of its solution and the its uniqueness was proved at mid XX century. The simplest and most common formulation of the problem is referred to the mono- dimensional case, with constant thermal properties and simple initial and boundary conditions. The solution of the analytical problem is often pointed out as "similarity solution", since it takes the form of a function of the single variable $S/t^{1/2}$, like the formulation reported at Equation (2.1.5), where S is the thickness [m] and t is the time [s].

The numerical approach

The numerical approach to the phase change problem has been deeply analyzed for technical applications since 1970s: the first studies employ the finite difference method and refer to the mono-dimensional case or a simple bi-dimensional geometries, such as the flat plane [21]. Later further methods have been deepened: the first technical applications use opportune simplifications to model the PCM in air- and water-based plants [23].

The enthalpic method

The PCM has been modeled by many authors with the enthalpic method, f.i. Bony and Citherlet [24], Lacroix [25], Voller [22]. The method numerically solves the Equation (2.2.5), that is the enthalpic formulation of the energy conserved equation.

Voller and Cross [26], as well as Voller [22], use a control volumes discretization. In his works Voller describes the step-like trend of both the temperature history and the phase change movement; he suggests some remedial schemes to predict the points of agreement between the analytical and the numerical solutions and to recover the enthalpy solution. The region in which both the liquid and the solid state coexist ("mushy region") acts as a dumper for these oscillations ([26]). However, many of the remedial schemes reported for the mono-dimensional problems can not be extended to the multidimensional ones. In the second paper a formulation for the mono-dimensional cylindrical geometry is provided (see Section 3.1.1).

Methods to treat the typical non linearity

The most common methods to treat the typical non linearity occurring when a phase change problems is solved with an implicit scheme, as summarized at Subsection 2.2.5, are the source update method, the enthalpy linearization method and the apparent heat capacity method (see 2.2.5, [21, 22]).

The convection effect

Many authors [27, 28], proving their conclusions on experimentally tests, state that, for many engineering applications, the convective motions in the mushy and especially liquid phase can't be neglected. Sparrow, Larson, and Ramsey [27], in particular, state that in the melting process the natural convection dominates the heat transport mechanism. The phase change controlled by natural convection is now well documented in the literature, but, especially in the initial approaches, many numerical techniques had been developed to solve the phase change problem taking into account the only diffusive heat transfer.

Sparrow et al. [29] show the impact of the convection on the freezing PCM starting from two different initial conditions. They carry on two experiments: in the first one the PCM initial temperature for the solidification process is the fusion temperature (non superheated case), while in the second one the PCM initial temperature is above the fusion value (super-heated case). In the first case no convection is present; in the second case the convection takes place and the heat transport is driven by both conduction and convection. For this experiment, if corresponding frozen specimens at equal run times are compared, the amount of solid material is sharply reduced when the convection is present. In other words, in presence of convective motions the PCM freezes in a longer time.

Voller et al. [28] describe an implicit upwind technique to solve the conserved heat and momentum equations with the control volumes finite difference method, for a bi-dimensional problem. A detailed explanation of the method to simulate the convection in the PCM through Computational Fluid Dynamic (CFD) is provided in [22].

Hibbert et al. [30] employ the enthalpic formulation of the conservation equations to simulate the solidification and the building-up of a solid crust in a pipe with a laminar flow. Both the heat transfer typology, conduction and convection, are modeled in the PHOENIX code and the results are compared with literature experimental data. When the simulation starts, the solid layer is thin and almost constant along the length of the pipe; then the double curvature, at the inlet and at the outlet of the pipe, as well as the solid thickness, increases with the time and with the longitudinal coordinate. The solidification proceeds from the pipe outlet and continues until the crust completely blocks the pipe and stops the flow.

A comparison among the implementations of convection models in the molten PCM, carried on by several authors, is contained in [31].

An other, simpler, approach to model the convection effect is to choose an opportune empirical correlation and use it to modify the conduction coefficient when the convection is supposed to take place. The strategy to take into account the convection in the liquid phase through correlations is common in the literature. The liquid conductivity could be multiplied by a power of the Rayleigh number, pointed out experimentally, and an other empirical factor in order to find out an effective conductivity. In TRNSYS [24, 32] the effective conductivity is calculated multiplying the actual conductivity by the PCM Nusselt value, calculated with different correlations for rectangular and spherical cavities. Farid and Hussian [15] model the convection in the melt phase by using an effective thermal conductivity for the liquid as a function of Rayleigh number, based on the melted layer thickness. Contrary to what happen in the melting process, during the solidification the natural convection in the liquid phase has not a great impact on the heat transfer

because of the greater resistance in the solid layer. A comparison between numerical and experimental studies on a PCM-heat exchanger, where the PCM is stored in vertical plates and the air flows from the bottom to the top, demonstrates that the used correlation, even if extrapolated for that particular model, is not accurate in describing the PCM temperature when the convection is taking place. The temperature of the boundary air, in this case, is stratified and it becomes higher flowing towards up. In the modeled molten wax, in fact, a thermal stratification due to buoyancy takes place, and it results highly two-dimensional. A single correlation calculated from the experimental case to evaluate an average values of k (k_e) does not estimate the more severe convection at the uppermost position of the plate: it predicts much lower convection compared to that found previously for convective melting of wax from below. Vice-versa, the experimental results for a shell-and-tube geometry presented by Lacroix [25] match the results obtained numerically with using selected correlations; the implemented correlations are similar to those used by Farid and Hussian [15] for an electrical application. A scheme resuming the correlation coefficients for a few geometries is summarized also in [33]. Adine and Qarnia [33] study a water tank with PCM shell-and-tube vessel and verifies the results obtained with correlations by comparing his results with the experimental ones reported in Lacroix [25]. Laouadi and Lacroix [34] provide similar correlations taking into account also the liquid layer thickness and the total PCM layer thickness.

Shatikian et al. [35] study the effect of the PCM stored between fins, and assert that while in a first stage of the melting process the flow in the liquid PCM is not strong and its impact on the melting process is weak as well, in a second stage the convective flow appears stronger. For narrow geometries at the first stage the liquid layer can be considered an additive resistance, later the vortices created in the liquid phase complete the erosion of the solid fraction. They state that the two stages compensate each other, and the error made not considering the convection may be considered low. During the melting process the vortices are formed in the lower and upper part of the domain, so the PCM solid phase is eroded from both above and below. They conclude that the impact on the convection on the the melting process depends on the width of the system, because in such geometries the convection starts at the early stage of the process. The effect of the system height on the melting process features is not sensible.

The cylindrical geometry

A cylindrical geometry has been chosen by several authors for the PCM modules: in the context of the LHSU the 2 models that have been considered more frequently are the shell-and-tube one, where the PCM fills the shells and the Heat Transfer Fluid (HTF) flows through them, and the strictly cylindrical one, where the HTF surrounds them. The first one allows a high efficiency [25], because of the high S/V ratio and because the problem is strongly coupled with the convective heat transfer from the surrounding fluid, but it is supposed to be more expensive for its production. [25] study, for water and air-based systems, storage tanks configurations with PCM shall-and-tube modules that cover all the length of the tank; a similar configuration has been chosen by [36] for air-based solar systems. Voller and Cross [26], Ghoneim [23] and Esen and Durmus [37] consider a cylindrical geometry for the modeled PCM and compute through numerical

methods the axial and radial conduction in the PCM neglecting the resistance of the container.

The spatial discretization

The spatial discretization of the PCM can be based on either fixed or deforming grids. Adopting the latter approach two methods can be chosen. With the first one, called "moving mesh method", the mesh is adapted to the simulating object according to the position of the solid-liquid interface, fixing the nodes on it: in other words, a coordinate generator has to be used at each time increment [21, 22]. With the second one, at each iteration, the initially uniform grid is refined locally at the moving boundary, such that further nodes are added or removed to obtain the requested accuracy. A PCM-water matching grid is achieved when the height of the PCM cells is the same of the water nodes and each boundary cells match exactly the water layers. Such grid is described in [14] as the classical (and obsolete) discretization scheme for the PCM. In TRNSYS several water nodes have been dissociated to overcome accuracy problems connected with such a discretization: this strategy realizes the compromise to preserve acceptable calculation times and keep a good accuracy.

The implementation of PCM modules as component enhancement

A phase change model algorithm has been developed and implemented by Bony and Citherlet [24] into a TRNSYS water tank component and then validated by Schranzhofer et al. [32]. The TRNSYS PCM model is based on the enthalpic method and describes the conduction, the convection, the hysteresis and the sub-cooling phenomenon in the PCM. In the TRNSYS component several geometries may be chosen: cylinders, plates or spheres. For the validation tests, an inorganic PCM is preferred to the organic one, since the latter consists of hydrocarbons with different chain length that melt at different temperature: this is, f.i., the case of the paraffin. The PCM-tank model validation in TRNSYS is based on experimental tests using both paraffin and acetate trihidrate (SA), contained in polypropylene cylindrical boxes. The experimental tests that have been numerically replicated are a charging and discharging process of a tank with 7 paraffin or SA+graphite modules. The numerical results that have been compared refer to the PCM heat flux and temperature variables.

An optimized configuration

The melting period is a crucial parameter that should be taken into account in determining the size and the shape of the PCM modules. Their size has to be related to the total PCM that changes phase during the day [38], so that the LHSU reaches its maximum efficiency. These achievements are true for a non solar application, but the issue becomes more complicated if the PCM charging depends on the solar energy.

Esen and Durmus [37] reformulates the same concepts and assert that the time at which the whole PCM changes phase is an essential criteria for choosing the PCM technical parameters and its geometrical characteristics .

The conclusion that a water tank with immersed PCM need an optimized configuration and design can be drawn as long ago as 1993, when Lacroix [25] asserted that the design and technical data of a given PCM must be precisely chosen, to improve at the higher level the storage unit performances. He has performed a numerical analysis of a shell-and-tube geometry in a water tank, simulating a water flow rate through the it, with the inlet water temperature always higher than T_{pc} and the initial PCM temperature lower than it. The results have been carried out for 3 different configurations having different shell radius, water flow rate and inlet temperature. The results point out that these parameters strongly influence the performance of the storage unit. The stored energy varies linearly with the inlet temperature and the curve increases his slope for higher flow rates.

Talmatsky and Kribus [39] enlightens the lack of studies about PCM-DHW system long-term performance and the overall improvements that the PCM may offer in realistic operating conditions. Simulations of such systems have been carried out by Ibáñez et al. [40] with the plants simulating software TRNSYS, by using the developed component 60PCM. If the issue mentioned above is analyzed together with Talmatsky and Kribus [39]'s and Kousksou et al. [36]'s conclusions, it will appear not possible to leave the analyzed system optimization out of considerations.

Ibáñez et al. [40] optimize a SDHW PCM-tank with reference to the next data: a draw profile of 200 liters/day, a hot water set-point temperature fixed at 45°. It is linked to a solar collector of 5 m^2. The results of this optimization is in terms of yearly solar fraction and collectors' efficiency. The discrete optimization variables are the number of modules inserted into the tank and the phase change temperature (45°and 55°C). The solar fraction is intended as "the solar energy contribution to the total load in terms of the fractional reduction in the amount of primary energy". The authors state that with PCM the solar fraction can be enhanced from 4% to 8% respect to those reached without PCM, depending on the phase change temperature. As conclusion of their work they observe a lack of influence of PCM-water tank on the mean yearly collector efficiency. Moreover, they spot a "saturation phenomenon" happening when the improvement to the solar fraction given by large amounts of PCM is not sensible. For this reason they state that the design phase of the tank is crucial in terms of volumes. They finally point out an other issue in the PCM-tank design, that is the choice of the phase change temperature. Anyway, this optimization is based on few design variables: this work does not inquire about the impact of the design parameters on the system performance. It can not be taken for granted that the design parameters that are considered optimal are effectively optimal, because an analysis on the design parameters is missing.

The aim of the thesis

The aim of the storage is to harmonize the supply and the demand of hot water in terms of time, power and location [41]. The main obstacle of the mentioned purpose is that in such systems the availability of solar energy and the energy demand is quite random and bring to overlaps in time between supply and demand, so that the risk of inefficiency is quite high. One of the most crucial point of this work is to find out if an integration of PCM into a solar storage tank may improve the performance of the system, and the particular issue is to quantify their impact for an optimized design. If the storage capacity

is improved, the overall system performance will rise up its efficiency: this means a better use of energy and implies a reduction in GHG emissions for the same performance; on the other side it leads to a reduction in the running cost and/or the investment. The thesis describes the implementation of a phase change model in ESP-r, with reference to an existing model of storage tank. The definition of the geometry and the computation of the thermal flux exchanged between the PCM modules and the tank water are collected in different subroutines among the ESP-r code. For the calculation of the PCM heat flux two different and somehow connected algorithm have been implemented: the explicit and the implicit Euler methods for the conductive heat transfer with phase change. A validation, based on literature experimental test, had been carried out, in order to verify the model and compare the results with the PCM actual behavior. The model neglects some aspects, like the hysteresis effect in the PCM. This phenomenon can be actually neglected for the ultimate purpose of this thesis, that is optimize the problem, carried on a time interval of one year and subject to the almost cyclic variation of temperature and flow rates during the days. Finally an optimization of the storage tank had been performed, considering for this operation a simple SDHW plant for the production of warm water.

2

Conduction problem with phase change

2.1 The analytical solution

The Stefan problem represents the non-linear problem of the solid-liquid moving interface, when a phase change occurs. If referred to a pure substance and applied to a semi-infinite body in a mono-dimensional scheme, the analytical solution of a phase change problem can be easily identified after some simplifying hypothesizes have been assumed. For the solidification problem illustrated in Figure 2.1, the moving interface solid-liquid can be traced adopting the next assumptions:

- Only the latent heat is stored (the influence of the sensible heat on the process is negligible if compared to the latent one, thus the temperature distribution in the solid phase is linear);
- the heat is transferred only through conduction (therefore the heat flux is proportional to the temperature gradient);
- at $t < t_0$: $T_f = T_{pc}$
- for $t \geq t_0$, $T_a = \text{cost} < T_{pc}$

where t is the time, T is the temperature, T_{pc} is the phase change temperature, 0 stands for initial, previous, f for fluid and a for air. If the temperature distribution in the solid phase is linear, the thermal flux passing through a layer S is reported in Equation (2.1.1):

$$\phi'' = \frac{T_f - T_a}{R''_{tot}} = \frac{T_f - T_a}{\frac{1}{\alpha} + \frac{S}{k}} \tag{2.1.1}$$

and does not depend on the coordinate x where the interface solid-liquid takes place. ϕ" is the specific thermal flux, R" is the specific resistance, α is the convection heat transfer coefficient, S is the layer thickness and k is the conductivity. At the spatial coordinate x,

that is when the temperature value is T_{pc}, the transferred thermal flux is absorbed as latent heat, thus:

$$\phi'' = \rho L \frac{dx}{dt} \tag{2.1.2}$$

where L is the latent heat.

The equivalence of Equation (2.1.1) and Equation (2.1.2) is written in the integral form of Equation (2.1.3): the thermal flux extracted from the solid phase equals those emitted by the liquid one.

$$\int_0^{t_S} dt = \int_0^S \frac{\rho L}{T_f - T_a} \left(\frac{1}{\alpha} + \frac{x}{k} \right) dx \tag{2.1.3}$$

where ρ is the density and t_S is the time requested for the solidification of the layer $S(x)$, calculated with Equation (2.1.4):

$$t_S = \frac{\rho L S}{\alpha \left(T_f - T_a \right)} \left(1 + \frac{\alpha S}{2k} \right) \tag{2.1.4}$$

The Equation (2.1.5) calculates the position of the solid-liquid interface: in the particular case in which R_α can be neglected ($\alpha \cong \infty$), it is a time function:

$$S_x \left(t \right) = \sqrt{\frac{2 t_S k \left(T_f - T_a \right)}{\rho L}} \tag{2.1.5}$$

In the mathematics's sector, the interest conveyed to this problem is essentially addressed to the study of the time dependent moving interface issue, while in the engineering sector the interest focuses on practical applications, or rather, the physical implications of the PCM enhanced devices adoption [28].

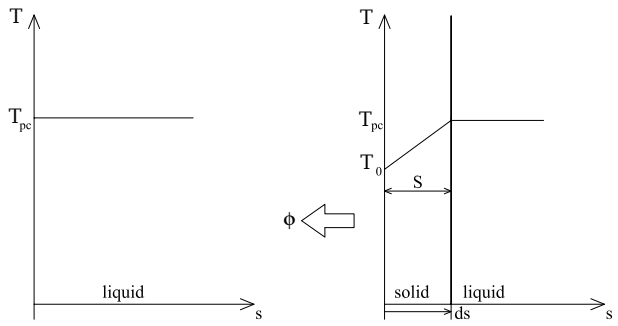

Figure 2.1: Solidification for a pure substance: instant t_0 and t

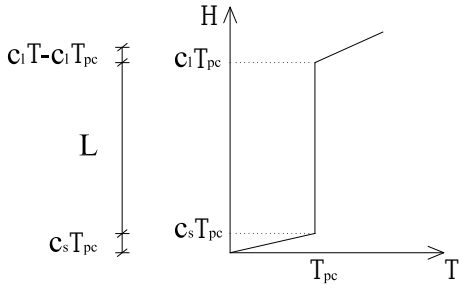

Figure 2.2: Enthalpy graph as function of the temperature for a pure substance

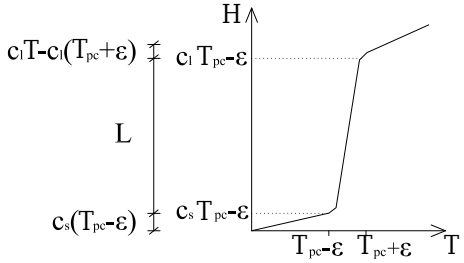

Figure 2.3: Enthalpy graph as function of the temperature for a PCM

2.2 The numerical problem

One of the preset tasks of this thesis was to implement in a building/plant simulation code an algorithm to solve the heat transfer problem with phase change.

A well documented method to solve numerically the Stefan problem is the enthalpic method. A deep description of it is reported in Subsection 2.2.1. The calculation of the discretized geometric values cited in the following sections is reported in Chapter 3.

2.2.1 The enthalpic method

The algorithm implemented in ESP-r is based on a simplified version of the general formulation of the energy conservation:

$$\frac{\partial}{\partial t}(\rho c_p T) + \nabla \cdot (\rho \mathbf{w} c_p T) = \nabla \cdot (k \nabla T) + \phi \tag{2.2.1}$$

If the only conductive heat transfer is considered for the phase change, the Stefan problem is expressed with Equation (2.2.1) written both for the solid and the liquid phases:

$$\frac{\partial}{\partial t}(\rho_s c_{p,s} T_s) = \nabla \cdot (k_s \nabla T_s) \tag{2.2.2}$$

$$\frac{\partial}{\partial t}\left(\rho_l c_{p,l} T_l\right) = \nabla \cdot \left(k_l \nabla T_l\right) \tag{2.2.3}$$

and a heat balance, written at the sharp solid-liquid moving interface Γ:

$$k_s \nabla T_s \cdot \mathbf{n} - k_l \nabla T_l \cdot \mathbf{n} = \rho L \mathbf{v} \cdot \mathbf{n} \tag{2.2.4}$$

where $\mathbf{v}$ is the velocity of the interface motion, $\mathbf{n}$ is the vector normal to the surface, s stands for solid and l stands for liquid. Equation (2.2.4) is the so called Stefan condition and states the equivalence between the net heat flux across the phase change interface and the amount of heat referred to the undergoing phase change.

The Stefan problem, described by the three Equations 2.2.2 - 2.2.4, can be expressed through a single formulation. Equation (2.2.5) is the reference Equation for the enthalpic method.

$$\rho \frac{\partial H}{\partial t} = \nabla \cdot (k \nabla T) \tag{2.2.5}$$

The enthalpy value H, that appears in the accumulation term, is a function of the temperature. The upper case symbol used to indicate $H(T)$ is common in the literature [22] and means that both the latent and the sensible heat are taken into account. Equation (2.2.6) is the correspondent integral form, written for the general Control Volume (CV):

$$\frac{d}{dt}\int_V \rho H \, dV = \int_A k \, \nabla T \, \mathbf{n} \, dA \tag{2.2.6}$$

where V is the cell volume and A is its interface area.

If T_{pc} is the phase change temperature, the enthalpy-temperature relation can be expressed through the Equation (2.2.7):

$$H = \begin{cases} c_s T & T < T_{pc} \\ c_l T + (c_s - c_l) T_{pc} + L & T \geq T_{pc} \end{cases} \tag{2.2.7}$$

As affirmed by Voller and Cross [26], the discontinuity shown at the former formulation is not desirable from a practical point of view: Voller and Cross [26] described three possible approaches to overcome the problem. The first suggests to measure $H(T)$ experimentally over the region of interest; the second proposes to smooths the jump in $H(T)$ over a small interval $T_{pc} \pm \varepsilon$ and to employ the formulation reported in Equation (2.2.8);

$$H(T) = \begin{cases} cT & \text{if } T \leqslant T_{pc} - \varepsilon \\ c\left(T_{pc} - \varepsilon\right) + \left(\dfrac{c_s + c_l}{2} + \dfrac{L}{2\varepsilon}\right)\left(T - T_{pc} + \varepsilon\right) & \text{if } T_{pc} - \varepsilon < T < T_{pc} + \varepsilon \\ c_l T + L + T_{pc}\left(c_s - c_l\right) & \text{if } T \geqslant T_{pc} + \varepsilon \end{cases} \tag{2.2.8}$$

the third expresses T as a function of H, using the same temperature range $T_{pc} \pm \varepsilon$, as

reported in Equation (2.2.9).

$$T(H) = \begin{cases} \dfrac{H}{c} & H < c\,(T_{pc} - \varepsilon) \\ T_{pc} + \varepsilon \dfrac{(H - cT_{pc} - L/2)}{c\varepsilon + L/2} & c\,(T_{pc} - \varepsilon) \leq H \leq c\,(T_{pc} + \varepsilon) + L \\ \dfrac{H - L}{c} & H > c\,(T_{pc} + \varepsilon) + L \end{cases} \tag{2.2.9}$$

The interval $T_{pc} \pm \varepsilon$ defines a mushy zone between the two phases. If the proposed remedy is used, it is not necessary to trace the change phase interface Γ.

The method described in the next Subsections, suggested by Voller [22, 26], has been chosen for the implementation in ESP-r for its efficiency, or rather, for its robustness, flexibility and accuracy in solving the phase change problem [22].

2.2.2 A further approach to the phase change study

The enthalpic method, that has been previously cited and that will be deepened in Sections 2.2.3 and 2.2.5, has been implemented in the ESP-r code to calculate the thermal flux of the PCM embedded in a water storage tank.

An other method to handle the phase change problems consists in focusing on the solid-liquid interface moving. To understand the Equation (2.2.5) it is useful to focus on the solid-liquid interface Γ movement taking into account the percentage of the 2 phases that coexist for the same node. Considering the volumes where the phase change takes place, the problem is solved through the definition of S_{pc}, that is the portion of the CV which has undergone the phase change. In these terms, the variation of enthalpy in the volume identified by P results, for a time-step:

$$\frac{dH_P}{dt} = \begin{cases} -L\,\dfrac{dS}{dt} & \text{freezing} \\ \\ L\,\dfrac{dS}{dt} & \text{melting} \end{cases} \tag{2.2.10}$$

It means that when Γ passes through the CV associated to the node P, the variation of the enthalpy in the time-step is proportional to the rate at which the discrete volume changes phase. Finally, Equation (2.2.7) can be re-written as Equation (2.2.11), taking into account the interval in which the enthalpy varies during the phase change:

$$c\,T_{pc} \leq H_P \leq c\,T_{pc} + L \tag{2.2.11}$$

The S, expressed in Equation (2.2.12):

$$S = \begin{cases} (c\,T_{pc} + L - H_P)/L & \text{freezing} \\ (H_P - c\,T_{pc})/L & \text{melting} \end{cases} \tag{2.2.12}$$

permits to calculate the amount of material that has changed phase. It is written for the considered volume and depends on the nodal enthalpy. If a phase change temperature

range is considered, a more general formulation can be adopted:

$$S = \begin{cases} (L - \Delta H_P)/L & \text{freezing} \\ \Delta H_P / L & \text{melting} \end{cases} \tag{2.2.13}$$

with:

$$\Delta H_P = \begin{cases} 0 & \text{if } T_{pc} - \varepsilon \geq T \\ \dfrac{L}{2\varepsilon}(T - T_{pc} + \varepsilon) & \text{if } T_{pc} - \varepsilon < T \leq T_{pc} + \varepsilon \\ L & \text{if } T > T_{pc} - \varepsilon \end{cases} \tag{2.2.14}$$

Subsection 2.2.4 summarizes some problems, due to the association of continuous variables to their numerical representation.

2.2.3 The Euler Explicit method

The general compact numerical expression of Equation (2.2.5), written with the Euler explicit time integration, is the following Equation (2.2.15):

$$\rho a_P^0 H_P = \rho a_P^0 H_P^0 + \sum_{nb} (a_{nb}^0 T_{nb}^0 - a_{nb}^0 T_P^0) \tag{2.2.15}$$

where P is the index referred to the considered node, nb stands for neighboring and 0 refers to the past and known time-step. The definition of the coefficients is reported in the Appendix (7.2.3).

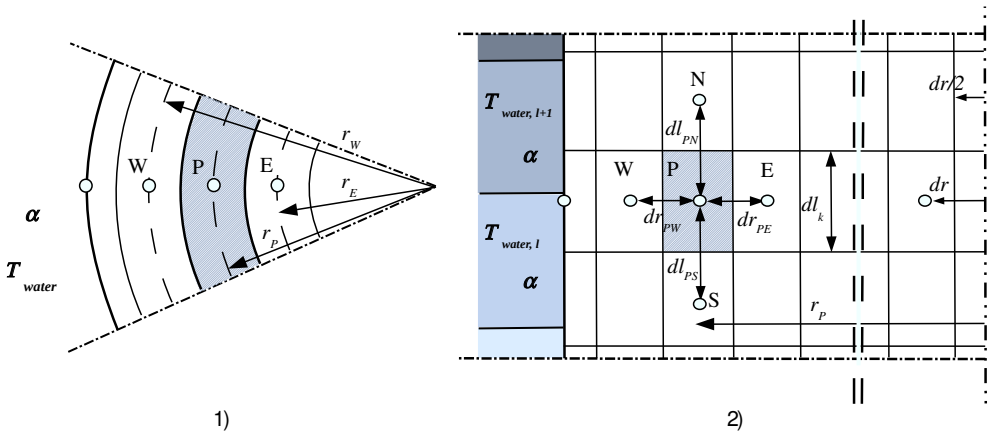

Figure 2.4: PCM module and tank water discretization.

In the implemented code the PCM density, ρ, can assume the liquid or solid value. After the former Equation has been solved and the enthalpy value has been calculated

for each node through Equation (7.2.3), the T field is updated at each time step with Equation (2.2.16).

$$T_P = \begin{cases} \dfrac{H_P}{c_s} & H_P < c_s T_{pc} \\ T_{pc} & c_s T_{pc} \leq H_P < c_s T_{pc} + L \\ \dfrac{H_P - (c_s - c_l)T_{pc} - L}{c_l} & H_P \geq c_s T_{pc} + L \end{cases} \tag{2.2.16}$$

To assure the convergence of the solution, the time step maximal value has to be calculated through the stability limit (see Subsection 2.2.3). For the computation of the PCM heat flux, it is not necessary to calculate the portion of the CV which has undergone the phase change.

Stability

The explicit method needs a stability limit to assure the convergence. This condition has the following general form:

$$\rho a_P^0 - \sum_{nb} a_{nb} \geq 0 \tag{2.2.17}$$

Referring to the coefficients values defined in the Appendix (7.2.3), Equation (2.2.17) was written using the enthalpic formulation, as reported in Equation (2.2.18),

$$\rho V \frac{H_P - H_P^0}{\Delta t} = \sum_i \frac{k_i A_i}{\Delta s_{PI}} (T_I - T_P) \tag{2.2.18}$$

and was adapted to the cylindrical symmetry in the bi-dimensional case, that is the discretization chosen for the implemented code. In particular, i=e, w, s, n is referred to the interface areas among cells and I=E,W,S,N is referred to the neighboring cells nodes. s is the general spatial coordinate. According to the uniform discretization, for the radial direction it results:

$$\Delta s_{PI} = \Delta x_{PE} = \Delta x_{PW} = \Delta r \tag{2.2.19}$$

and for the axial direction results:

$$\Delta s_{PI} = \Delta y_{PN} = \Delta y_{PS} = \Delta l. \tag{2.2.20}$$

The relations:

$$A_n = A_s = A_y \tag{2.2.21}$$

and:

$$A_e \neq A_w \tag{2.2.22}$$

come out from the cell annular shape [1]. Furthermore, since both the phases of the material have to be considered, the next formulation of the stability limit, written for the general case cell *(i,j)*:

$$\frac{\rho \cdot c \cdot V}{\Delta t} - \left(\frac{k\left(A_w + A_e\right)}{\Delta r} + \frac{kA_y}{\Delta l} + \frac{kA_y}{\Delta l} \right) \geq 0, \tag{2.2.23}$$

that is re-managed as:

$$\Delta t \leq \rho \cdot c \cdot V \cdot \left(\frac{k\left(A_w + A_e\right)}{\Delta r} + \frac{2kA_y}{\Delta l} \right)^{-1}, \tag{2.2.24}$$

becomes:

$$\Delta t \leq \rho_{st} \cdot c_{st} \cdot V \cdot \left(\frac{k_{st}\left(A_w + A_e\right)}{\Delta r} + \frac{2k_{st}A_y}{\Delta l} \right)^{-1} \tag{2.2.25}$$

where *st* indicates the liquid or the solid state. The minimum value for Δt has to be selected considering both the two values for the variables ρ, c and k and taking into account all the cells dimensions.

For the general cell the considered thermal flux depends on the conductive heat transfer among the cells; for the border cells an imposed thermal flux is considered. Regarding the CV in contact with the water, at the boundary face(s) the diffusive terms, that appear in Equation (2.2.18), are replaced by the convective contributes written in Equation (2.2.26)[2].

$$\alpha_w A_{face} \cdot \Delta T_{i,w} \tag{2.2.26}$$

If the controls listed in Footnote 3 were written for each cell, the code might appear redundant and cause also an useless computational effort. Therefore, it is convenient to point out the most unfavorable condition, that is the condition which, once satisfied, the stability is satisfied for all the model. This condition can be identified as the formula

[1] Vice-versa, if the discretization in axial direction is not uniform the stability condition for the boundary cells (at cylinder top and bottom) need to take into account different heights:

$$\Delta l_{bot} \neq \Delta l_{top} \neq \Delta l = \text{Water node height}$$

This is just one of the reasons that led to adopt the uniform grid: in spite of a grid reflecting the water layer discretization.

[2] The nodes of the border cells are located on the border (see Figure 2.4 and their width, in the direction normal to the cell border face, is halved. For this reason, when the water side of the cell is analyzed, there are no contributions for the conduction heat transfer to be considered. In theory, but it can't be applied to a PCM, if it was chosen a discretization, that put the node at the center of the cell also for the border cells, also a conduction contribution should had been added (see Subsection 3.1.5).

written for the general cell on the axis (Equation (2.2.31)) [3]:

$$\Delta t \leq \frac{\rho_{st} c_{st} V_P}{\frac{k_{st} A_w}{\Delta r} + \frac{2 k_{st} A_y}{\Delta l}} \tag{2.2.31}$$

If this Equation is satisfied, the stability condition is satisfied for the rest of the cells.

2.2.4 Time-Temperature graph

After the phase change interface and the solid-liquid coexistence for a cell have been presented at Subsection 2.2.2, some further observation can be added to the numerical representation of the phenomenon. Some preliminary simulation tests confirmed what is reported in the literature [22, 26]. If a solidification problem is simulated with the explicit fixed grid enthalpic scheme, it may happen that the resulting temperature profile shows oscillations. It is assumed that a PCM, having T_{pc}=0, at the initial time t_0=0 is in the liquid state, with $T_0 > 0$. At $t > 0$ the temperature of one surface is lowered to $T < T_{pc}$ and maintained constant. For simplicity the mono-dimensional case is considered and the thermal properties ρ, c, k are assumed constant.When the latent is much larger than the sensible heat (low Stefan number) the numerically predicted temperature profile shows large oscillations, composed by alternations of plateaus and sharp drops. This behavior is typical of the enthalpic method and it is due to the temporary blind in the pseudo steady state region constituted by the solid phase. In other words these plateaus depend on the way in which the numerical phase change interface proceeds, and this is considered in the following paragraph. Vice-versa, when the Stefan number is high, or rather when the latent heat effects are low, it can be observed a sound correspondence to the analytical solution. The same behavior occur for the front movement: again the step-like graph is caused by the discrepancy between the actual development of the phenomenon (continuous) and the discretized model adopted to describe the phase change. These behaviors have no consequence on the performance, in terms of heat flux, associated

[3] The limiting value for Δt should be obtained from the stability condition written for all the cells:
General lateral border cell (i,1), i = 2,...,nY

$$\frac{\rho_{st} \cdot c_{st} \cdot V}{\Delta t} - \left(\frac{k_{st} A_e}{\Delta r} + \alpha_{w,lat} A_{xb} + \frac{k_{st} A_y}{\Delta l} + \frac{k_{st} A_y}{\Delta l} \right) \geq 0 \tag{2.2.27}$$

General cell on axis (i,nX), i = 2,...,nY

$$\frac{\rho_{st} \cdot c_{st} \cdot V}{\Delta t} - \left(\frac{k_{st} A_w}{\Delta r} + \frac{k_{st} A_y}{\Delta l} + \frac{k_{st} A_y}{\Delta l} \right) \geq 0 \tag{2.2.28}$$

Bottom lateral border cell (1,1), top lateral border cell (nY,1),

$$\frac{\rho_{st} \cdot c_{st} \cdot V}{\Delta t} - \left(\frac{k_{st} A_e}{\Delta r} + \alpha_{w,lat} A_{xb} + \frac{k_{st} A_y}{\Delta l} + \alpha_{w,bot/top} A_y \right) \geq 0 \tag{2.2.29}$$

Bottom cell on axis (1,nX), top cell on axis (nY,nX)

$$\frac{\rho_{st} \cdot c_{st} \cdot V}{\Delta t} - \left(\frac{k_{st} A_w}{\Delta r} + \frac{k_{st} A_y}{\Delta l} + \alpha_{w,bot/top} A_y \right) \geq 0 \tag{2.2.30}$$

with the PCM; they occur because the temperature distribution is quasi-steady during the phase change process [42]. When the phase change is undergoing in one CV, while the cell volume gradually changes state in the time, the solid-liquid interface remains fixed at the coordinate corresponding to that node. Then, only when the phase change take place at the successive node, the interface shifts to it, and this causes a jump in the interface position. Some remedial schemes to this problem can be found in the literature, for example a linear interpolation or the introduction of a small phase change temperature range around T_{pc}. The definition of the actual interface proceeding or the pointing out of a continuous temperature history graph is not a purpose of the thesis. These aspects do not influence the calculation of the thermal flux needed to evaluate the contribution of the PCM on the water maintenance at a certain temperature.

2.2.5 The Euler Implicit method

In the explicit scheme the stability condition depends on the selected grid as well as the material characteristics, therefore the maximum time- step for the simulation is automatically defined. Vice-versa an implicit scheme always converges, or rather, the convergence does not depend on the time discretization. For this reason it is not necessary to divide the tank time-step into smaller intervals, as done for the explicit method.

The conduction with phase change equation, written at Equation (2.2.5), can be solved with the Euler Implicit formulation, as reported at Equation (2.2.32):

$$\rho a_P^0 H_P = a_P^0 H_P^0 + \sum_{nb} (a_{nb}^0 T_{nb} - a_{nb}^0 T_P) \tag{2.2.32}$$

where, again, P is the index referred to the considered node, nb stands for neighboring and 0 refers to the past and known time-step. Refer to the Appendix 7.2.3 for the coefficients values.

As reported in [22] and [21], the most common approach to treat and overcome the non linearity of this discretized formulation is to linearize it and to employ an iterative solution. The most common adopted methods in the literature are the source update method, the enthalpy linearization method and the apparent heat capacity method. The formulation that had been implemented in the ESP-r code is the second one and it is formulated in the following paragraphs; a descriptive scheme of the other two methods is summarized later in this Subsection.

The enthalpy linearization approach

The enthalpy linearization method assumes that the phase change takes place on an arbitrarily thin temperature range (see Subsection 2.2.1), such that the enthalpy is a

piecewise continuous function of the temperature, as reported in Equation (2.2.33):

$$H(T) = \begin{cases} c_s T & \text{if } T \leqslant T_{pc} - \varepsilon \\ c_s \left(T_{pc} - \varepsilon\right) + \left(\dfrac{c_s + c_l}{2} + \dfrac{L}{2\varepsilon}\right)\left(T - T_{pc} + \varepsilon\right) & \text{if } T_{pc} - \varepsilon < T < T_{pc} + \varepsilon \\ c_l T + L + T_{pc}\left(c_s - c_l\right) & \text{if } T \geqslant T_{pc} + \varepsilon \end{cases} \tag{2.2.33}$$

where 2ε is an arbitrarily small temperature interval over which the phase change occur. The accuracy and the efficiency of the method do not depend on the size of this interval. After the enthalpy is calculated, it can be derived respect to the temperature; then, the value of c^A, interpreted as apparent heat capacity value, is pointed out with the formulation reported at Equation (2.2.34).

$$c^A = \frac{dH}{dT} = \begin{cases} c_s & \text{if } T \leqslant T_{pc} - \varepsilon \\ \dfrac{c_s + c_l}{2} + \dfrac{L}{2\varepsilon} & \text{if } T_{pc} - \varepsilon < T < T_{pc} + \varepsilon \\ c_l & \text{if } T \geqslant T_{pc} + \varepsilon \end{cases} \tag{2.2.34}$$

The defined value of $H(T)$ and c^A can be employed for the linearization of the Equation (2.2.32) written in the following iterative form:

$$\rho a_P^0 H_P^n = \rho a_P^0 H_P^0 + \sum_{nb} a_{nb} T_{nb}^n - a_P T_P^n \tag{2.2.35}$$

where n is the current iteration and 0 refers to the value of the previous time-step, that is known. Applying the Taylor series expansion:

$$H_P^n = H_P^{n-1} + \frac{dH_{n-1}}{dT}\left[T_P^n - T_P^{n-1}\right] \tag{2.2.36}$$

the Equation (2.2.35) becomes:

$$\left(a_P + \rho c^A a_P^0\right) T_P^n = \rho c^A a_P^0 \cdot T_P^{n-1} + \sum_{nb}\left(a_{nb} T_{nb}^0\right) + \rho a_P^0\left[H_P^0 - H_P^{n-1}\right] \tag{2.2.37}$$

with the a_P and a_P^0 coefficients values defined in the Appendix (7.2.3).

The detailed proceeding of the calculation is summarized as follows. The convection coefficient for the PCM border cells, α, is calculated once per tank time-step as function of the PCM border cells mean temperature and the water layer temperature which is in contact with the module surfaces[4] for the lateral module surface. The cell conductivity and density is upgraded as function of the previous time step nodal temperature. In case that also the convection effect in the mushy-liquid phase is taken into account, an effective

[4]Or the water layers averaged temperature, if the surface is in contact with two water layers.

value of conductivity is calculated, as reported in Section 2.3. Finally the equation system coefficients reported in the Appendix 7.2.3 are calculated. The general initialization of the iterative values can be considered concluded after these operations are finished, at the beginning of the time step. After this first initialization has been done, the iterative process of PREDICTION-CORRECTION starts and continues until the convergence is reached, or rather until the residual falls below a fixed tolerance. The first stage consists in calculating c^A from Equation (2.2.34) with the temperature and enthalpy field known from iteration $n-1$ and upgrading the temperature field at iteration n by solving the Equation (2.2.37). The resulting system to be solved can be summarized with the classical formulation reported below:

$$A_P T_P + A_E T_E + A_W T_W + A_S T_S = S_P. \tag{2.2.38}$$

This formulation has been implemented, as well as the explicit one, for the new component of ESP-r: see the Appendix for further information about the equation system coefficients (see Appendix 7.2.3). As described in Chapter 3, the PCM module has been discretized with a bi-dimensional scheme, therefore, the resulting matrix, that is the **LHS** term in the Equation (2.2.40), is penta-diagonal. The scheme used to build up the matrix is reported in Figure 2.5; the scheme points out also the indexing of the conductivity values (k_x referred to the x direction and k_y referred to the y direction) that refer to the cells interfaces.

The CORRECTION stage consists in updating the nodal enthalpy field at iteration n through Equation (2.2.35) and in assuring the consistency with the nodal temperature field through Equation (2.2.39)

$$T_P^n = \begin{cases} \dfrac{H_P^n}{c_s} & H_P^n \leqslant c_s\left(T_{pc}-\varepsilon\right) \\ \dfrac{H_P^n + \left[\left(c_s-c_l\right)/2 + L/\left(2\varepsilon\right)\right]\left(T_{pc}-\varepsilon\right)}{\left(c_s+c_l\right)/2 + L/\left(2\varepsilon\right)} & c_s\left(T_{pc}-\varepsilon\right) < H_P^n < c_s T_{pc} + c_l\varepsilon + L. \\ \dfrac{H_P^n - \left(c_s-c_l\right)T_{pc} - L}{c_l} & H_P^n \geqslant c_l\left(T_{pc}+\varepsilon\right) + L \end{cases} \tag{2.2.39}$$

As already run over, the system described by the Equation (2.2.38) can be expressed through the following compact formula:

$$\mathbf{LHS} \cdot T = \mathbf{RHS} \tag{2.2.40}$$

The Left Hand Side (LHS) is the coefficients matrix: if $nXnY$ is the total number of cells, its dimension is $nXnY$ x $nXnY$. It contains the coefficients of the array T at the current iteration, so that it is referred to unknown values. Right Hand Side (RHS) is the array of the known values, calculated at the previous iteration.

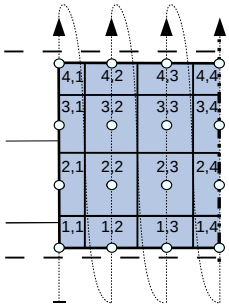

4,1	k_x(4,1)	4,2	k_x(4,2)	4,3	k_x(4,3)	4,4
k_y(3,1)		k_y(3,2)		k_y(3,3)		k_y(3,4)
3,1	k_x(3,1)	3,2	k_x(3,2)	3,3	k_x(3,3)	3,4
k_y(2,1)		k_y(2,2)		k_y(2,3)		k_y(2,4)
2,1	k_x(2,1)	2,2	k_x(2,2)	2,3	k_x(2,3)	2,4
k_y(1,1)		k_y(1,2)		k_y(1,3)		k_y(1,4)
1,1	k_x(1,1)	1,2	k_x(1,2)	1,3	k_x(1,3)	1,4

$A_{P,11}$ $A_{N,11}$ $A_{S,21}$ $A_{P,21}$ $A_{N,21}$ $A_{S,31}$ $A_{P,31}$ $A_{N,31}$ $A_{S,41}$ $A_{P,41}$	$A_{E,11}$ $A_{E,21}$ $A_{E,31}$ $A_{E,41}$		
$A_{W,12}$ $A_{W,22}$ $A_{W,32}$ $A_{W,42}$	$A_{P,12}$ $A_{E,12}$ $A_{S,22}$ $A_{P,22}$ $A_{E,22}$ $A_{S,32}$ $A_{P,32}$ $A_{N,32}$ $A_{S,42}$ $A_{P,42}$	$A_{E,12}$ $A_{E,22}$ $A_{E,32}$ $A_{E,42}$	
	$A_{W,13}$ $A_{W,23}$ $A_{W,33}$ $A_{W,43}$	$A_{P,13}$ $A_{N,13}$ $A_{S,23}$ $A_{P,23}$ $A_{N,23}$ $A_{S,33}$ $A_{P,33}$ $A_{N,33}$ $A_{S,43}$ $A_{P,43}$	$A_{E,13}$ $A_{E,23}$ $A_{E,33}$ $A_{E,43}$
		$A_{W,14}$ $A_{W,24}$ $A_{W,34}$ $A_{W,44}$	$A_{P,14}$ $A_{N,14}$ $A_{S,24}$ $A_{P,24}$ $A_{N,24}$ $A_{S,34}$ $A_{P,34}$ $A_{N,34}$ $A_{S,44}$ $A_{P,44}$

Figure 2.5: Building up of the pent-diagonal matrix.

Other methods to treat the conduction with phase change

The source update method is based on Equation (2.2.41),

$$\rho c \frac{\partial T}{\partial t} = k\nabla^2 T - \rho L \frac{\partial g}{\partial t} \tag{2.2.41}$$

that is the result of the substitution of Equation (2.2.42):

$$H = [gc_l + (1-g)\, c_s]\, T + g\,(c_s - c_l)\, T_{pc} + gL \tag{2.2.42}$$

into Equation (2.2.32). g is the liquid volume fraction [-].

The numerical discretization of the previous Equation (2.2.41) is written, in the implicit formulation, in the following Equation (2.2.43):

$$(\rho c a_P^0 + a_P)T_P = \rho c a_P^0 T_P^0 + \sum_{nb}(a_{nb}T_{nb}) + \rho L a_P^0 (g_P^0 - g_P) \tag{2.2.43}$$

c is calculated as the average of the phases characterizing each volume. This approach isolates the non linearity, typical of the phase change problems, in the source term.

The apparent heat capacity method is based on a reformulation of the governing equation Equation (2.2.5) in terms of apparent heat capacity, such that:

$$\frac{\partial H}{\partial t} = \frac{\partial H}{\partial T}\frac{\partial T}{\partial t} = c^A \frac{\partial T}{\partial t} \tag{2.2.44}$$

and thus:

$$\rho c^A \frac{\partial T}{\partial t} = k\nabla^2 T. \tag{2.2.45}$$

With this formulation the non linearity, due to the phase change, is absorbed into the apparent heat capacity term. The previous Equation, as well as the next Equation (2.2.46), represents the general formulation of a heat conduction with a non linear specific heat. Equation (2.2.46) represents the discretized form of Equation (2.2.45):

$$(\rho c^A a_P^0 + a_P)T_P = \rho c^A a_P^0 T_P^0 + \sum_{nb}(a_{nb}T_{nb}). \tag{2.2.46}$$

The Stefan problem can be solved identifying an appropriate approximation for c^A. If ε is too small, Equation (2.2.34) can not be used to substitute the c^A value, thus, other schemes, proposed in the literature, have to be employed.

Both the cited approaches proceed with an iterative method based on alternations of "PREDICTION-CORRECTION" phases.

2.2.6 Method remarks and observations

The main observations on the two described Euler methods can be summarized in the following issues:

- The nodal temperature remains fixed at T_{pc} for all the phase change time interval;

- the liquid fraction g at the node where the phase change is undergoing is included in the range [0;1];
- in one-dimensional problems only one node at a time can be affected by the phase change at any time step.

Moreover, considering the enthalpy linearization in the implicit method, a phase change temperature scaled to T_{pc}=0 is required for its efficiency and accuracy. If ε is small (for example 0.1°C), the apparent heat capacity term $c^A = dH/dT$ will become large and the prediction temperature T_P will results close to 0 in the cells where the phase will be changing. For this reason, if $T_{pc} \neq 0$, a bigger value for ε has to be chosen (for example 1°C). An other observation on the enthalpy linearization method is that the convergence is almost always reached quickly, within one iteration, except for the case in which the phase change is taking place.

In case a fixed grid is adopted to discretize the PCM, it is suggested to treat the discontinuous thermal properties with particular care. For what concern the density and the heat capacity, a mean weighted value on the quantity of solid and liquid phase coexisting in the CV should be considered. Vice-versa, the value of the k should be calculated with a Kirchhoff transformation [43]. This method is accurate and efficient and need neither the Γ tracing, nor the g calculation at the interface cell areas. If the arithmetic average is used, it may be run the risk of obtaining a poor accuracy and the convergence failure. This approach consists in approximating conductivity, for example at the east cell interface area,through the next Equation (2.2.47):

$$k_e = \frac{T_E}{T_E - T_P} k_e + \left(1 - \frac{T_E}{T_E - T_P}\right) k_P \tag{2.2.47}$$

A re-managed form of it, reported at Equation (2.2.48), is the computational formulation implemented into the code.

$$k_e = k_P + \frac{T_E(k_E - k_P)}{T_E - T_P + \varepsilon} \tag{2.2.48}$$

ε is here a small number that avoids division by zero: in the model implementation ε<1E-5. e refers to the east interface cell, while the caps, E (East) and P, denote the nodal variables.

2.3 The convection effect

The method implemented in the ESP-r code does not take into account the natural convection inside the liquid phase, in fact the formulas contain only the accumulation and diffusive terms. The literature provides a large quantity of scientific works describing the convection effect in the molten PCM (see 1). The main features emerging from it can be resumed in the following concepts:

- the effect of the convection is sensible for wide PCM modules (in thin modules the vortices can not be established);

- the convection effect rise up the melting velocity;
- the correct and accurate approach that better describe this phenomenon is to solving the mass conservation equations;
- a reasonable approach that is a good compromise between computational effort and results quality is to use correlations to calculate a k_e for the phase where the convection can be established.

In the implemented code the convection in the molten PCM fraction is taken into account through the following correlation, that permit to minimize the computational complexity.

$$\frac{k_e}{k_l} = CRa^n \tag{2.3.1}$$

The implemented C and n values are respectively 0.12 and 0.25. The assumption on which this correlation is based is that the Rayleigh number for the PCM is 5000 [20, 44].

3

PCM module

3.1 The geometry

3.1.1 Axi-symmetric problem

A way to solve the Stefan problem through the enthalpic method in an axi-symmetric geometry has been purposed by Voller and Cross [26]. The formulation reported at 2.2.2, Equation (2.2.13), can be written as:

$$S = \frac{1}{2} \pm \frac{\delta r}{8r} \tag{3.1.1}$$

and the corresponding value of the nodal latent heat as:

$$\Delta H_P = \begin{cases} L(1-S) & \text{freezing} \\ LS & \text{melting} \end{cases} \tag{3.1.2}$$

3.1.2 The adopted PCM grid

The PCM module was modeled as a cylinder, thus, for simplicity, an uniform structured fixed grid was defined. The number of the cells, both in the axial and in the radial direction, can be chosen by the user. Figure 3.1 shows the chosen discretization and the implemented labeling. The node centered grid was defined starting by the position of the central and border nodes for the radial direction and those of the top and the bottom for the axial direction. Then, the resulting dimension of the cell depends on the refinement chosen by the user (see Sub subsection 4.2.2).

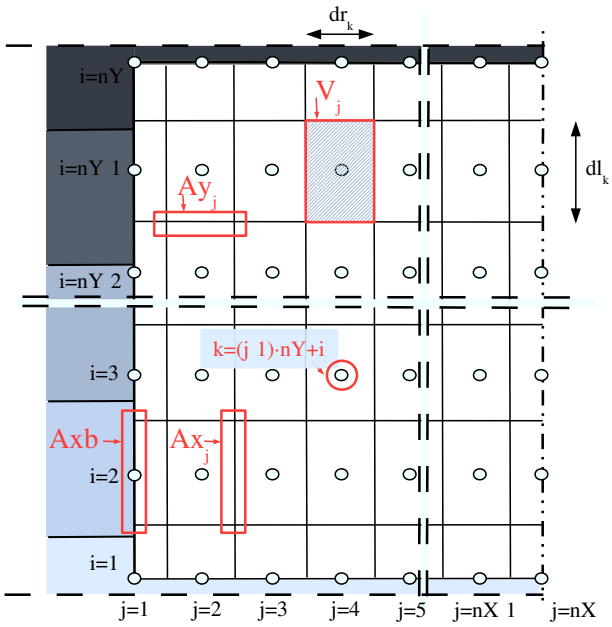

Figure 3.1: PCM cells numbering.

Except for the cells located on the axis, that are cylindrical, the general cells have an annular shape: in particular, all the cells characterized by the same index j have the same north-south interface area and volume. The border cells at the top and the bottom of the PCM moodule have been halved and those laying on the cylindrical surface have an halved thickness. This strategy avoids problems when the phase change occur, since in that cell the temperature is fixed for all the cell.

After the general cell height and thickness and the nodes position in the radial direction are calculated, the cells areas and volumes are computed. To save memory each interface area is calculated once, since the east face of the cell i, j is the same of the west one of the cell numbered $i, j + 1$.

The Equation (3.1.3) gives the values of A_x for all the interface areas among the cells that are adjacent with the East and West area (j=1,...,nX-1) [1]

$$A_{x,j} = 2 \cdot \pi \cdot \Delta l \cdot \left(r_{P,j} - \frac{\Delta r}{2} \right) \tag{3.1.3}$$

where r is the radius, distance axis-node [m], Δr is the distance among nodes in radial direction [m] and Δl is the distance among nodes in axial direction [m]. The lateral border areas are calculated with the Equation (3.1.4)

$$A_{x,b} = \pi \cdot D_{cyl} \cdot \Delta l \tag{3.1.4}$$

[1] Like in figure Figure 2.5, A_x is the area perpendicular to the x direction and A_y is those perpendicular to the y direction.

where b stays for border, D stays for diameter [m] and *cyl* stays for cylinder.

The Equation (3.1.5) calculates the general $A_n = A_s = A_y$ (j=2,...,nX-1)

$$A_{y,j} = 2 \cdot \Delta r \cdot r_{P,j} \cdot \pi \tag{3.1.5}$$

The Equation (3.1.6) expresses the value of A_y for the outer cell (j=1):

$$A_{y,j} = \Delta r \cdot \left(r_{P,j} - \frac{\Delta r}{4} \right) \cdot \pi \tag{3.1.6}$$

while Equation (3.1.7) expresses the value of A_y for the the inner cell (j=nX):

$$A_{y,j} = \left(\frac{\Delta r}{2} \right)^2 \cdot \pi \tag{3.1.7}$$

The cell volume, V, is then straightforward calculated as:

$$V_j = A_{y,j} \cdot \Delta l \tag{3.1.8}$$

this value is halved for the top and bottom cells.

3.1.3 Discretization correspondence among PCM cells and water layers

While for a matching discretization among PCM cells and water layer (see subsection 3.1.6 the correspondence is straightforward identified, for a non-matching grid, like the uniform one described here, the code calculates the number of the water layer that correspond to the PCM cells row.

A first check assures that the PCM grid is more refined than the water one: the cell height should be smaller, or, at maximum, equal to the water layer one, such that at each PCM row can be at maximum in contact with 2 water layers.

At a later stage the code identifies a correspondence among the progressive PCM cells row and the water layer number: this is reported in Figure 3.2.

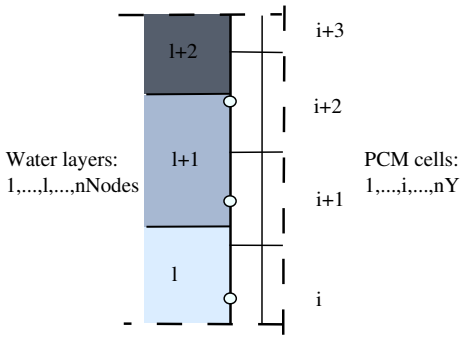

Figure 3.2: PCM cells and tank water layers matching.

Finally the code calculates the percentage of the PCM cell border surface that is in contact with each boundary layers.

3.1.4 The border condition - water side

To calculate the convection coefficients on the module top, bottom and lateral surfaces, different correlations have been used. These values depend on the surface position and the water flow inside the tank: inside the tank natural or mixed convection motions may established.

Averaged temperatures for the PCM module lateral surface and the tank water are used inside the correlations, derived from [45].

Fot the horizontal module surfaces the following formulation had been implemented. If the cylinder top surface temperature was higher than the boundary water, and if the cylinder bottom surface temperature was lower than the water one Equation (3.1.9) or Equation (3.1.10) had been used; when the top or bottom cylinder surfaces had a lower or higher temperature than the surrounding fluid respectively, Equation (3.1.11) had been chosen:

$$Nu_n = 0.54 \cdot Ra^{1/4}; \qquad 10^4 \leq Ra \leq 10^7 \tag{3.1.9}$$

$$Nu_n = 0.15 \cdot Ra^{1/3}; \qquad 10^7 \leq Ra \leq 10^{11} \tag{3.1.10}$$

$$Nu_n = 0.27 \cdot Ra^{1/4}; \qquad 10^5 \leq Ra \leq 10^{10} \tag{3.1.11}$$

Nu is the Nusselt number, Ra is the Rayleigh number; n stands for natural. For the cylinder lateral surface a condition of mixed convection has been considered, and the Nusselt value, calculated with Equation (3.1.14), depends on both the natural and forced convection, as reported at Equation (3.1.12) and Equation (3.1.13).

$$Nu_n = \left[0.825 + \frac{0.387 \cdot Ra^{1/6}}{\left[1 + (0.492/Pr)^{9/16}\right]^{8/27}}\right]^2 \tag{3.1.12}$$

$$Nu_f = 0.664 \cdot Re^{1/2} \cdot Pr^{1/3} \tag{3.1.13}$$

$$Nu^3 = Nu_n^3 + Nu_f^3 \tag{3.1.14}$$

Re is the Reynolds number; the subscript f stands for forced. For what concerns Equation (3.1.12), a vertical cylinder may be treated as a vertical flat plate when Equation (3.1.15) is verified:

$$\frac{D}{L} \geq \frac{35}{Gr_L^{\frac{1}{4}}} \tag{3.1.15}$$

The code assumes that this condition is verified and does not implement any further alternative formulation. The same formulation is implemented also in TRNSYS [14].

The convection heat transfer coefficient [W/(m^{2}K)] is therefore calculated with the following Equation (3.1.16)

$$\alpha = \frac{Nu \cdot k_w}{X} \tag{3.1.16}$$

where X is the characteristic length of the module considered part, that are the height of the cylinder for the lateral value of α and the value calculate with Equation (3.1.17) for the top/bottom cylinder surface.

$$L = \frac{A_s}{P} = \frac{\frac{D_{module}^2}{4} \cdot \pi}{D_{module} \cdot \pi} \tag{3.1.17}$$

An extra resistance is added to simulate the presence of the PCM containment: this is implemented throughout an equivalent convection coefficient that includes the resistance of a PVC vessel of 1 mm.

$$R''_{ext} = \frac{1}{\alpha_w} \tag{3.1.18}$$

$$\alpha_{w,eq} = \frac{1}{R''_{ext}} = \frac{1}{R''_{ext} + R''_{PVC}} \tag{3.1.19}$$

$$R''_{PVC} = \frac{s_{PVC}}{k_{PVC}} = 6.6 \cdot 10^{-3} \frac{m^2 K}{W} \tag{3.1.20}$$

3.1.5 The border condition - PCM side

During the phase change the temperature does not vary until all the CV material has changed phase; moreover the temperature at the node is the same as those at the border. This reason motivated the choice of localizing the nodes of the border cells on the module boundary surface, considering for those cells half width and/or half hight (see Subsection 3.1.2). With this strategy the coefficients of the solving equations can be calculated as $\alpha_w \cdot A_{bc}$, where α_w is the convection heat transfer coefficient [W/(m^{2}K)] value, calculated once per *tank* time step, w stays for water and bc stays for border cell.

3.1.6 An alternative grid for the PCM

The implemented code for the PCM imposes that the axial discretization of the module has to be more refined than the water one. This is the only constraint applied on the module discretization. The discretization of the stratified storage tank component for ESP-r is reported in Section 4.2.1. It may happen that the number of the PCM cells in this direction is high and the tank discretization is not refined. For this reason it may be criticized that such discretization for the PCM (or the lack of a control on it) is not reasonably in terms of computational effort. Even though the PCM model is based on the CFD calculation, the considered tank is just a component of a plant and not a CFD model. For this reason it may appear more reasonable to choose a discretization for the PCM that matches the water layers. This discretization had been firstly implemented and was effectively efficient for several test simulations. Such grid, however, may result

highly irregular because it depends on the position at which the module is located, on its height and on the water discretization. Depending on the position and the height of the module, the lower and the upper PCM cells may result much smaller than the general cell height and a non homogeneous grid is thus generated. Moreover, if the explicit Euler method is chosen to simulate the phase change it may happen that a useless small time-step is obtained for the simulation. The choice of implementing a water-PCM matching grid resulted necessary after the decision to work with an optimization tool (ModeFRONTIER, see Chapter 5) that manages the simulation variables exposed at Section 7.2.1. The optimization code varies the position and the height of the module without controls on the grid uniformity, thus highly non-uniform grids may result if a matching discretization is used. The matching discretization, implemented at first, had been used as term of comparison for the homogeneous grid (the test discretization for the matching and no-matching cases is reported in Figure 3.3). Concluding, the gridding scheme chosen makes very little difference to the results, assuring in the same time less computational problems.

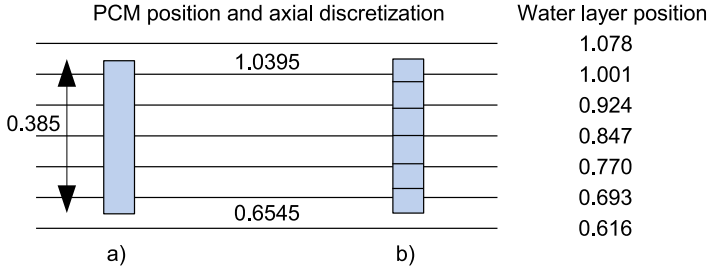

Figure 3.3: Reproduction of the same axial discretization for the matching and uniform discretization.

In TRNSYS the PCM module height is a multiple of the node height of the water tank [14]: the tank node is calculated on the basis of the module height. The definition of the exact PCM hight that have to be simulated depends, therefore, on the degree of refinement of the water discretization. The choice of fixing the PCM module height and dividing it as a function of the tank discretization is more reasonable than the vice-versa.

Further considerations have been added in Subsection 3.1.7 on the numerical error introduced changing the spatial discretization.

3.1.7 Sensitivity analysis

A sensitivity analysis had been executed on the simulation results of a stratified tank model with 2 coils inserted in the typical SDHW plant described in Chapter 4.

A first test had been considered to verify the correspondence of the PCM cylinders modeled through the matching and not-matching discretization. In this context the same cells number has been selected, after the module position and height had been chosen such that the top and bottom cells for the matching discretization are half of the general cells.

The cylindrical module was positioned at a height of 0.65450 m respect to the bottom of the tank, the chosen module height was 0.38500 m and, only for the uniform model (the only one that consent the choice), 6 layers had been chosen. For the not-matching model the input geometry values, together with the number of water layers chosen, automatically define the number of PCM cells in the axial direction. For the current test a tank of 1.54 m height had been defined and the water contained in it had been divided into 20 layers. A radial discretization consisting on 20 cells has been chosen for these simulations. The other details of the tank are those reported as "base case" at Section 7.2.1, Table 7.5; those referring to the plant are described at Chapter 4. The convection heat transfer coefficient, α, had been fixed at 500 W/(m^{2}K) A sketch of the compared discretization is reported in Figure 3.3.

The results in terms of primary energy consumption, given in output for each minute, show an error of less than 3 decimal places; this results in an error of one unit order of magnitude if the plant performance for a period of one year is simulated.

Table 3.1: Optimized designs. Primary energy consumes for an year simulation time [kWh].

6 cells, matching discretization	1397.2
6 uniform cells	1397.0

Table 3.2: Sensitivity analysis on the tank performance. Primary energy consumes for an year simulation time [kWh].

		cells axi		
		6	10	15
cells rad	10	1397.2	1401.0	1400.8
	15	1397.4	1401.0	1401.0
	20	1397.2	1401.0	1400.9

Table 3.3: Sensitivity analysis on the simulation CPU runtime (s).

		cells axi		
		6	10	15
cells rad	10	502	720	1002
	15	1323	2063	2989
	20	1826	4712	6890

The sensitivity analysis analyzes the effect of increasing the number of cells in the axial direction: this can be done from the input file just choosing the number of PCM cells rows, for the not-matching case, or refining the water stratification, for the matching case.

The sensitivity test results are listed in table Table 3.2. Concluding, the resolution of grid made little difference to the results.

3.1.8 CPU calculation time

Some data about the calculation time are reported in Section 3.1.7 Table 3.3 for the explicit method. The simulations performed to obtain the results included in Chapter 5 were carried out choosing the explicit method, since a small time step has to be chosen for the tank model (see Sub subsection 4.2.1), and there was no point to use an already small time step for the implicit method. Moreover, the firs temporary choice of a LU decomposition[2] to solve the PCM system is not suitable and other quicker methods should be selected.

As example, Table 3.4 reports a comparison between the CPU time of the explicit and implicit method referred to a one year simulation carried on the "base case" plant model described in Section 7.2.1. The tank contains 8 PCM cylindrical modules, 0.6545 m height, located at the position of 0.385 m from the tank bottom (see Figure 3.3). The module diameter is 4 cm.

The simulations use the matching discretization. The PCM module is discretized through 6 cells in the axial direction and 10 cells in the radial direction. The results, in terms of primary energy consumption, are the same for both the methods.

Table 3.4: Comparison between the CPU time of the explicit and implicit method

	time [s]
explicit	387
implicit	966

The heat capacity of each node decrease with their size; if the node number in the radial or axial direction is increased n times, the stability condition will calculate a time step for the simulation that will be n^2 times smaller, and the CPU time will increase [14].

3.2 The PCM enhanced tank feasibility

To avoid the user inserting too many PCM modules in the tank, or in a position where they can't be located, a geometrical control is run when the variables are initialized.

A specific check verifies the feasibility of the internal geometry of the tank: on one side it takes into account the location of the PCM modules in the vertical direction, considering their height and position (see Figure 3.4); on the other side the control tests the tank viability considering the number of modules that could be inserted, taking into account the number and the diameter of the modules and their reciprocal position with the tank section and the coils location (see Figure 3.5).

[2] The Lower-Upper decomposition is a direct method for the resolution of algebraic equation systems. It is a variation of the Gauss method and provide for factorizing the matrix **A** as product of a triangular upper matrix **U** and a triangular lower matrix **L**:

$$\mathbf{A} = \mathbf{LU}.$$

Since **L** and **U** are full, the storage of these matrix needs much memory.

The latter control is related to the circle packing problem and it is solved by referring to some solutions that have been found in the literature [46]: in the case of a 2 coils tank, the available space corresponds to the section of the tank whether the PCM is below the first coil, above the second one or between the two coils; the free space corresponds to the coils diameter (excluding the coil encumbrance itself) whether the PCMs are totally or partially enclosed within the coils. Figure 3.5 shows the section of the tank having, for example, 12 modules inserted. The smaller dots indicate the contact points.

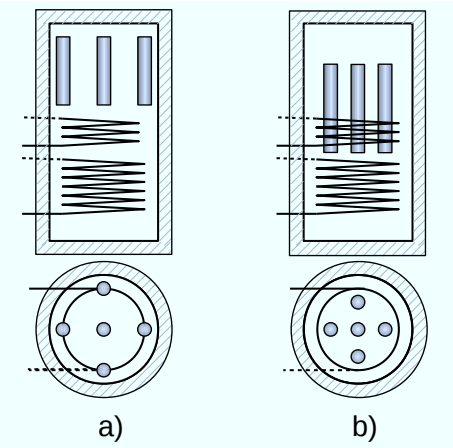

Figure 3.4: Geometrical feasibility of the PCM tank: the modules can cover all the section of the tank for the tank height where there are no coils. PCM tank axial section.

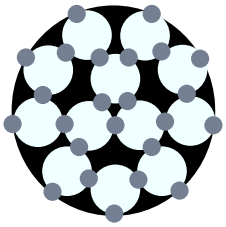

Figure 3.5: Geometrical feasibility of the PCM tank: the maximum number of modules that could be inserted is calculated referring to a circle packing problem. Example: 12 modules. PCM tank transversal section.

4

Simulated SDHW systems

4.1 The simulation code

The ESP-r code had been firstly developed at the University of Strathclyde - Glasgow. It is a versatile tool that permit to forecast the performance of a building/plant integrated system, subjected to defined internal and external loads and prescribed controls. Much information about the algorithms implemented in this code is described in the Energy Systems Research Unit (ESRU) Ph.D. thesis pages, freely accessible. The ESRU team of developers, based at the Strathclyde University, was born in 1987. The working-group research topics are themes concerning the reduction of the energy demand and the adoption of sustainable energy in the building sector. The research carried on by this group aims at enhancing the efficiency of the energy supplying systems and exploiting the renewable energy sources.
The next subsections describe the structure of the code and the process for the simultaneous solution of the different aspects facing the building design.

4.1.1 The subversion system

The primary connotation of an open source code is the free access to it. Such a code is maintained by a developers community that allows and promotes its free study, modifications and enhancement. A suitable and typical structure for supervising such a tool permits a separate and independent development of the code and a correct management of the implementations realized by anybody wants to improve it. A system like the described one is the *version control system*. The *subversion* is a version control system that manages the source code files and directories by maintaining a track of the incremented versions over time. The subversion *repository* is the tool which permits to explore the changes uploaded in each version and allows to recall them. The personal changes of the code made by the developers on the personal computer (*sand box*) can be accessed by all the community if these change are uploaded on the repository. The personal *branch* is modified starting from the common version, known as *development version*, that is independent of any other branch, or from an other developer version. The development branch can be incremented by the archivist with the contribution contained in a specific version. In other words it can be improved with particular *revisions* of the code [47].

ESP-r is an open source code for the integrated simulation of building/plant systems. It can be locally modified by any user who need to model a specific building element, a plant component or generally a design variable that can not be modeled jet through the release branch algorithms. The contribution of the developers community are managed through the software version control system. The subversion consent to maintain and periodically upgrade the different enhancement of the code developed by different users, as it is described in Figure 4.1, taken from the ESP-r Developers Guide [48].

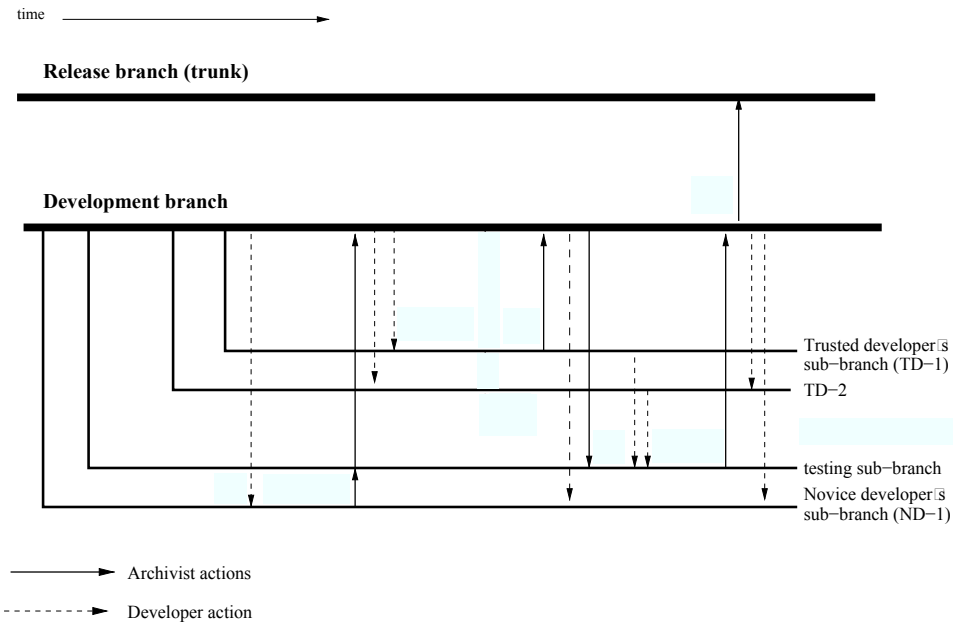

Figure 4.1: ESP-r repository scheme.

ESP-r users of the development community can *check out* any specific version of the code and work on the personal sand box localized on the personal computer. The modified code produced by the developer on the personal sand box may be *merged* back into the repository through *commitments* and eventually uploaded in the development branch if some *tests* are passed. The development branch is to preserve the quality of the distribution before the modifications are available through the *trunk* version.

4.1.2 An integrated system

The simulation is a process that can be divided in different stages. The building is discretized through a finite volume approach and reduced to a series of nodes. These nodes represent, in particular, the room air and the fabric compounding the construction. The plant associated to the considered building is composed by a series of components: each component is represented by one or more nodes and the nodes are linked by connections.

Finally, also the environmental conditions are described through one or several nodes. The conservation equations that take into account the inter-nodal transfer of energy, mass and momentum, are simultaneously written and solved for all the cited nodes and for all the time-steps in which the total simulation time is divided. With this approach it is possible to obtain the future value of the nodal state variable on the basis of the current state.

The discretization of a construction element

A construction detail of a building can be modeled in ESP-r as a *construction* element, containing the information about the thickness and the *material* of each compounding layer. Each of these homogeneous layers is represented by 3 nodes: one node is located at the center of the layer, two of them are interface nodes and are located on the two surfaces of the layer. For the construction elements, constituted by one or more layers, the internal nodes represent the finite volumes where the energy balance is calculated for the capacity/insulation system, while the surface nodes are connected with one internal node, with other surface nodes and with the nodes representing the boundary fluid, that is in contact with the element. Figure 4.2 shows a mono-dimensional discretization for a construction of 2 homogeneous layers.

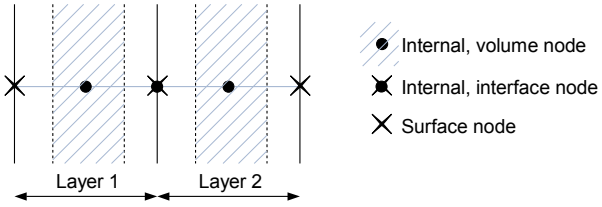

Figure 4.2: Construction nodes.

The discretization of a plant

Before describing the modeled plant components and connections, a description of a generic plant in ESP-r is here briefly reported: the literature (for example [49] and [9]) provides a deep description of the plant schemes. In order to perform the energy and mass balances describing a system, the components of a plant are modeled through nodes and connected together. Logically, the nodes that represent water can only be connected to nodes representing water and the same happen for the air nodes. The balance equations are collected in a system written through matrices, processed together with the building/zones ones and simultaneously solved. Generally the plant time-step is a fraction of the building one, so the plant matrices are solved n times for each building time step, if n is the number of sub-divisions.

Consider, for example, the simple system shown in Figure 4.3, representing a connection between 3 nodes. Considering the only plant and neglecting the building for the moment, the shown nodes are characterized by their own volume, mass and thermal capacity. To each node are associated a temperature and a mass flow rate values, one for each phase of

the fluid. The node i exchanges heat with the environment (env); an internal generation of heat (ϕ) is assumed. The balance of energy for this scheme is:

$$\begin{aligned} \bar{c}_i M_i \frac{\partial T_i}{\partial t} &= R_{i,j}\dot{m}_{a,j}c_{pa}\left(T_j - T_i\right) + R_{i,j}\dot{m}_{v,j}c_{pv}\left(T_j - T_i\right) + \\ & R_{i,k}\dot{m}_{a,k}c_{pa}\left(T_k - T_i\right) + R_{i,k}\dot{m}_{v,k}c_{pv}\left(T_k - T_i\right) + \\ & UA\left(T_{env} - T_i\right) + \phi_i \end{aligned} \tag{4.1.1}$$

where a stands for air and v stands for vapor, $R_{i,j}\dot{m}_j$ is the mass flow rate through the connection i,j, where $R_{i,j}$ is known as mass diversion ratio [-], c_p is the specific heat capacity at constant pressure of the fluid, $\bar{c}M$ is the weighted heat capacity where $\bar{c}$ is the mass weighted average specific heat capacity of the components[1]. M is the mass, U is the U-value that refers to the total heat loss from node i to the environment, and A is the corresponding component area.

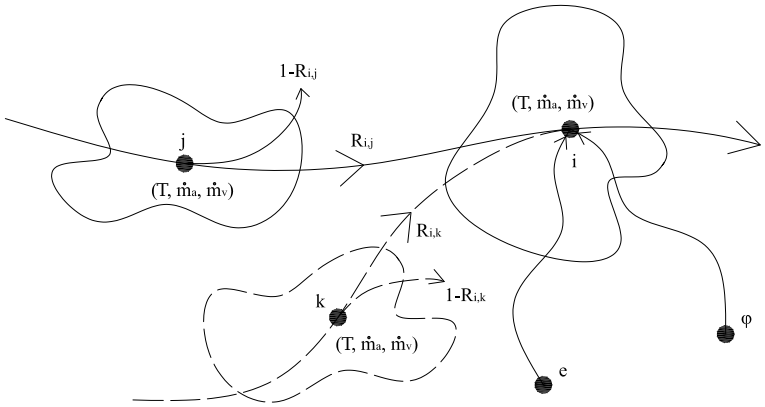

Figure 4.3: Plant nodes scheme

If more than 2 connections are linked to the node i, the equation 4.1.1 will contain more terms that are similar to the first and second line ones. The Equation (4.1.1) is solved through the method of the finite differences and, using the following notation:

$$C_{i,j} = R_{i,j}\dot{m}_{a,j}c_{p,a} + R_{i,j}\dot{m}_{v,j}c_{p,v} \tag{4.1.2}$$

can be written through an explicit and implicit formulation just choosing α=0 or α=1 respectively.

$$\begin{aligned} \left[\alpha\left(-C_{i,j} - C_{i,k} - UA\right) - \frac{\bar{c}_i M_i}{\Delta t}\right] T_i + \left[\alpha C_{i,j}\right] T_j + \left[\alpha C_{i,k}\right] T_k &= \\ \left[\left(1-\alpha\right)\left(C^0_{i,j} + C^0_{i,k} + UA^0\right) - \frac{\bar{c}_i M_i}{\Delta t}\right] T^0_i & \end{aligned}$$

[1]The storage tank described after is a multi-nodal component: it is represented by a water node, a node representing the boiler coil and, in case, the solar panel coil. For multi-nodal components the global heat capacity is calculated making an average of the different component regions.

$$+\left[(1-\alpha)\left(-C_{i,j}^{0}\right)\right]T_{j}^{0}+\left[(1-\alpha)\left(-C_{i,k}^{0}\right)\right]T_{k}^{0}$$
$$+\left[-\alpha UAT_{env}-(1-\alpha)\,UA^{0}T_{env}^{0}-\alpha Q_{i}-(1-\alpha)\,Q_{i}^{0}\right] \tag{4.1.3}$$

where 0 indicates that the variable is already known for the considered time-step. Equation (4.1.3) represents the fundamental equations of the plant side and their coefficients are collected in the matrix describing the plant at the considered time step.

The formulation shown at Equation (4.1.3) is always written in a matricial form:

$$\mathbf{A}T=\mathbf{B}T^{0}+\mathbf{C}=\mathbf{Z}. \tag{4.1.4}$$

and then solved with the building equations. **A** T form the unknown (LHS) and **B** T^0 +**C**=**Z** is the known (RHS).

If the interaction between a building and a plant (Heating, Ventilation, and Air Conditioning (HVAC)) should be represented and in the case where there are multiple zones to be represented,

a similar matrix is written for each time step by the simulating code: each single zone becomes a sub-matrix of the complete matrix describing the modeled system. The matrices that describe each zone and/or plant are assembled through many cross-coupling coefficients. For example, the connection between the different zones and between a zone and the plant is established through cross-coupling coefficients (see Figure 4.4) [2].

[2] In case the independent variable is not the temperature, the matrix will be similar and the vector containing the terms T_i Will be replaced by a containing similar generic variables ψ_i

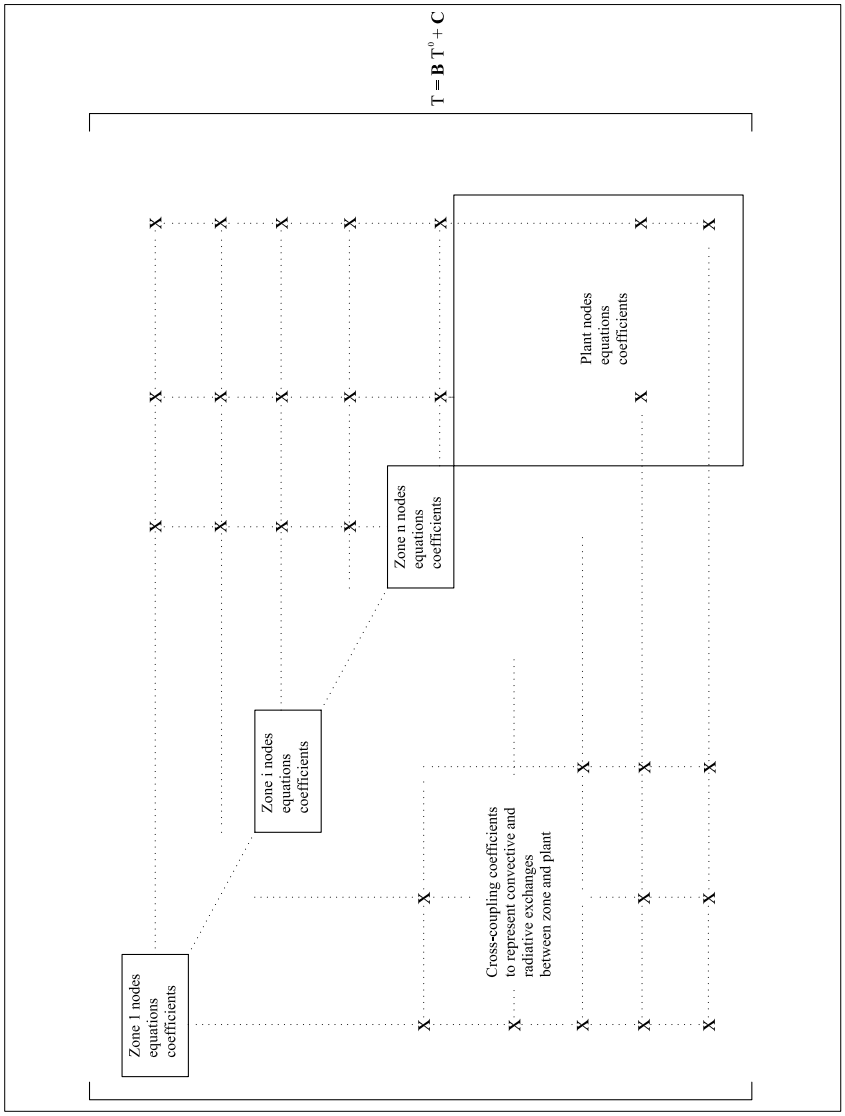

Figure 4.4: Generic building-plant system written in matricial form

4.2 The plant

A water tank is the typical energy storage system employed in the construction sector and it is adopted in the plants apt to the climatization and/or the DHW production. The

European legislation imposes the use of the renewable energy source. For this reason, the plants typology that have been chosen for the simulations is the typical SDHW system. In a typical SDHW plant the water tank, which provides the hot water to the users, is connected to a solar collector and a boiler. The PCM tank, that is the heat storage system described in Subsection 4.2.1, is the key component of the SDHW plant that had been simulated and optimized in this thesis. The plant scheme that has been modeled through ESP-r is graphically represented in Figure 4.5. The plant components and their controls are described in the next paragraphs.

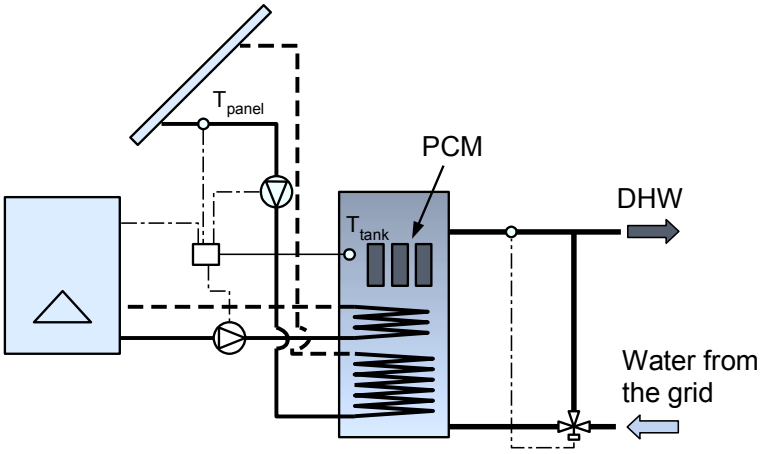

Figure 4.5: Analyzed system.

The plant to be simulated, and then optimized, can be discretized as shown in Figure 4.6.

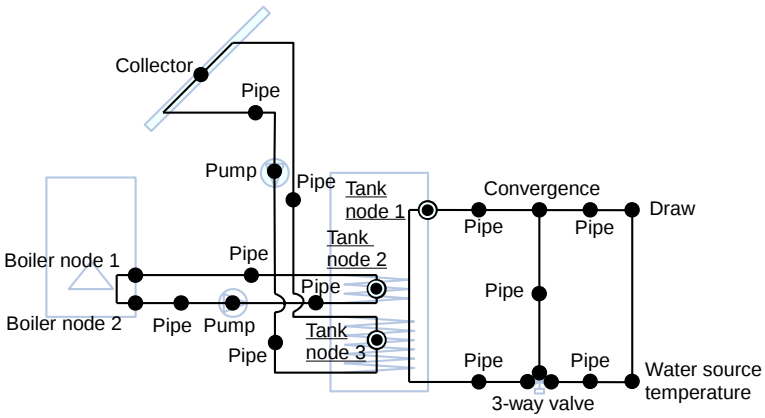

Figure 4.6: Nodes and connections of the simulated plant.

4.2.1 The tank

The description of the component is taken from the component documentation cited in [50]. The main aim of this thesis was to simulate and optimize a simple SDHW plant and its PCM storage tank. The PCM storage tank component was a modified version of the *stratified storage tank with 2 immersed heat exchangers component*. A phase change modelization, a cylindrical geometry in a bi-dimensional scheme and all the features described in Chapter 2 had been linked to this existing component and to the associated model with a single coil. The existing tank components, contained in the current ESP-r trunk version as component 103 and 104, have been developed by Thevenard and Haddad [50]. His tanks have been defined starting from the implementation of a stratification model and from the modelization of an heat flux released by heating coils. In other words, the complexity of the existing components can be summarized in the following points:

- one or two heat exchanger models are included in the tank;
- the water and the two coils outlet temperature are represented by different nodes, so three nodes are needed to represent the tank. The nodes temperature depend also on the combination of several water nodes (layers) collected together forming a single water node. The resulting water node represent the water leaving the tank.
- the balance for the single water layer, and the sections resulting from the layer mixing, accounts several contributes. The balance for one node is reported at Subsubsec 4.2.1;
- the natural convection in the water is simulated through the mixing of the water sections inside the tank.

The energy balance

The energy balance for the general tank node is subjected to the contributes listed as follows:

- the heat losses to the environment. The environment corresponds to the location where the tank is contained, in the simulated model a room at the fixed temperature of 20°C. The thermal exchanges from the environment to the tank are upgraded through the integrated simulator. The contribution is described by the term:

  $$UA_S(T_{env} - T_i)$$

  where A_s is the area of the water layer in contact with the tank surface, i is the counter referred to the tank node, *env* stays for environment. It computes the lateral vertical cylindrical surface for the general node and also the plane horizontal top and bottom tank surface for the upper and lower nodes respectively. The U is unique for all the surfaces compounding the tank (rather for the top, bottom and cylindrical vertical surfaces).

- the conductive heat transfer between the considered general node and the 2 nodes that are in contact with it.

$$\frac{(k_w + k_t)}{\Delta z} A_c (T_{i-1} - T_i) \text{ and } \frac{(k_w + k_t)}{\Delta z} A_c (T_{i+1} - T_i)$$

  A_c represents the tank cross-section, k_w is the thermal conductivity of water and k_t the additional thermal conductivity equivalent to heat a conduction along the wall.

- the forced convective heat transfer from (or to) the layer below (or above). This represents the net fluid motion due to the circulation of the water entering the tank from the tank inlet[3] The term describing this contribution is:

$$\dot{m}_{up} c_p T_i \text{ and } \dot{m}_{up} c_p T_{i-1}$$

  or

$$\dot{m}_{down} c_p T_{i+1} \text{ and } \dot{m}_{down} c_p T_i$$

  The first two terms are computed if the resulting mass flow rate $\dot{m}$ is upwards, while the second two terms if the resulting flow rate $\dot{m}$ is downwards. The sense of the flow rate is given by the water inlet and outlet position.

- the flow rate entering and going out the two water layers where the inlet and outlet is located. The term is straightforward identified as

$$\dot{m}_{in} c_p T_i \text{ and } \dot{m}_{out} c_p T_i$$

Since in the modeled tank the cold water coming from the grid enters at the lower side of the tank, the balance for the general water node is written as:

$$\begin{aligned} M_i c_p \frac{dT_i}{dt} &= U A_S (T_{env} - T_i) + \\ &\frac{(k_w + k_t)}{\Delta z} A_c (T_{i-1} - T_i) + \frac{(k_w + k_t)}{\Delta z} A_c (T_{i+1} - T_i) + \\ &\dot{m}_{up} c_p T_i + \dot{m}_{up} c_p T_{i-1} + \\ &\dot{m}_{in} c_p T_i - \dot{m}_{out} c_p T_i \end{aligned} \tag{4.2.1}$$

where M_i is the mass of the water referred to the node i. For the lower and upper tank layer the thermal exchange area towards the environment accounts also the bottom and top tank surfaces. Obviously, for the same nodes the conduction term between the lower and upper node respectively is not considered, since there are no any layers to exchange with.

The discretization of Equation (4.2.1) uses the Crank-Nicholson formulation. This scheme consent to use the explicit forward Euler scheme (first order, conditionally stable), implicit backward Euler scheme (first order, unconditionally stable) or the full Crank-Nicholson scheme (second order, unconditionally stable). The tank internal time step dt_{tank} has often to be smaller than dt_{plant} generally dt_{tank} is chosen such that the water motion in the vertical direction does not exceed a fraction of one node.

[3]The model provide the possibility to implement easily a second couple of inlet-outlet for the tank component.

The heat exchanger

The heat exchanger model is implemented in a separated routine and calculates the heat flux to be transfered to the water. The heat flux takes into account the contribution of the forced convection in the water inside the coil, of the conduction through the wall of the coil, finally of the free and forced convection in the tank water.

The nodes, the sections and the mixing algorithm

The heat and mass transfer equations are solved among the layers. In the tank model a maximum of 100 layers can be chosen. The code evaluates the temperature of each layer. A mixing algorithm calculates the actual sections of water that are homogeneous for temperature value: considering a general layer, it may happen that the temperature of the layer below is higher than those of the considered one. This unstable inversion of the temperature value contrasts the natural stratification of the water, that depends on the density value. In this case the algorithm applies a mixing by joining all the neighboring nodes, in this way the nodes are mixed into an unique section with an homogeneous temperature. After the mixing, the equilibrium determined by the natural convection is reestablished and the sections temperature profile grows towards the tank top.

The tank time step

The tank governing equations are solved once per tank time step, that is a fraction of the plant one. The possibility of subdividing the plant time step, operation that can be done by the user at the beginning of the simulation, allows a better accuracy. The plant simulation time step, that is already a fraction of the building one, may be too big respect to the distance traveled by the forced motion of the fluid between two layers nodes, thus the so called *internal time step* should be used. The time step for the PCM equals the tank internal time step when the Euler implicit method is chosen; vice-versa the tank internal time step has to be sub-divided to obtain the PCM time step when the explicit Euler method is chosen, due to the method stability limit.

As deeply described in Chapter 2 and 3, the new component PCM enhanced tank can contain several PCM modules. The code that had to be implemented to carry on the research simulates the PCM performance and calculates the heat flux to be exchanged with the tank water. The implementation had been done putting a particular care into the updating of the previously calculated PCM temperature, because the tank water temperature may be scaled to those of the previous time step if the plant time-step does not match the tank one. For the PCM no sub-cooling problems are treated, therefore the adopted model can only be used for those materials for which these phenomena can be neglected.

4.2.2 The implementation of the PCM modules in the tank component

The Figure 4.7 outlines the code for the simulation of a PCM enhanced tank with one or two coils. The right side summarizes the implemented new routines, the left side describes

the existing tank routines. The PCM routines are called by the tank calculation routine, or rather the routine that execute the balance on the nodes described in Equation (4.2.1). The call to the PCM routines is situated at the same location of the call to the routines for the calculation of the heat exchangers thermal flux. The PCM routines, like those of the heating coils, are called ones per tank time step. Vice-versa, the energy balance for the water layers (or sections) may be computed several times for a tank time step, until the mixing algorithm has defined the uniform temperature sections.

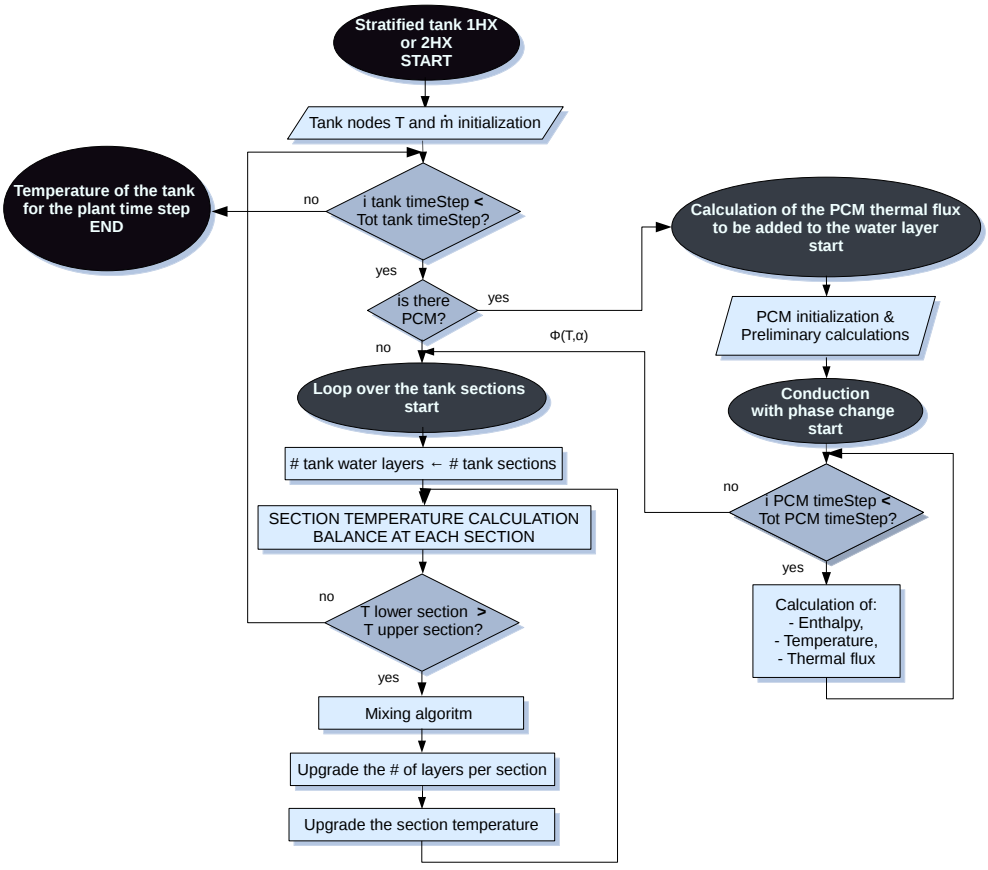

Figure 4.7: Flow chart describing the calculation of the PCM enhanced tank.

When the routines for the calculation of the tank are called, the PCM modules geometry initialization (see Subsection 3.1.2) and the geometrical feasibility test (see Section 3.2) has already been done. They are calculated, in fact, just once, that is when the PCM tank component is read for the first time.

If the Euler implicit scheme is chosen for the calculation of the PCM thermal flux, the time-step used for the PCM is those of the tank. In this case it is not need to sub-divide the tank time step because the same method is implicitly stable (see Chapter 3). When

the Euler explicit scheme is chosen for the PCM, the tank time-step is sub-divided in order to satisfy the stability condition; then the thermal flux obtained for each PCM time-step is then averaged in the tank time step. The PCM time-step is thus generally shorter than the tank one. The values obtained for the n PCM time-steps, in which the tank-time step is divided, is then averaged over the tank time-step. The thermal flux, that results from the energy balance applied on all the PCM cells, is then passed to the tank water layers where the PCM modules are located. To be more clear, refer to Subsection 3.1.3. If a module cell that stays on the border cylindrical surface is in contact with only one layer, the thermal flux $\phi_{i,1}$ is automatically assigned to the corresponding water layer; otherwise, if it is in contact with 2 layers, the thermal flux is divided into two contributes, one fraction is assigned to one layer, the other to the next one. The thermal flux that is assigned to each water layer is the sum of the contribution of all the cells pertaining to the same layer, multiplied by a "pertaining factor". The pertaining factor is calculated as the percentage of the cell area in contact to each water layer.

A flow-chart describing the implementation of the Euler explicit and implicit scheme and the managing of the PCM algorithms by the tank routine is reported at Figure 4.8 and Figure 4.9.

The implemented tank component, stored in the database of plant components, can be used and adapted to the user need (2 views of the code screen can be seen in Figure 4.10 and Figure 4.11).

4.2.3 An alternative approach to model the tank component

The premise exposed in this section introduces the possibility of modeling a plant component, such as a storage tank, through two alternative approaches. The first one is to model it as a plant component, specifying the product parameters and connecting it to the previous and following components. Its simulation is based on a sequential approach: as shown in the scheme reported in Figure 4.12, the output variables, calculated for the previous component, are the input variables assigned to the next. The plant is solved when the network convergence is assured, and this is obtained through an iterative solution. A considerable number of plant components is stored in the existing databases; each database component offers a series of parameters that can be modified by the user via graphical interface. The component and its manufacture details can be quickly modeled just filling out the form contained in the components database.

The potentiality of ESP-r allows to model a plant component in a much more specific and detailed way. A possible approach to describe the component in a very detailed way is to model the component as it was made of building construction/material elements. Choosing this method means performing the simulation of the component through a simultaneous approach. This modelization is very demanding, especially if the whole plant has to be modeled (using flow networks and suitable controls), but very useful to calibrate a model, in particular when the variables of the component are difficult to be represented through the first method.

The simulation of a PCM enhanced stratified storage tank, at the state of the art, can be carried out only with the second approach, modeling the hypothetical different layers through zones of a water network, the tank wrapper (steel and insulation) as

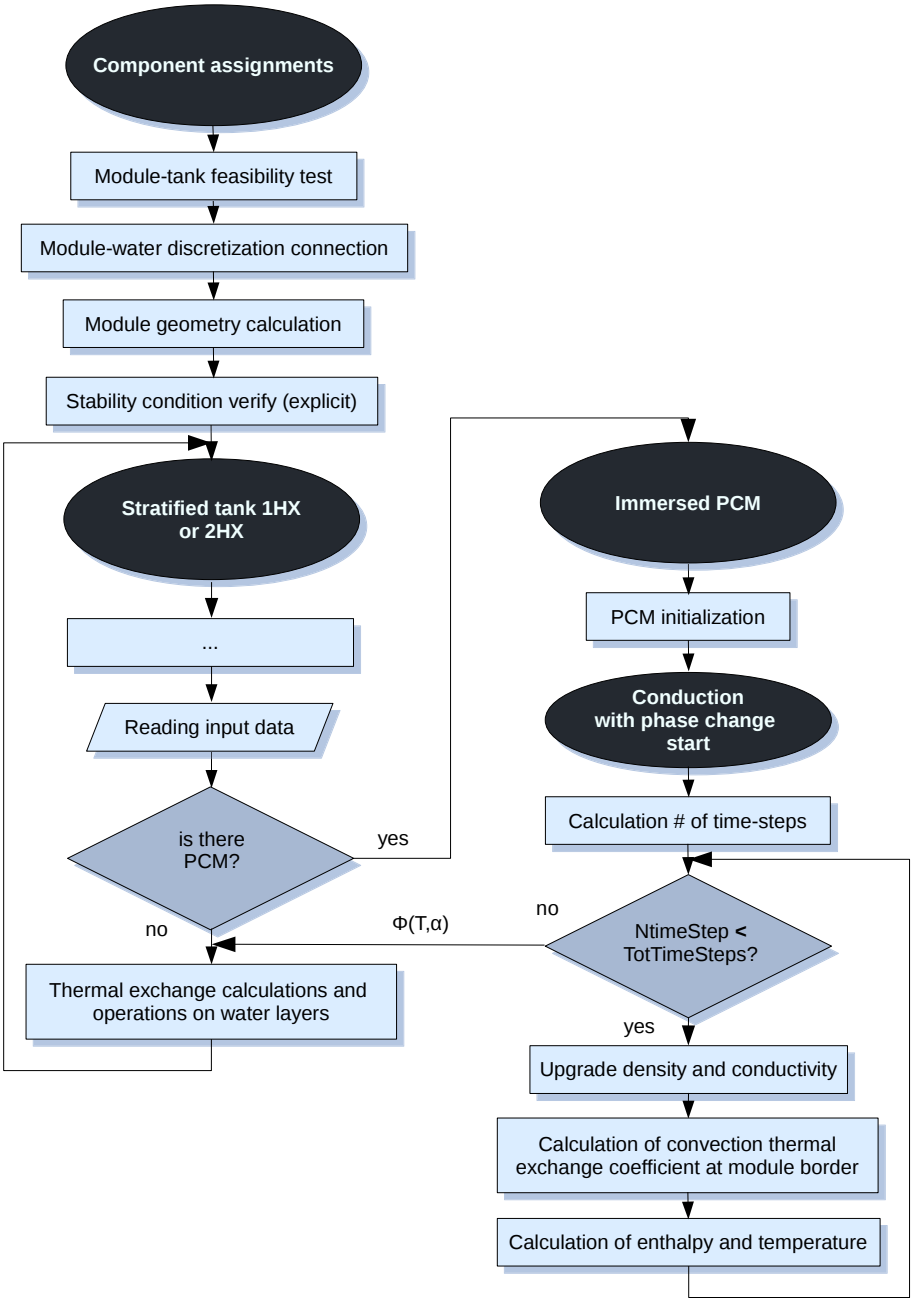

Figure 4.8: The Euler explicit scheme.

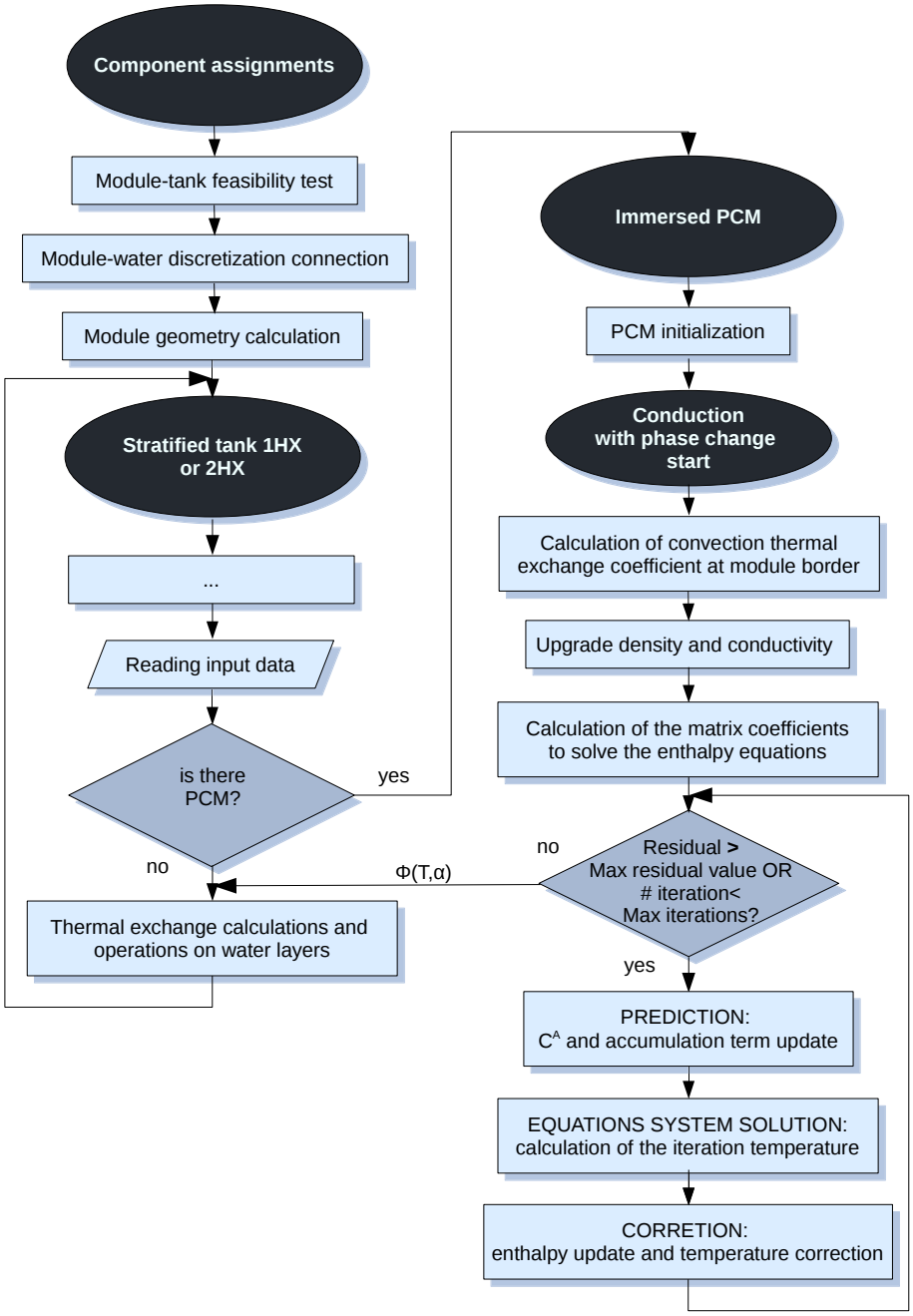

Figure 4.9: The Euler implicit scheme.

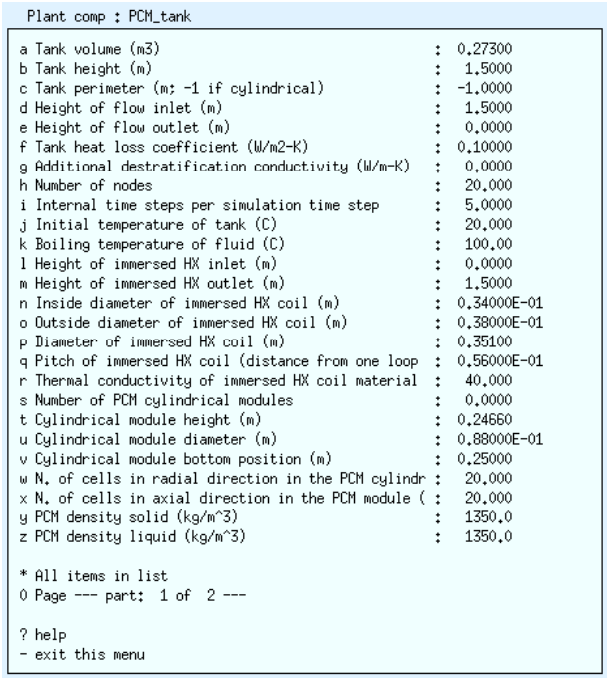

```
Plant comp : PCM_tank

a Tank volume (m3)                                    :  0.27300
b Tank height (m)                                     :   1.5000
c Tank perimeter (m; -1 if cylindrical)               :  -1.0000
d Height of flow inlet (m)                            :   1.5000
e Height of flow outlet (m)                           :   0.0000
f Tank heat loss coefficient (W/m2-K)                 :  0.10000
g Additional destratification conductivity (W/m-K)    :   0.0000
h Number of nodes                                     :   20.000
i Internal time steps per simulation time step        :   5.0000
j Initial temperature of tank (C)                     :   20.000
k Boiling temperature of fluid (C)                    :   100.00
l Height of immersed HX inlet (m)                     :   0.0000
m Height of immersed HX outlet (m)                    :   1.5000
n Inside diameter of immersed HX coil (m)             :  0.34000E-01
o Outside diameter of immersed HX coil (m)            :  0.38000E-01
p Diameter of immersed HX coil (m)                    :  0.35100
q Pitch of immersed HX coil (distance from one loop   :  0.56000E-01
r Thermal conductivity of immersed HX coil material   :   40.000
s Number of PCM cylindrical modules                   :   0.0000
t Cylindrical module height (m)                       :  0.24660
u Cylindrical module diameter (m)                     :  0.88000E-01
v Cylindrical module bottom position (m)              :  0.25000
w N. of cells in radial direction in the PCM cylindr  :   20.000
x N. of cells in axial direction in the PCM module (  :   20.000
y PCM density solid (kg/m^3)                          :   1350.0
z PCM density liquid (kg/m^3)                         :   1350.0

* All items in list
0 Page --- part:  1 of  2 ---

? help
- exit this menu
```

Figure 4.10: PCM-tank input data.

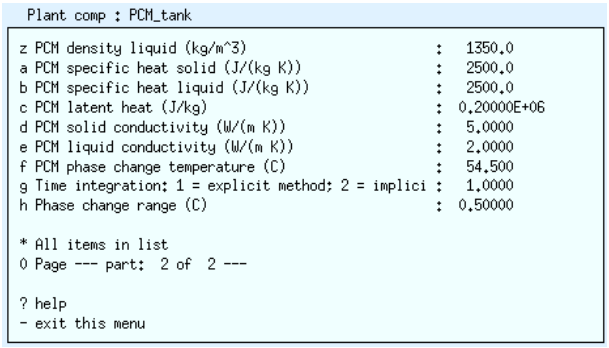

```
Plant comp : PCM_tank

z PCM density liquid (kg/m^3)                         :   1350.0
a PCM specific heat solid (J/(kg K))                  :   2500.0
b PCM specific heat liquid (J/(kg K))                 :   2500.0
c PCM latent heat (J/kg)                              :  0.20000E+06
d PCM solid conductivity (W/(m K))                    :   5.0000
e PCM liquid conductivity (W/(m K))                   :   2.0000
f PCM phase change temperature (C)                    :   54.500
g Time integration: 1 = explicit method; 2 = implici  :   1.0000
h Phase change range (C)                              :  0.50000

* All items in list
0 Page --- part:  2 of  2 ---

? help
- exit this menu
```

Figure 4.11: PCM-tank input data.

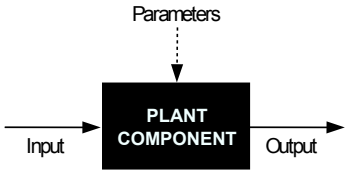

Figure 4.12: ESP-r component.

"building fabric", and finally applying "active materials" connotations to the inertial mass representing the inserted PCM. The PCM material is indeed already implemented in ESP-r, but it can be used only for the building simulation: the PCM technical parameters (such as density, conductivity, specific heat capacity and latent heat) can be assigned to particular nodes of the fabric, specifying the percentage of the building layer characterized by the phase change data.

The simulation and the optimization of the SDHW plant chosen for this research would have been a hard and challenging work if a new plant component reproducing a PCM tank had not been implemented. However a building modelization to calibrate the PCM tank component had been carried out and a cooling down test had been performed. This is reported in Subsection 6.3.

4.2.4 The solar collector

The description of the component is taken from the component documentation cited at [51]. The solar panel chosen for the plant simulation is the ESP-r component 84, that is a simplified flat solar collector modeled through 1 node. To this node, that is connected to the second tank coil through some pipes an a pump, is assigned the temperature value of the water flowing out from the panel. The equation calculating the node temperature is reported in Equation (4.2.2)

$$M\bar{c}\frac{\partial T_k}{\partial t} = -\dot{m}c_p(T_k - T_j) + \eta_{0,out}AG - \eta_{1,out}A(T_k - T_a) \tag{4.2.2}$$

where k denotes the solar collector node and j the node of the component that is backwards connected to it; *out* stands for outlet, a for air. M is the collector mass, $\bar{c}$ is the collector mass weighted average specific heat capacity, T is the node temperature, t is the time, $\dot{m}$ is the water-glycol flow rate throw the collector, c_p the collector fluid specific heat capacity, A is the gross collector area and G is the solar radiation incident upon the collector. $\eta_{0,out}, \eta_{1,out}$ are parameters characteristic of the panel. The scheme that has been described is reported in Figure 4.13: the finite volume on the left represents the collector pump, those on the right represents the collector one. To each finite volume is assigned a node. These two nodes are connected together, and linked to the third tank node, or rather the second tank coil, as shown in Figure 4.6. Obviously in the adopted connections web the mass diversion ratio [-] R=1.

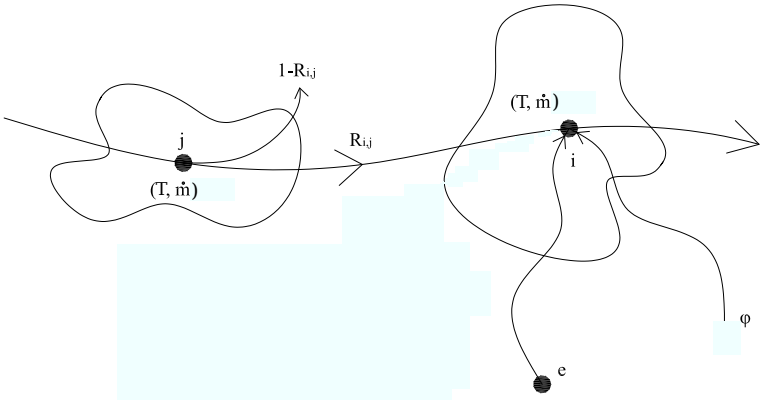

Figure 4.13: Solar collector node and connection.

The collector efficiency is calculated with Equation (4.2.3). To define the efficiency, the coefficients values η_0,η_1,η_2, that are respectively the constant (-), linear [W/(m^{2}C)] and quadratic [W/(m^{2}C^2)] coefficients of efficiency, have to be specified. These parameters characterize the collector and are generally reported on the commercially available products details.

$$\eta = \eta_0 - \eta_1 \frac{\Delta T}{G} - \eta_2 \frac{\Delta T^2}{G}; \tag{4.2.3}$$

In Europe ΔT corresponds to the difference of the air temperature T_a and the average of the collector inlet and outlet temperature [4] , as reported in Equation (4.2.4)

$$\Delta T = (T_{in} + T_{out})/2 - T_a \tag{4.2.4}$$

Equation (4.2.2) can be written as function of the inlet temperature and becomes:

$$M\bar{c}\frac{\partial T_{out}}{\partial t} = -\dot{m}c_p(T_{out} - T_{in}) + \eta_{0,in}AG - \eta_{1,in}A(T_{in} - T_{env}) \tag{4.2.5}$$

where *in* stands for inlet. With opportune rearrangements it can be written as:

$$M\bar{c}\frac{\partial T_{out}}{\partial t} = -\left(\dot{m}c_p - \frac{A\eta_{1,avg}}{2}\right)(T_{out} - T_{in}) + \eta_{0,avg}AG - \eta_{1,avg}A(T_{out} - T_{env}) \tag{4.2.6}$$

that is the linear collector efficiency equation and identifies the linear efficiency coefficient. The quadratic collector efficiency equation refers to the following Equation (4.2.7)

$$\eta = \eta_0 - (\eta_1 + \eta_2\Delta T)\frac{\Delta T}{G} \tag{4.2.7}$$

ΔT is calculated iteratively because of the non linear nature of Equation (4.2.7).

The parameters chosen for the adopted collector are summarized in Table 4.1. The reported values are those chosen for the collector in the plant simulation. where A_{coll}

[4]European test results generally use the average collector temperature, while the North-American ones are often reported in terms of inlet temperature.

Table 4.1: Solar collector parameters.

DESCRIPTION	VALUE
A_{coll} (m^2)	4.4
η_0 (-)	0.819
η_1 ($W/(m^2K)$)	3.125
η_2 ($W/(m^2K^2)$)	0.022
$\dot{m}_{test}$ (kg/s)	0.200
β (deg. from horizontal)	30
δ (deg., N=0)	180
μ_{gly} (%)	50
m_{coll} (kg)	80

is the collector surface, η_0, η_1, η_2 are, respectively, the constant, linear and quadratic coefficients of efficiency, $\dot{m}_{test}$ is the collector test flow rate, β is the collector slope (degree from horizontal), δ is the collector azimuth (degree N=0, E=90), μ is the mass fraction of propylene glycol, M_{coll} is the mass of collector; *coll* stands for collector and *gly* stands for glycol.

4.2.5 The boiler

A modulating condensing boiler had been added to the solar plant in order to provide a backup source of energy to maintain the tank set-point temperature when the solar collector is not enough. The boiler characteristics are summarized in Table 4.2, which lists also the normalized boiler efficiency performance parameters used in Equation (4.2.8), where r stays for return and f_L is the boiler fractional load factor [%]. The reported values are those chosen for the boiler in the plant simulation.

$$\eta_b = a_0 + a_1 \cdot T_r + a_2 \cdot f_L + a_3 \cdot f_L \cdot T_r \tag{4.2.8}$$

Table 4.2: Boiler parameters

DESCRIPTION	VALUE
$\dot{V}_{gas}$ (m^3/s)	3.73E-003
$H_{0,gas}$ (J/m^3)	3.50E+007
$T_{b,max}$ (°C)	65
$f_{b,min}$ (%)	10
a_1 (1/K)	0.353
a_2 (-)	141.45
a_3 (1/K)	-2.333
a_0 (-)	75.076

$\dot{V}$ is the full load gas firing rate, H_0 is the gas heating value at STP, $T_{b,max}$ is the

upper boiler temperature limit, $f_{b,min}$ is the lower limit of total differential, and the a are the coefficient for efficiency equation characterizing a commercially available boiler. b stands for boiler, gas is referred to the adopted fuel, that is methane.

4.2.6 The by-pass

To maintain the tank outlet DHW temperature at about 40°C a bypass had been added connecting the tank outlet and inlet pipe. This device lowers the temperature of the hot water by mixing a flow rate at 15°C, that is from the mains. A three node water flow diverger with control component had been used to connect the bypass pipe to the tank inlet pipe: the first node represents the fluid at the first outlet (pipe to the tank), the second represents the fluid at second outlet (by-pass pipe), while the third node represents fluid at inlet (pipe from the grid). An equi-percentage law had been assigned to the three-way valve: the percentage of the opening varies between 0 and 1, where 1 indicates that no flow through the bypass is allowed, as described in Subsection 4.2.8. A simple convergence, that is a single node component, is used to connect the other end of the by-pass pipe to the outlet pipe.

4.2.7 The user side: the DHW demand

The DHW demand is taken out from the ESP-r component n° 88 "water hourly draw profile". The graph shows two picks, the first one in the late morning, the second during the evening. It could be feasible for a typical family of 4 people (approximately 240 liters per day): during the morning a consistent draw is spilled for the habitual works of the housewife, while in the evening the people take a shower.

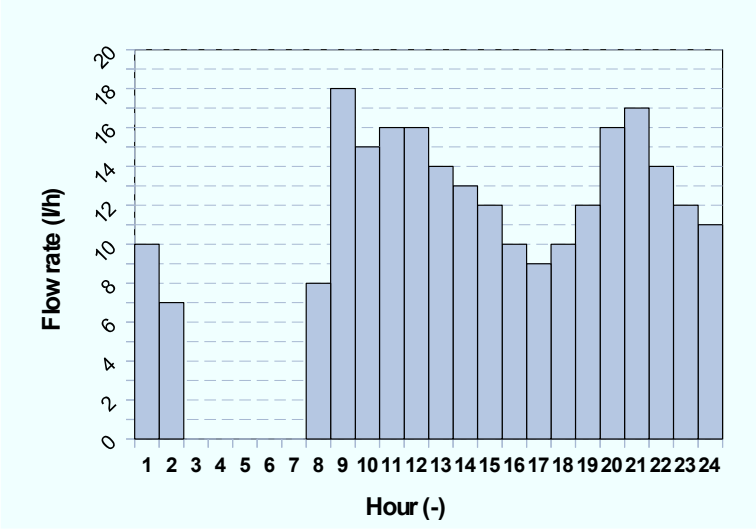

Figure 4.14: DHW flow rate profile for a family of 4 people.

4.2.8 The controls

The control on the solar collector pump is regulated by the difference between the collector temperature and the temperature at the middle height of the tank water. To find this last value a node had been added to the tank, exploiting the adaptable structure of the tank. When the difference is higher then 5 K the flow is activated through the pump and it is deactivated when it falls below 1 K. Advanced control logics had not been adopted because the objective was to simulate a plant standard installation: the PCM tank had been intended as simple replacement of a currently commercially available tank in standard installations.

The boiler operation is controlled by a sensor located in the tank that activates the boiler pump when the DHW outlet temperature from the tank falls below 45°C and deactivates it when the temperature rises over 55°C, while the flow rate is 4.5E-05 m^3/s.

The equi-percentage control relating to the three-way valve makes the flow capacity increased exponentially with valve trim travel. With such component and its relative control equal increments of valve travel are associated to equal percentage changes in the existing control valve. The control consists in the following formulation:

$$\frac{m_1}{m_{max}} = e^{XN\cdot(x-1)} \tag{4.2.9}$$

The output percentage vary between 1.0 (bypass closed) - when the tank outlet water is at 40°C - and 0.606 - when the tank outlet water is at 70°C.

To calculate the value of 0.606 the following balance on the convergence node had been evaluated: Figure 4.15 reports a detail of Figure 4.5.

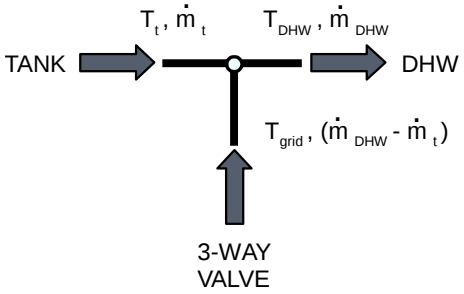

Figure 4.15: Balance on the convergence node.

$$\dot{m}_{DHW}\cdot T_{DHW} = \dot{m}_t\cdot T_t + (\dot{m}_{DHW} - \dot{m}_t)\cdot T_{grid} \tag{4.2.10}$$

In the first term $\dot{m}$ is the mass flow rate to be send to the users (DHW), in the second it is those spilled from the tank (t) and in the third it is referred to the water flowing through the pipe connecting the 3-way valve to the convergence. T_{grid} is the temperature of the water coming from the grid, T_t is the tank outlet temperature, T_{DHW} is the temperature of the water to be sent to the users. The value of x reported in Equation (4.2.9) is

calculated in Equation (4.2.11):

$$x = \frac{\dot{m}_t}{\dot{m}_{DHW}} = \frac{T_{DHW} - T_{grid}}{T_t - T_{grid}} \tag{4.2.11}$$

It means that the 3-way valve modulates between the 2 temperature values. A first approximation value for x is calculated assuming T_{grid}=15°C and T_{DHW}=40°C, for a tank water temperature of 40°C x=1, while for a tank water temperature of 70°C x=0.4545. Then, substituting the value of x=0.4545 in the Equation (4.2.9) and choosing a value of 2 for XN, it results:

$$x = \frac{ln0.4545}{2} + 1 \tag{4.2.12}$$

and a value of 0.606 for the minimum output had been found.

The graph reported at Figure 4.16 reports the temperature/flow rate ratio for the chosen equi-percentage valve.

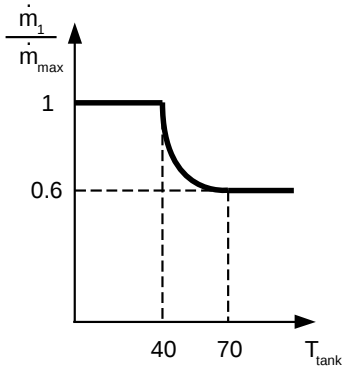

Figure 4.16: Graph of the temperature - flow rate ratio for the chosen equi-percentage valve.

4.2.9 The primary energy consumed

The boiler gas consumption [l/s] is given as output of the simulation for each plant time step, that is 1 minute. The simulation is made for one year period, therefore, known $\dot{V}$, the consumed gas flow rate and H_0, that is the gas heating value at STP [J/m^3], the primary energy consumption, Q, is straightforward calculated.

$$Q = \int_{year} \dot{V}_{gas} \cdot H_0 dt. \tag{4.2.13}$$

4.3 The climatic data

As suggested by the acronym, in a SDHW system the solar influence to the plant plays a prominent role in determining the efficiency of the plant, together with the efficiency

of the storage and the water draw demand. The locations assumed for the simulations are situated in Italy: Rome and Trieste were chosen for their different latitude and thus solar irradiation. The climatic data were obtained from a public domain databases, which is managed by the ASHRAE[5] [52] to consent the design and simulation of HVAC and dehumidification equipment for several sector of production. It includes climatic information for 6443 locations around the world, included the parameters to calculate clear-sky radiance. Other included data are the dry-bulb, wet-bulb, and dew-point temperatures; the wind speed with direction at various frequencies of occurrence; the monthly degree-days to various bases and the precipitations. This database is based on the Italian Gianni De Giorgio (IGDG) one [53]. De Giorgio based his data on the Thermal and Nuclear Research Center of ENEL[6] (CRTN), who elaborated the air temperature for each month calculated through the mean and the variance of the values registered in a range of 19 years (1951-1970). Moreover it collects the hourly total and diffuse irradiation calculated in function of the daily total and diffuse irradiation. The diffuse irradiation is calculated with the formulation developed by Y.Liu and Jordan [54], assuming that the ratio between the hourly diffuse solar irradiation on the horizontal plane and the daily diffuse irradiation can be approximated through the ratio between the irradiation on the horizontal plane, considered constant for an hour, and the daily irradiation on the same plane in absence of atmosphere. The hourly total irradiation is calculated as function of the daily total irradiation and several graphs have been produced to represent this relationship by assuming the daily distribution is symmetrical around the solar noon[7].

[5] American Society of Heating, Refrigerating and Air Conditioning Engineers

[6] National Agency for Electric Energy

[7] The IGDG database contains also the wind velocity at 10 m height from the ground, the air relative humidity, and the number of hours and tenths of an hour of sunshine that occurred throughout the day.

5

Optimization problem

5.1 The optimization analysis

All the optimization analysis described in this thesis had been carried out with the commercial code modeFRONTIER®, developed by ESTECO [55]. A thorough description of the optimization problems is given by Ranut [56].

An optimization problem is the issue of reaching the best result under given circumstances or rather the process of identifying the conditions which lead to the maximum or minimum value of one or more *objective function*, $f(\mathbf{x})$. In other words it can be seen as an evaluation criterion that compares different results and selects the best alternative.

To obtain acceptable solutions the *design parameters* (or *variables*), collected in the vector $\mathbf{x} = \{x_1, x_2, ..., x_n\}^T$, must satisfy the *design constraints*, f.i. *geometric constraints*, that are restrictions defining the solutions feasibility. A constraint is generally defined by a function $g_j(\mathbf{x}) = 0$. The *design space* is the n-dimensional Cartesian space having, as coordinate axes, the design variables x_i with i=1,...,n. In this way a *feasible space* is automatically defined and the feasible solutions are defined for $g_j(\mathbf{x}) < 0$

An optimization characterized by a single objective function is called *mono-objective* optimization, while those characterized by more than one objective function is a *multi-objective* one.

5.1.1 Mono-objective optimization

In a mono-objective problem at least one solution $\mathbf{x}^*$ exists in the feasible space which corresponds to the minimum objective value, and it is identified by the *optimum solution*. It can be mathematically expressed as:

Find	$\mathbf{x} = \{x_1, x_2, ..., x_n\}^T$	
which minimizes	$f(\mathbf{x})$	
subjected to	$g_j(\mathbf{x}) \leq 0 \quad j = 1, ..., m$	– functions of the inequality constraints
	$l_j(\mathbf{x}) = 0 \quad j = 1, ..., p$	– functions of the equality constraints
such that	$\mathbf{x}^{min} \leq \mathbf{x}^* \leq \mathbf{x}^{max}$	

5.1.2 Multi-objective optimization

In the Multi-objective problems the design variables, that have to be contemporary optimized, can be concurrent, and the objectives can be in conflict each others. Since it is impossible to identify a single set of parameters, or *solution*, that is optimal for all objectives simultaneously, the algorithm points out a series of optimal solutions that are aligned on the *Pareto frontier*. The Pareto frontier is a graph that collects all the parameter sets that are *non-dominated* by any other solution, or rather optimal in the sense of Pareto. If A and B are two designs, A dominates B if the design A is better then B at least in one purpose, while for others they might be equal:

$$A >_P B \Leftrightarrow (\forall i \, F_i(A) \geq F_i(B)) \cap (\exists j : F_j(A) > F_j(B))$$

This concept, graphically shown in Figure 5.1, can be mathematically expressed as:

$$\begin{array}{lll} \text{Find} & \mathbf{x} & \\ \text{such as} & f_i(\mathbf{x}) \quad i = 1, 2, ..., n_{obj} & \text{is a minimum} \\ \text{subjected to} & g_j(\mathbf{x}) \leq 0 \quad j = 1, ..., m & -\text{constraints} \\ & l_j(\mathbf{x}) = 0 \quad j = 1, ..., p & -\text{constraints} \\ \text{such that} & \mathbf{x}^{min} \leq \mathbf{x} \leq \mathbf{x}^{max} & \end{array}$$

where *obj* stays for objectives.

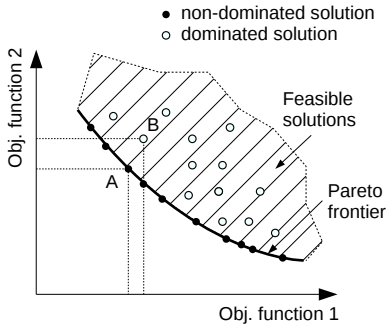

Figure 5.1: Minimization of two objective functions, f_1 and f_2: the Pareto frontier.

5.1.3 Optimization algorithms

The optimum solutions of the problem are pointed out through *classical* or *evolutionary* algorithms.

The first ones generally use a point-by-point approach and a deterministic procedure: one solution is updated to a new one in one iteration, starting from a random guessed solution and choosing a direction to proceed, following a pre-specified transition rule. The direction method is the connotation that differentiate the various classical algorithms.

A further classification divides the classical optimization methods, that are deterministic, into *direct search* and *descent* (or gradient) ones. In the first ones the only objective functions (and often the constraints) are used to guide the search strategy and they do

not need the partial derivatives of the function for the optimization to carry on. For this reason they are called zeroth-order methods. To cite one direct search method, the Nelder-Mead Simplex one is suitable for simple problems described by few variables [1]. In the gradient-based methods the search process is driven by the first and/or second-order derivatives of the objective function and/or constraints, in other words they use the objective function gradient as a direction of descent.

The classical methods are usually slow because derivative information is not used and, so, require several functions evaluations to converge. The gradient-based methods quickly converge to an optimal solution, but are not efficient in non-differentiable or discontinuous problems. The stochastic *evolutionary methods* have no strong mathematical basis and are direct search procedures[2]. Their algorithms are generic and represent robust search methods grounded on the analogy of the evolution theory. The main drawback of using the evolutionary algorithms is the large computing time, that is caused by the objective function value evaluation, but it can be mitigated by the parallel calculation.

The evolutionary algorithms are grounded on a population-based approach: the initial population is iteratively updated to evolve in a new population. The next population is generated through four main operators: the selection, the crossover, the mutation and the elite-preservation. The number of the population individuals needed by the algorithm depends on a numbers of factors related to the number of the designs variables, the complexity of the problem and others. As suggested by Ranut [56], for the Nondominated Sorting Genetic Algorithm (NSGA-II) described in Subsection 5.1.4, an acceptable number of individuals for the initial population could be identified as:

$$n.initial = n.variables \cdot n.objectives \cdot 2 + 1$$

5.1.4 Genetic algorithms

Among the Evolutionary methods, the most popular are the Genetic Algorithms (GAs), initially developed by Holland and De Jong, in 1975. A GA is an iterative optimization process handling a set of solutions (called *population*) for each iteration. The design solutions $\mathbf{x} = (x_1, x_2, ..., x_n)$ are also known as *individuals* and x_i are their design parameters. The *gene* corresponding to each individual is made up by several *chromosomes* $x_1, x_2, ..., x_n$, and each chromosome, that corresponds to the design variable in the optimization process, can be represented either as a real number (floating-point-coded GA) or as a string of bits (binary-coded GA). The analogy with the Darwinian evolution is and will appear clear.

The search begins from a population that may be generated by a Design of Experiments (DoE) method (see Section 5.1.4). The GA processes the entire population and can potentially explore the whole search space avoiding local optimal points. The three

[1] In the Simplex algorithm, if n are the real variables, the $n + 1$ vertexes ($\mathbf{x}_0$,$\mathbf{x}_1$,...,$\mathbf{x}_n$) representing the objective function values are compared and the better point moves gradually towards the optimum during an iterative process: if an optimization of 2 variables is considered, thus a triangle is formed, the algorithm replaces at each step the vertex with the highest function value with an other having a better value for the objective function, moving towards the optimum. The movement proceeds through reflection, expansion and contraction operations.

[2] They do not employ any gradient of the objective function.

operators - selection, crossover and mutation - are applied to update the population, or rather to carry out a new *generation*, until a termination criterion is satisfied.

The individuals defining a population can be identified as the *parents*, that are the individuals able to reproduce themselves and the *offspring*, that are the individuals of the following generation, generated by the parents. Finally, the *elite* represents the currently non-dominated individuals. An individual can contemporary be part of different groups. All the individuals are characterized by their capacity of surviving, known as *fitness* level: the fitness value depends on the values of the objective functions.

The *selection* is the first operator applied on the population, that simulate the Darwinian law of surviving for the most fitting individuals: in the case of a proportional selection, f.i., the fitness of an individual determines the probability he has to be chosen with a proportional law. The individuals above-average have more possibility to be selected. At this stage none new solution is created: the next stage (operator) provides to do it. The new offspring will be the result of the combination of two parents chromosomes or a copy of one of them, called *survival*. In the first case, the suitable combination of chromosomes is handled by variation operators to create better individuals.

The second operator employed is the *crossover*: it rises up the individuals diversity by randomly extracting two individuals from a generation and exchanging portions of the genes between them. The process used by this operator to exchange the genetic material between two individuals is summarized in two steps: firstly it cuts the DNA at a random location, and successively it pasts together the opposite segments that belong to the different individuals. The offspring solutions generated through this operator have not necessarily a better fitness than the parents, but the possibility to carry out better solutions is far higher than the a random choosing. If individuals with a better fitness are created, they will be picked up in several copies by the selection operator.

Finally the *mutation* operator produces a random change in the chromosomes, to simulate casual transcription errors that may happen with low probability.

In the evolution the best solutions are maintained by the *elitism operator*, that promotes the solution convergence. It simply copy a part of the best individuals of one generation to the next, while the rest of the offspring is created by the usual cited operators applied on all the individuals of the generation. The best offspring is not just passed between 2 generations, but also employed to create the following generation.

Together with their robustness, an advantage of the genetic algorithms is that, even if some evaluations fail, they are able to iterate further.

To conclude, lots of acceptable designs are produced by algorithms starting from one or some random solutions in the search space; then, the best alternative is/are searched in the feasible region on the basis of the objective function.

NSGA-II

The Nondominated Sorting Genetic Algorithm NSGA-II, conceived by N. Srinivas and K. Deb, has been improved by Deb et al. [57] and the NSGA-II has been developed. This is now considered the state-of-the-art for general purpose GAs. It is a standard binary-coded GA for the multi-objective optimization that uses, beyond the peculiarity of

an NSGA of emphasizing the non-dominated solutions, an elitist principle and an explicit diversity preserving mechanism.

The algorithm writes the chromosomes corresponding to the design variables through string of bits (it is a binary-coded GA).

The structure of the algorithm and its procedure to optimize the problem is deeply detailed in [57].

At each iteration two kinds of sorting are applied: at the first stage the solutions are collected in sub-groups (*fronts*) according to Pareto dominance; then the solutions are sorted for each front by an operator that promotes the individuals situated in the scarcely populated areas of the objective space (*crowding distance operator*).

Design of Experiments

The DoE is a methodology conceived by Fisher in the 1920s to explore the design variable space: its aim is to offer the widest knowledge for an assumed set of data. The DoE provides an optimization algorithm to create an initial population, but also can furnish a suitable set of solutions for a sensitivity analysis, to point out the input parameters mainly affecting the experiment.

The variables of the problem are simultaneously handled and more than one is made changed at the same time. The initial sample of experiments can be chosen through different methodologies, among them the most common are the Random and the Sobol techniques, that cover the design space by using a random definition of numbers.

Using a Sobol technique the number of designs fills uniformly the design space, while a Random technique causes more evident clustering effects. Figure 5.2 graphically reports the typical distribution of the designs.

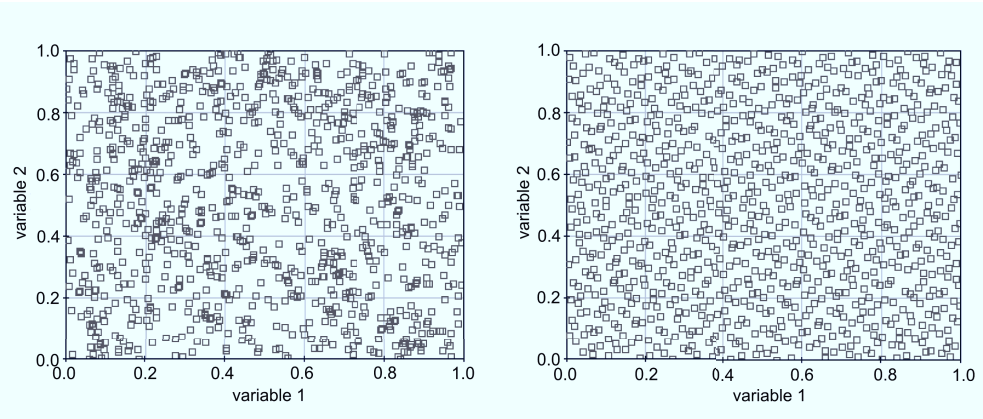

Figure 5.2: Random (on the left) and Sobol (on the right) space filling.

5.1.5 The performed optimization

The more water is contained in the tank, the more storage is established and the less energy consumption is demanded to provide the water at the set-point of 40°. Of course, and this is true in particular for the low- and ultra-low energy buildings, it is not always possible to have much space available, where to put a big tank. For this reason the reduction, or, at least, the restraint of the tank volume is considered as a crucial aspect. Therefore, the space occupied by the tank, that is the tank gross volume (insulation included), has to be minimized. To consider also this design target and enlarge the inspection of the optimal tank, it is necessary to perform a multi-objective optimization.

The simulations of the typical SDHW plant, that had been carried out with the ESP-r tool, were then managed by modeFRONTIER®. The initial population for the optimization process had been generated with a Sobol space filler, than two kinds of analysis had been performed.

To understand the effect of the PCM in the simulated plants it is useful to consider various analysis. A mono-objective analysis can answer to the question if it is possible to reduce the consumes of the plants just inserting PCM, in variable measure, into the storage tanks. A multi-objective analysis can specify if it is possible to obtain better results, taking into account also the space occupied by the tank. Finally a third optimization analysis is required to understand if the the best results obtained with a PCM tank are comparable with those obtainable using an optimized traditional tank.

For the mono-objective analysis the Simplex classical direct search algorithm can be chosen for its simplicity and facility to converge towards the solution; for the multi-objective analysis the NSGA-II genetic algorithm can be chosen for its robustness.

6

Tank preliminary analysis

6.1 Analysis on a traditional tank

The aim of this chapter is to focus on the working of the storage tanks. This is a preliminary analysis that had been fulfilled using several tools. The codes used to perform this study were a CFD simulation tool, ANSYS CFX®, and an optimization tool, modeFRONTIER®. These softwares had been somehow coupled with ESP-r and the results obtained from the simulations had been compared with the experimental data.

A first example of results comparison is a parametric analysis carried on a traditional tank: this is reported in the next Subsection.

In this test the experimental data, realized by the Italian national research council, Consiglio Nazionale delle Ricerche (CNR), had been compared to the simulation results. For this analysis the software ESP-r had been coupled with modeFRONTIER®. The optimization tool handles the simulation code until the parameter, that performs the solution more proximal to the experimental data, is identified. This is a useful analysis that can be used also as method to identify an hypothetical missing parameter of a given problem. The method, in fact, is based on a comparison among the system performance. In the case described in 6.1.1 the parameter to be identified is the tank U-value.

A second test has then been performed to understand the actual fluid dynamic in a water tank. To fulfill it, a CFD simulation had been realized: it can reproduce some phenomena that can not be considered with a 1-D analysis. A 1-D analysis is a suitable approach to reproduce a complex system performance regarding a long period: the calculation time is relatively short because the discretization of the model is based on few nodes (for example, referring to Subsection 4.2.1, the water nodes of the ESP-r tank component can vary from 1 to 100). If a CFD approach is adopted, the Navier-Stockes equations are applied on each CV in which the device is discretized[1]. Therefore, for the same simulation time, the time to carry out a CFD analysis is much longer. The first kind of simulation can not catch and reproduce some local phenomena, but can do it quickly. Vice-versa, a CFD simulation can reproduce the local dynamic of the fluid and can simulate the performance of the system, but requires a longer computational time.

[1] As reported in the Sub-subsection 6.1.2, the number of nodes adopted in the CFD analysis is much higher.

A CFD analysis helps to understand the ESP-r results through the simulation of simple problems. For example, some tests carried on with a CFD simulation tool can answer to questions like what kind of tank is better simulated by the ESP-r stratified tank routines. It allows also to answer to the following questions: What is the impact of a deflector on a cooling down test? Do the ESP-r routines catch at best the performance of the cooling down of a tank provided or not by a deflector? Can the difference in the performance be ascribed also to the *mixing algorithm* implemented in the existing model (see 4.2.1)?

Also the experimental data relative to this test had been carried out by the CNR: its results had been used to compare and discuss the simulation results. In particular, the temperature and flow rate values of the experimental test had been used as input data for two different numerical representations with the same dynamic: the 1-D problem had been carried on with the ESP-r simulation tool, the 3-D simulation had been performed with ANSYS-CFX®[58].

The design of the tank is shown in Figure 6.1.

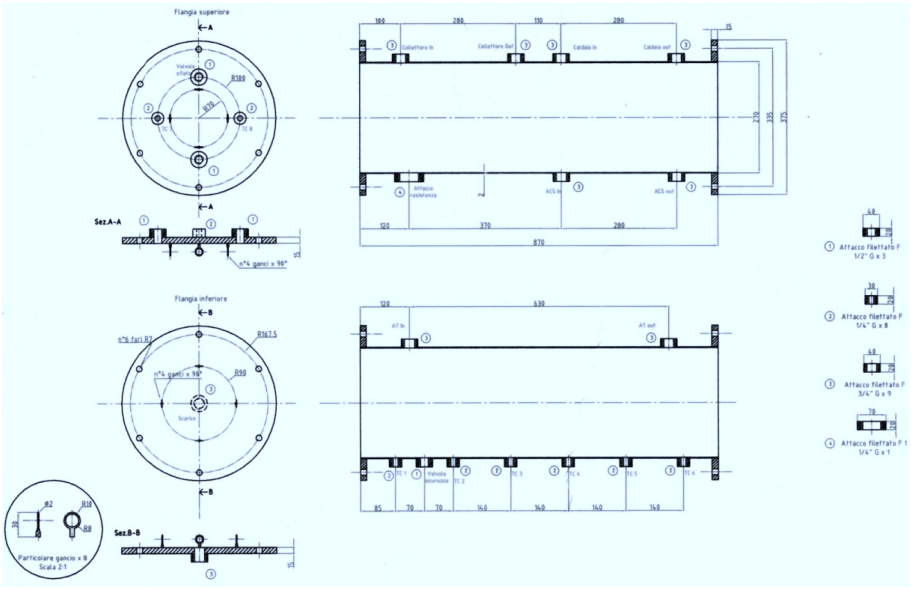

Figure 6.1: Design of the tank used for the cooling-down test.

6.1.1 The cooling-down test

This Subsection describes the first test that has been previously introduced. The performed simulations that reproduced the first CNR experimental test were based on the cooling-down of the tank water: it had been previously warmed up to a temperature of about 70°C by means of an entering water flow, then it was leaved in a stand-by condition, at constant room temperature, until its temperature has been decreased to ~ 40°C.

The tank contains about 47.5 liters an its height is 0.87 m. The height of the flow outlet is at 0.75 m, while the height of the flow inlet is at 0.12 m from the bottom of the tank.

Handling the ESP-r simulations of the traditional tank with one coil (component # 103) through the optimization tool, it had been possible to identify the global mean U-value, identified as unique variable of the optimization problem. For the simplicity of the problem a SIMPLEX algorithm had been used. The optimization objective was the minimization of the standard error between the simulated output water temperature and its experimental value.

A plausible conductivity value of 0.04 W/(mK) had been assumed for the insulation material; fixing it, the U-value can be calculated with the known formulation:

$$U = \frac{1}{\frac{1}{\alpha_{ext}} + \sum_i \frac{S_i}{k_i} + \frac{1}{\alpha_{int}}} \tag{6.1.1}$$

where S is the thickness of the layers and k is the conductivity of the material; α_{int} and α_{ext} are the convection heat transfer coefficients at the external and internal side of the tank.

For the ESP-r simulations an uniform initial value of 70°C had been adopted for the water layers. A simulation of 1 day had been performed: for this problem it was not necessary to set a start-up simulation period since the output file data containing the temperature values was generated directly from the tank routine. The points where the temperature had been monitored are located at 0.225, 0.365, 0.505, 0.645 m height from the tank bottom (see Figure 6.2): in ESP-r a linear interpolation on the layers calculated the temperature at these precise points.

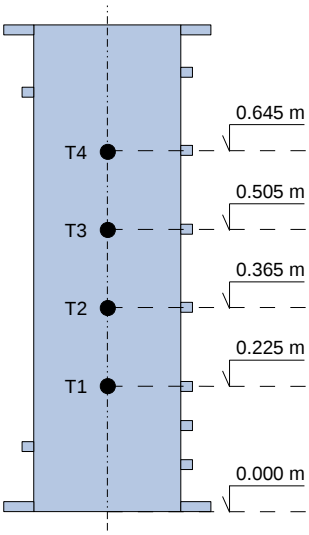

Figure 6.2: Sensor location for temperature monitoring.

Figure 6.3 reports the monitored temperature and the simulated temperature plot for the 4 surveyed points in the tank. The optimized tank, whose temperature values are reported here, is the tank whose performance is as similar as possible to the real tank one. The best simulated tank had an U-value of 2.7 W/(m^{2}K), that corresponds to the actual real value.

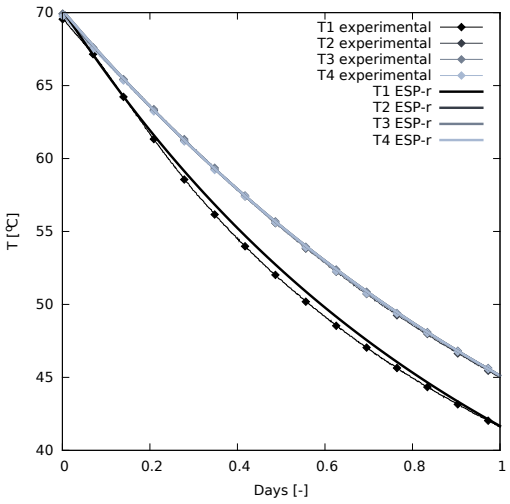

Figure 6.3: Experimental cooling-down test and simulation results.

6.1.2 A calibration test

The second experimental test consists of a continuous supply of hot water for a family house. The tank is charged up through a hot water inlet flow rate until an average temperature of about 70°C is reached, then it is discharged through a flow rate of 8-10 liter/min. The temperature of the hot water spilled by the tank is controlled by a mixing valve automatically set on 39°C. The test is stopped when the hot water temperature falls below 35°C. Thus, the test could be resumed in a charging and discharging phase. The monitored temperature refers to the 4 points in the tank cited in the previous Subsection.

In order to understand how precisely the ESP-r tank component described the reality, a CFD analysis had been performed. The simulation was aimed to understand the effect of a deflector surface added at the pipe side entering the tank, so 2 cases had been simulated, with and without deflector. Moreover, this analysis was aimed also to understand the effect of the water mixing in the tank, thus 2 further simulations, with and without mixing algorithm (see Subsection 4.2.1), had been performed.

To fulfill the CFD analysis, the tank had been modeled, meshed and simulated through two different softwares: its geometry and mesh were generated with ANSYS ICEM CFD®, the CFD simulation was performed with the ANSYS-CFX®code.

In ANSYS ICEM CFD®the symmetrical geometry had been meshed directly as non

structured and the following dimensions had been chosen for the grid. The maximum size selected for the cells located in the tank zones that did not need to be refined was 25 mm. The maximum width of the outlet and the inlet zone was 2 mm. As inlet zone has to be intended the area that included the inlet tube section entering the tank and the water volume inside the tank next to the inlet; in case that a deflector is included, it taken into account also the deflector. A total of 53021 nodes for the case with deflector was obtained. Figure 6.4 shows a mesh detail at the tank water inlet.

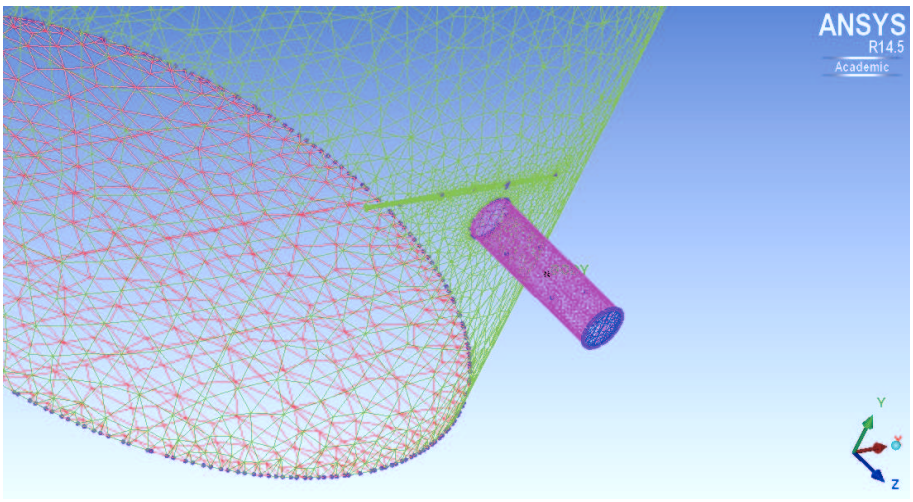

Figure 6.4: ANSYS ICEM CFD refined mesh.

To carry on the simulation with ESP-r a *tdf* (temporal definition file) had been employed. In this specific case, the *tdf* file reported the values of the temperature and the flow rate that has been experimentally monitored every second. These data had been assigned to the tank inlet water as control of the system. This kind of control permits to impose to the model some known dynamic variables. The minimal time-step for the simulations of plants is by default equal to 1 minute. For this simulation the plant time step was divided in 60 intervals to obtain a time step of 1 second; the *tdf* allowable maximum number of time-steps in an hour had been risen to 3600 values per hour.

Such a small time-step permitted to reproduce exactly the experimental test.

A water flow rate warmed up the tank water in about 7660 seconds. The simulation of the charging stage is not reported here: the next part of the Sub subsection covers the discharging test. In the discharging stage the water flow rate was 0.17 kg/s. It started around the 7830 second after the beginning of the charging, and was constant for the remaining part of the experiment. The following graphs report the inlet water the temperature plots.

The simulation of the charging stage was needed to assign the correct, non-uniform, temperature to the water layers: the lower layer, below the inlet position, for example, was not much affected by the entering water. If a charging-stage simulation had not been

performed, the simulation of the discharge stage would have started form an uniform tank temperature. This is the reason that prevented from starting the simulation on the basis of the only discharge data.

As shown in the plots reported in Figure 6.5 - Figure 6.11, in the first stage of the test the temperature of the inlet water is lower than the tank average temperature; then, the tank water cools down and, at a certain point, the inlet water is hotter than the tank one.

Considering the simulation results before the plateau, the slope of the temperature graph is quite representative of the reality for the lower layers. The more the abscissa increases, and the higher layers are considered, the more the temperature graph slope is dissociated to the experimental one.

This can be due to the mixing algorithm, that operates among too little time steps when the temperature of the inlet (lower position) water is higher than the temperature of the tank layers (higher position). For this reason it had been supposed that a better performance could be reached deactivating the mixing algorithm. To perform the correct stratification in the discharging phase the mixing algorithm, that is contained in the ESP-r $stratified\_tank\_calc$ routine, has thus been disabled in order to avoid the creation of mixed sections. The results had been compared with those of the case where the mixing is allowed. A comparison of the results is reported in Figure 6.5 and Figure 6.6. If the mixing algorithm is not computed and the creation of uniform sections is avoided, the representation of the cooling-down slope, before the plateau, is much more similar to the real case. In the same case, the ESP-r simulation graph shows also a peak in the water temperature, at the beginning of the plateau. This peak is more pronounced for the lower layers.

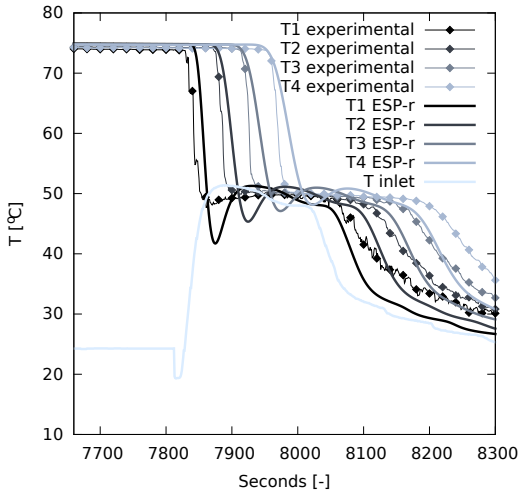

Figure 6.5: Discharge result comparison experimental - ESP-r, case no mixing.

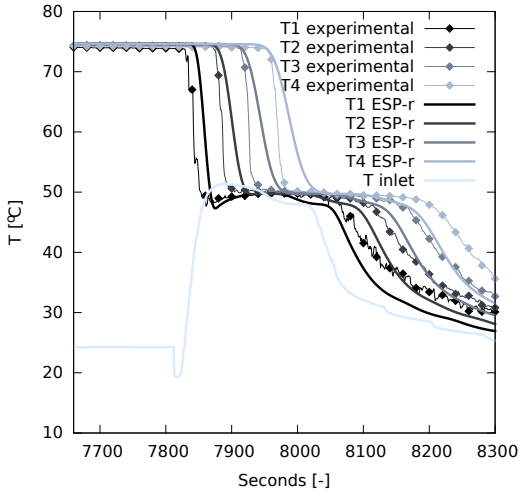

Figure 6.6: Discharge result comparison experimental - ESP-r, case with mixing.

The CFD transient analyses are very time consuming. For this reason, the simulation realized with ANSYS CFX®covered the only discharging phase. The temperature field obtained with ESP-r at the end of the charging phase, corresponding to those at the beginning of the discharging one, had been used as initial condition for the discharging simulation performed with ANSYS CFX®.

A transient analysis had been carried on for the cooling-down of the tank. It held over 485 s; a time-step of 0.1 s had been chosen. The water inlet flow rate experimental values had been used, also in this simulation, as input data.A boundary temperature of 22°C for the air surrounding the tank had been chosen and a heat transfer coefficient of 2.17 W/(m^{2}K) had been taken, in conformity with the optimized value pointed out in Subsection 6.1.1. The turbulence had been modeled with the shear stress transport method.

A high resolution scheme had been selected for the advection and the turbulence, a second order backward Euler transient scheme had been chosen and a value of 1e-5 had been adopted as residual target. The CFD simulation showed on the one hand the presence of vortices in the lower part of the tank, on the other hand the water tendency of stratifying. The turbulence of the water in the middle-high part of the tank was very low.

To better understand the water fluid dynamics in the tank, a comparison test has been carried out: its results show the water dynamics if a deflector would be present at the tank inlet. Figure 6.7 - Figure 6.10 plots the 2 cases performed with ESP-r, that are the case with and without the mixing, and the 2 cases performed with ANSYS CFX®, that are the cases with and without the deflector. Again the temperature refers to the 4 monitor points defined in Subsection 6.1.1. The abscissa axes report the time in seconds, the timing is referred to the duration of the entire test.

Inspecting Figure 6.8 - Figure 6.10 it results that, before the plateau, the temperature

plot in ESP-r reproduces better the CFD one where the deflector is included into the model.

This happens if the mixing algorithm is allowed. For these simulations also the peak is better reproduced. In the case with the deflector the temperature of the water in the tank after the plateau is much more uniform than in the case without deflector. Vice-versa, the temperature plot at the plateau obtained from ESP-r is more similar to those performed through ANSYS CFX in the case without the deflector. From the comparison between the CFD and the experimental results it appears that peak, or rather the sharp temperature drop and successive rise at the beginning of the plateau, is more marked in the case with the deflector. The deflector modifies the turbulence generated by the inlet water: this affects the water stratification, that is more marked in the case the deflector is present.

The results of the CFD analysis show that the deflector makes the temperature more uniform, in particular after the plateau. This effect can not be catch by ESP-r. Therefore, regarding the temperature graph after the plateau, ESP-r catch best the performance of a tank without a deflector. This happen for both the cases, with or without the mixing algorithm. On the other side the ESP-r simulations without the mixing algorithm can reproduce well the sharp temperature drop at the beginning of the plateau, that is more marked in the CFD results of the tank with the deflector.

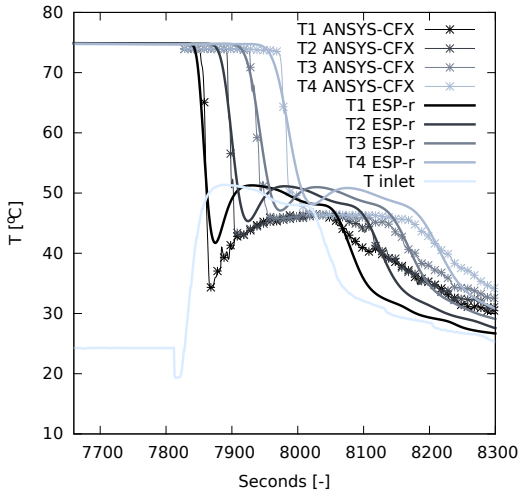

Figure 6.7: Discharge result comparison ANSYS CFX - ESP-r, case no mixing, with deflector.

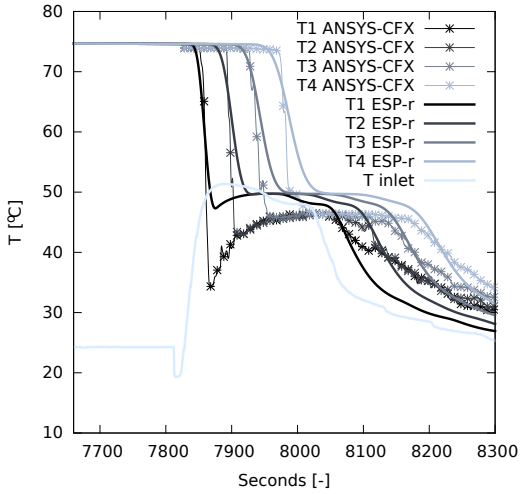

Figure 6.8: Discharge result comparison ANSYS CFX - ESP-r, case with mixing, with deflector.

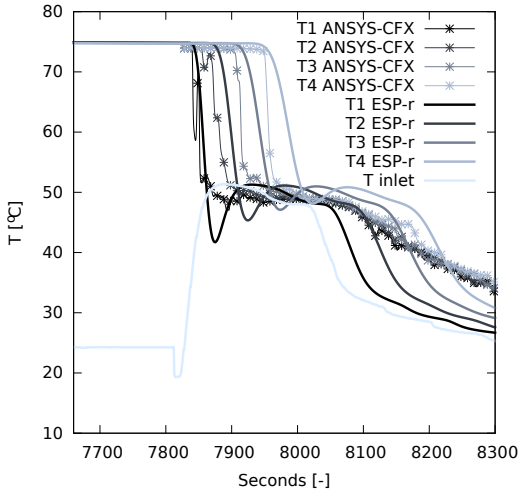

Figure 6.9: Discharge result comparison ANSYS CFX - ESP-r, case no mixing, no deflector.

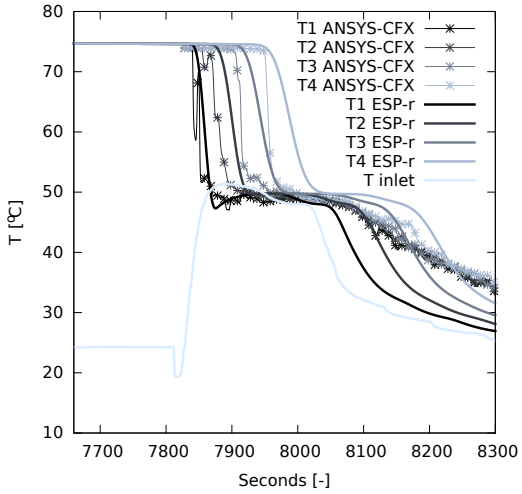

Figure 6.10: Discharge result comparison ANSYS CFX - ESP-r, case with mixing, no deflector.

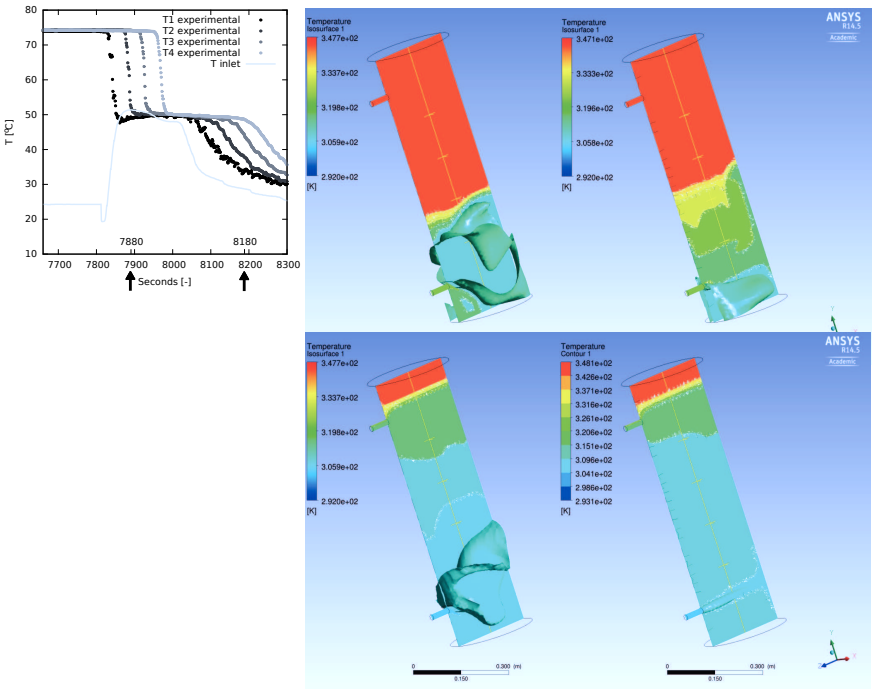

Figure 6.11: ANSYS CFX output, case with (at left) and without (at right) deflector, 60th (upper) and 360th (lower) second after the beginning of the discharging test.

The temperature distribution of two instants, before and after the plateau, is shown in Figure 6.11. The four figures exported from ANSYS-CFX show the isothermal surfaces referred to the two different models (with and without the deflector, respectively the two figures on the left and the two figures on the right) at two different instants (the 60th and the 360th second of the simulated 485 seconds after the beginning of the discharging test). On the top two isosurfaces at T=35°C are shown (60th second after the beginning of the discharging test), while on the bottom two isosurfaces at T=40°C (360th second after the beginning of the discharging test) are located.

The deflector reduces the turbulence generated by the water entering the tank and limit it at the lower part of the tank, at the inlet position. This can be deduced comparing the two top figures, showing a different stratification: the buoyancy effect is more marked in the figure on the left. By comparing the two figures on the bottom, it appears that the isosurface at T=40°C is much wider in the case with deflector than the other. Here the water spread shows that the deflector slows down the velocity of the water mixing. Combining this information with those obtained from Figure 6.10, it results that the mixing algorithm is fundamental to simulate at best a tank where there is no deflector (comparison of the peaks at the 60th second). Vice-versa, if a tank with a deflector has to be simulated, the mixing algorithm should be deactivated.

An important observation is that the ESP-r time step has to be sufficiently small to catch the rapid mixing in the second part of the test (water cooling down).

6.2 The PCM tank validation

The core of the work fulfilled in this thesis is the enhancement of two sensible storage tank components for ESP-r. The improvements upon the code consists in the possibility to simulate the presence of PCM, located in cylindrical vessels. Some of the ESP-r tank components had been enhanced with the possibility of adding PCM into cylindrical plastic vessels.

A first trial tank model, where the phase change had been implemented, was a concentrated parameters tank: for such a component the phase change had been described with a simple mono-dimensional model [59].

The PCM model had been validated by comparing the simulated results to experimental data gained from the literature. The test chosen to perform the validation was similar to one of those that Ibáñez et al. [40] carry out for TRNSYS. The reference test was the cooling down of a tank having an homogeneous initial water temperature of 80°C. The tank contained 2 PCM modules: the PCM initial temperature was maintained at the same temperature of the water. The water cooling activated the PCM solidification. The tank stored 147 l of water: it was 125 cm high and had a diameter of 39 cm. The geometry and position details and the material technical data of the modules are summarized in Table 6.1, where D_m is the diameter of the PCM module, h_m, is its height, $h_{m,b}$ is the height of the module from the bottom; ρ is the PCM density, c is the PCM specific heat capacity[2], k is the PCM conductivity and T is the phase change temperature of the PCM

[2]The implemented mono-dimensional model used an unique value for the solid and liquid specific heat capacity [J/(kg K)].

for the melting solidification.

Table 6.1: PCM module details simulated in the validation test.

PARAMETERS	VALUE
D_m [cm]	8.8
h_m [cm]	24.7
$h_{m,b}$ [cm]	0.85
ρ [kg/m^3]	1350
c [J/(kgK)]	2500
L [J/(K)]	180000
k [W/mK]	2
T_{pc} [°C]	56

The literature module actual height is 31.5 cm. Since the vessels are filled with 1.5 l of PCM, a height of 24.7 cm had been considered in the simulation. The conductivity high value is due to the presence of a graphite matrix in the PCM. The graphite rises up the conductivity and, in the same time, blocks the convection motions in the liquid PCM. The technical data for the PCM are reported in Table 6.1.

The graphs reported in Figure 6.12 and Figure 6.13 validate the concentrated parameters tank. Here the radial discretization of the module consist of 20 cells. Figure 6.12 reports the plot of the water temperature: it can be seen a curve flattening in correspondence of the registered phase change. The duration of the solidification and the temperature value at the end of the cooling down process match the values reported by Ibáñez et al. [40].

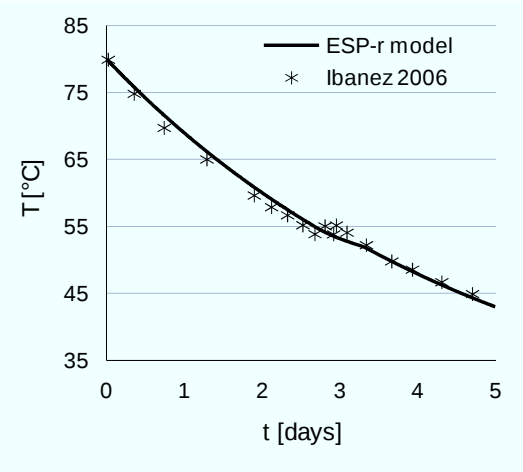

Figure 6.12: Temperature comparison between the simulated and the literature values.

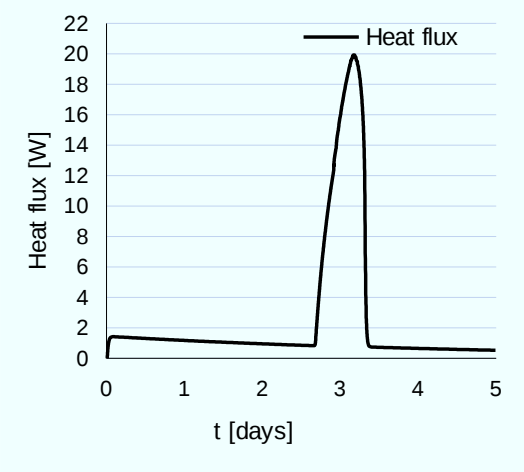

Figure 6.13: Corresponding exchanged heat flux between the PCM and the water, concentrated parameters tank model.

The limit of the concentrated parameter tank model, which induced a discretization refinement, was that such test is characterized by a sensible stratification effect.

A refined PCM tank could be obtained by implementing the phase change for stratified tanks models: the components # 103, stratified storage tank with 1 heat exchanger (2 nodes model) and # 104, stratified storage tank with 2 immersed heat exchangers (3 nodes model) had therefore been enhanced [60]. The phase change bi-dimensional model, described in Chapter 2, had been implemented and the PCM modules, described in Chapter 3, had been linked to it, as described in Chapter 4.

The same simulation had been repeated using a 10 layers stratified tank component. The obtained results, reported in Figure 6.14 and Figure 6.15, are similar to the previous ones: the simulation could reproduce for this tank model the experimental stratification registered in the water. Four layers, at 30, 60, 90 and 110 cm from the bottom, are considered for the temperature plotting: a strong stratification in the hot water is present in the upper part of the tank, that is where the PCM modules had been installed. The presence of the PCM modules, that spanned from 112.5 cm to 118.75 cm from the bottom of the tank, directly affected the temperature of the 7th layer.

The implemeted model for the PCM, applied to a storage tank, performed the same results of the considered literature test: this validation was important to assure a ground to the more complex simulations (SDHW plants with PCM tanks) that had to be performed.

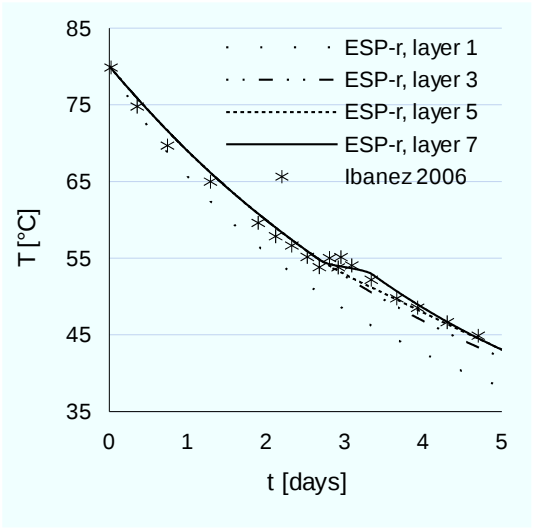

Figure 6.14: Temperature comparison between the simulated and the literature values, stratified tank model.

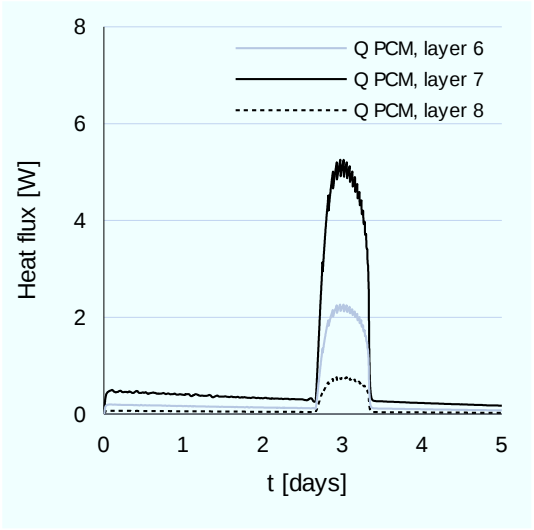

Figure 6.15: Corresponding exchanged heat flux between the PCM and the water, stratified tank model.

6.3 Calibration of a PCM tank modeled through building elements

The test is based on the cooling down of the tank water, starting by an uniform temperature of 80°C. The simulated tank is located in a room at a fixed temperature of 20°C. Two tests are performed, one for the traditional tank without PCM, one for the PCM enhanced tank.

The modelization of a PCM tank through thermal zones and constructions, in spite of using a database component, allows to specify details that could not be specified adopting the other approach: for example it permits to boost the description of the tank envelope and specify a different U-value for the different surfaces orientations (for example see Table 6.2 and Table 6.3 that resume the values used in the described simulation).

Table 6.2: Zone modeled tank envelope description.

LAYER	MATERIAL	THICKNESS [m]	CONDUCTIVITY $\left[\frac{\mathrm{W}}{\mathrm{mK}}\right]$
s_{ins}	Glass wool	0.08	0.04
$s_{mech.res}$	Steel	0.005	50

Table 6.3: U-values for the different surface orientation.

ORIENTATION	U-value $\left[\frac{\mathrm{W}}{\mathrm{m^2K}}\right]$
h	0.461
u	0.467
d	0.452

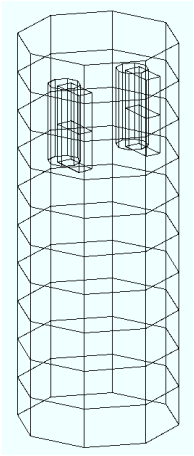

Figure 6.16: Thermal zones representing 10 water layers.

The used routines for the zonal approach model the convection in the liquid phase of the PCM through the correlation described at Section 2.3. Figure 6.16 shows the discretization of the tank water: 10 water layers had been modeled as 10 different zones.

The general layer is in contact with those that stay up and down through *fictitious* constructions. The PCM had been modeled as additive inertial mass and had been inserted in the chosen 2 water layers. The PCM data had been assigned to the central node of the three nodes representing a construction layer. With reference to Figure 4.2 in Sub subsection 4.1.2, the node where the PCM material characteristics have to be assigned are the "internal, volume nodes". As reported in Table 6.4, the surface where the phase change data had been assigned is 8 cm wide and 8 cm thick.

Table 6.4: PCM data.

PCM geometry and parameters	Values
n_m [-]	2
h_m [m]	0.20
t_m, w_m [m]	0.08
$h_{m,b}$ [m]	0.70
ρ_s $[\mathrm{kg/m^3}]$	880
ρ_l $[\mathrm{kg/m^3}]$	770
c_s [J/(kgK)]	2 100
c_l [J/(kgK)]	2 100
L [J/kg]	178 000
k_s [W/(mK)]	0.2
k_l [W/(mK)]	0.2
$T_{melting}$ [°C]	55
$T_{solidification}$ [°C]	59
ν $[\mathrm{mm^2/s}]$	32.49
ΔV [%]	14

The parameters used in the simulation, typical for a commercial PCM, are summarized in Table 6.4. The inserted values are described as follows: h_t is the height of the tank, s_{ins} is the thickness [m] of the insulation, n_m is the number of the PCM module, h_m, t_m, w_m are respectively the module height, thickness and width, $h_{m,b}$ is the height of the module from the bottom. ρ is the PCM density, c is the PCM specific heat capacity, L is the PCM latent heat, k is the PCM conductivity, T is the phase change temperature of the PCM for the melting solidification, ν is the kinematic viscosity, ΔV is the thermal expansion coefficient; s stands for solid and l stands for liquid.

For the layers where the PCM modules are located, the water mass had been subtracted. Figure 6.17 describes a water node, or rather, the water zone contained between two fictitious layers, a tank wrapper section, and the PCM nodes.

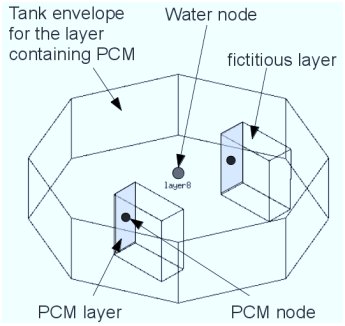

Figure 6.17: PCM assignment to the selected node.

A general calibration of the stratified tank model without PCM has been carried on by comparing the zone model tank with a plant stratified tank component (cmp. # 104). It is assumed that is not possible to obtain the same temperature results for the 2 models because the geometry is different and the U-values calculated in the zone model is function of the surfaces positions. If a mean U-value of 0.35 $\left[\mathrm{W/(m^2K)}\right]$ is assigned to the plant component, the temperature drop is matched (see Figure 6.18). Figure 6.18, Figure 6.19 and Figure 6.20 report the temperature range for a tank without PCM: the Figures illustrate the results obtained from the two models and the stratification effect.

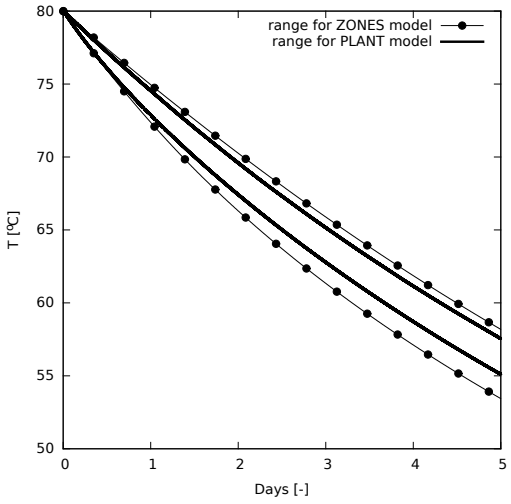

Figure 6.18: Comparison between plant model results and zonal approach results.

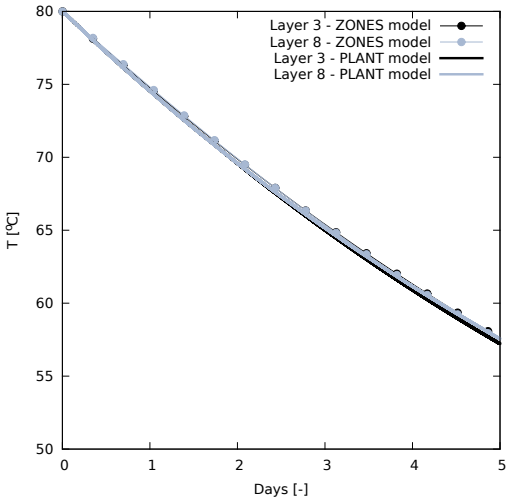

Figure 6.19: Comparison between the two models temperature considering the 3rd and the 8th layers.

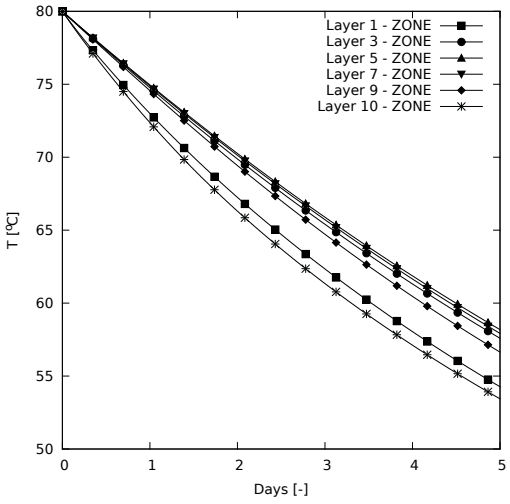

Figure 6.20: Temperature of the water zones.

If a sensible-latent tank is considered, the PCM can be modeled taking into account the convection effect in the liquid phase or avoiding considering it: the error on the water temperature is very small choosing one or the other (it can be seen from Figure 6.21). If the convection effect is computed, the water layer temperature is a bit higher than in the

case in which it is neglected. The temperature difference is more emphasized for the 8 th layer than for the 9th layer, but in general the impact is not appreciable. For these layers, the maximal value of the difference between the two cases is 0.15°C (for the layer number 9 the maximum difference is 0.12°C).

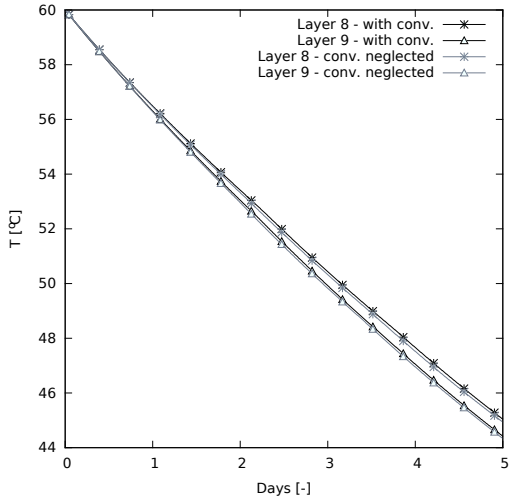

Figure 6.21: Effect of the convection in the liquid PCM on the temperature of the water zones, layer 8 and 9.

The implemented PCM tank component did not allow to simulate the sub-cooling phenomenon. The zonal approach is useful to fill this gap, since some routines related to the constructions permit to set up a sub-cooling degree. This phenomenon can be easily implemented in the new tank component, and can be intended as future work.

The convection and sub-cooling effect on the water tank temperature had been compared with the performance obtained if no one of them was considered[3]. Figure 6.22 reports the impact of these phenomena on the water temperature at the 8th layer and Figure 6.23 shows the PCM temperature plot. The modeled sub-cooling is simulated with a 2°C skip.

[3]The simulation of the two phenomena used two different routines that refer to the building description.

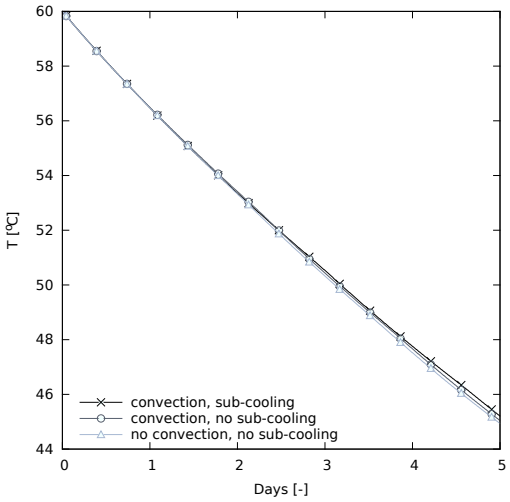

Figure 6.22: Water temperature at layer 8.

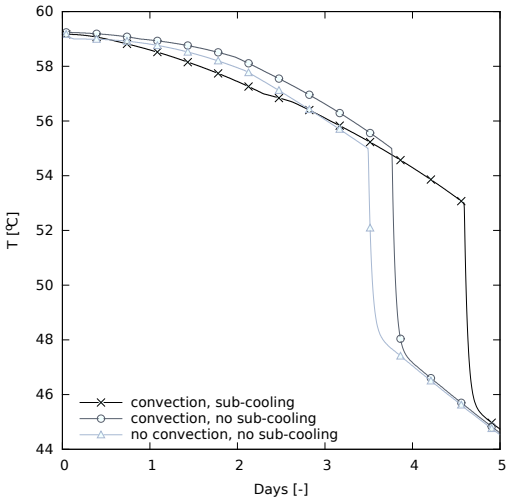

Figure 6.23: PCM temperature for the module section set located at layer 8.

The sub-cooling effect is positive at the end of the simulation, because the PCM temperature is maintained at a higher temperature for a longer time. Even if the effect of the heat transmission/phenomenon appears sensible in the PCM nodes, their effectiveness on the water temperature is marginal. The method is stable even if a not refined space grid is adopted. A time step of 5 minutes is adequate for this purpose.

The zonal approach presented in this Sub Section can be intended as a further test. The comparison between the two models results proves again the validity of the code implemented for the tank plant component. Moreover, this calibration underlines the necessity of a simple, rapid and convenient method to simulate the PCM enhanced tanks without resorting to complex models elaborated ad hoc: this is also one of the aims of the thesis.

7

Simulations results

7.1 The PCM tank initial simulations

The validity of the simulation code for the PCM had been verified by the literature cooling-down test. After this test, it was possible to proceed with the simulations needed to test the impact of the PCM in a SDHW system. A preparatory set of simulations is important to understand the impact that the PCM technology offers to the system: if the PCM brings improvements, it is worth inspecting an approach to exploit at the best its potentiality. A simple SDHW plant, similar to those described at Chapter 4, had been simulated for a period of one week in July and in September. The simulated plant was situated in two different location, that are Rome and Trieste (see Section 4.3).

Objects of the analysis were four tanks. The first two was characterized by a volume of 147 liters and by the same geometry described in Subsection 6.2. The first was a traditional/sensible tank, the second was enhanced with PCM modules. The third and the least tank were smaller than the first two and contained 73 liters: they had the same diameter of the first two, but with 80 cm height. The third was a sensible/traditional tank, the least was enhanced with PCM modules. The PCM tanks contained 8 modules filled with a total of 12 l of the sodium tetra-hydrate salt included in a graphite matrix. The PCM characteristics are described in Table 7.1. The PCM modules were located at 0.55 m from the bottom of the tank. where ρ is the PCM density, c is the PCM specific

Table 7.1: PCM parameters.

PARAMETERS	VALUE
ρ [kg/m^3]	1300
c_s [J/(kgK)]	2500
c_l [J/(kgK)]	2500
L [J/kg]	1.8 E-8
k_s [kW/(mK)]	2.0
k_l [kW/(mK)]	2.0

heat capacity, L is the PCM latent heat, k is the PCM conductivity; s stands for solid and l stands for liquid.

The boiler providing the heat flux when the solar collector was not sufficient was a non-condensing boiler with aqua-stat control, thus different from those described in Subsection 4.2.5. The used component provided water at the temperature of 60°C; the boiler pump was activated when the temperature of the tank water fallen below 45°C and was deactivated when the temperature rose over 50°C.

The considered solar panel area was 4.72 m^2.

An equi-percentage control, like those described in Chapter 4, had been used to maintain the supply water temperature, but the tank outlet temperature range for the modulation was narrowed to 40-60°.

Figure 7.1 shows the effect of the PCM modules presence on the water temperature at mean height for a 73 l tank in a week of September and Figure 7.2 shows the same for a 147 l tank.

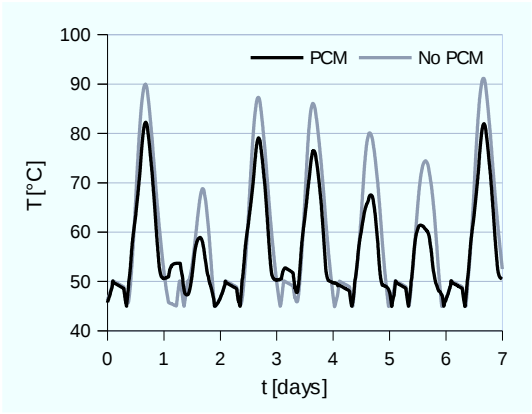

Figure 7.1: Water temperature in a 73 l tank for a week of September.

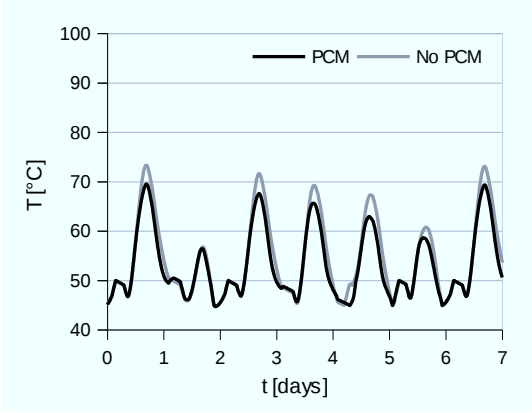

Figure 7.2: Water temperature in a 147 l tank for a week of September.

It can be noted that the temperature values oscillate more in the water of the smaller tank than of the bigger. This is obvious because of the lower storage capacity of the water. The effect of the PCM in the smaller tank is far more pronounced: the peaks in the oscillations can be reduced till about 10 K, while in the bigger this impact is of much less effect. It might be possible that the reduced effect in the bigger tanks depends on the quantity of PCM that had been inserted. For this reason it may be assumed that embedding more PCM can produce better results. From these simulations seems that the quantity of PCM is a variable that influences the results of such applications. For the simulated weeks the fractional thermal energy savings parameter had been calculated with the formulation proposed by Heimrat and Haller [61]:

$$f_{sav,therm} = 1 - \frac{Q}{Q_{ref}} \tag{7.1.1}$$

$f_{sav,therm}$ measures the percentage of non solar energy input for heating that can be reduced by the solar system. The denominator of the fraction shown in Equation (7.1.1), Q_{ref} represents the primary energy consumption of the corresponding plant without the solar panel, and the numerator, Q, represents the primary energy consumption in the described solar system. The primary energy consumed is calculated as described in Subsection 4.2.9 for one year simulations.

Table 7.2 resumes the obtained values for the climate of Rome and Table 7.3 summarizes the results of the corresponding plant located in Trieste.

Table 7.2: $f_{sav,therm}$ for different cases in Rome.

Volume [l]	Cases	July	September
147	no PCM	0.940	0.732
	PCM	0.945	0.748
73	no PCM	0.912	0.717
	PCM	0.934	0.742

Table 7.3: $f_{sav,therm}$ for different cases in Trieste.

Volume [l]	Cases	July	September
147	no PCM	0.751	0.519
	PCM	0.759	0.521
73	noPCM	0.750	0.520
	PCM	0.767	0.527

The reported results show that the presence of the PCM modules can only marginally improve the performance of the SDHW system for the simulated weeks. In the same weeks, the warmer climate outcomes were better than those obtained for the cooler climate. If the plants located in Rome had been considered, the performance obtained in both tanks in June are higher than those obtained for September, because of the higher solar contribution. In September the obtained $f_{save,therm}$ for the smaller PCM tank was

higher then those obtained with the larger traditional tank. In July, the small PCM tank efficiency was higher than those obtained for the traditional tank having the same size, but was lower than those obtained for the same week using the bigger traditional tank (the values were in any case comparable: 0.934 and 0.940).

Then, a successive analysis had been carried on for a period of 1 year: it included the stratification effect. The model and the presentation of the results are similar to those previously described. The stratified tank model corresponds to the component # 104[1] of the ESP-r trunk and development version enhanced with PCM. In the simulated plant, a gas fired boiler (component # 17) provided water at the constant temperature of 60°C. These simulations compared the impact of different PCM phase change temperature, while the other PCM technical data were the same as before. The impact of this variable was considered crucial for the PCM storage capacity, thus the phase change temperatures of 55° and 60° had been considered.

Also for these simulations the $f_{save,therm}$ had been calculated and the results are summarized in Table 7.4

Table 7.4: $f_{sav,therm}$ for different cases.

Volume [l]	Cases	Trieste	Rome
147	No PCM	0.483	0.680
	PCM 55	0.489	0.688
	PCM 60	0.486	0.686
73	No PCM	0.455	0.635
	PCM 55	0.462	0.636
	PCM 60	0.460	0.635

The T_{pc} had a sensible impact on the global performance of the SDHW systems, even if, also in this case, the $f_{save,therm}$ was not dramatically improved by the employment of PCM. For this reason it had been considered emblematic the choice of the temperature that maximizes the tank performance. Again, the impact of the PCM was higher if it was embedded in low volume tanks, vice-versa it is marginal if it was inserted in the higher volume tanks. So, the performance of the tank must be evaluated taking into account, as crucial design parameters, the volume of PCM. As reported in [60], the improving of the discretization for both the tank and the PCM did not give sensibly different results[2].

As conclusion of the performed simulations, it can be pointed out the necessity of additional analysis to tune up the parameters of the model in order to optimize the system. Further than the phase change temperature, it must be taken into account also the position of PCM modules inside the tank, since, here, the temperature distribution is not uniform. Considering the impact of the latent heat, the design parameters that have to be tuned to obtain the better performance of the tank are: the PCM volume, the tank inner geometry and the phase change temperature. Further simulations that are not

[1] The ESP-r plant components are identified by a progressive number, generally depending on the implementation order.

[2] In these simulations a matching grid water-PCM for the axial discretization had been used.

reported here confirmed the necessity, spotted by Esen and Durmus [37], of exploiting all the inserted PCM volume.

7.2 The tank optimizations

The conclusions of the performed simulation confirmed that the efficiency of the LHSU depended on several factors, as the dimension of the vessels where the PCM was located and the phase change temperature, confirming what has been remarked by Esen and Durmus [37], Rostamizadeh et al. [38] and Ibáñez et al. [40]. The simulations enlighten the necessity of optimizing the problem: this kind of analysis and its results are reported in the next Subsections.

The optimization of the tanks presented in this Section refers to the plant described in Chapter 4. The defined main and crucial objective was to minimize the plant (or boiler) primary energy consumption during a whole year: this performance is calculated with the formulation reported in Subsection 4.2.9. The aim of this optimization was to analyze the possibility to reduce the fuel consumption just by acting on the PCM quantity that has to be inserted maintaining constant the tank external geometry. It is clear, also from the previous simulations, that the more water is contained in the tank, the more storage is established and the less energy consumption is demanded to maintain the water at the set-point of 40°. Of course, and this is true in particular for the low- and ultra-low energy buildings, it is not always possible to have much space available, where to put a big tank. For this reason both the reduction and the restraint of the tank volume becomes a crucial aspect. Therefore, the space occupied by the tank, that is the tank gross volume (insulation included), has to be minimized. To consider also this design target it is necessary to perform a multi-objective optimization.

The adopted algorithm was the NSGA-II for both the mono- and the multi-objective analysis. The optimization problem started by the definition of a reference case, also called *base case*, that is the tank with characteristics described in Section 7.2.1. To initiate the optimization an initial population of 31 individuals had been created for both the analyses. In order to reduce the effort to explore all the possible solutions a Sobol space filler had been used, so that the initial population was uniformly distributed in the design space. The optimization code permits to define the probability of the operators to be applied to the population: the cross-over probability was set at 70%, the mutation probability at 5%. The optimization considered a population of 30 generations.

The analyses that will be reported in the following sections consider one or two objectives simultaneously and are carried out for both the traditional tanks without PCM and the PCM enhanced tanks [62–64]. The objectives are the same for both the tank typology, without or with PCM. The optimization performed on the traditional sensible tanks are useful to understand how much the energy consumption and the tank volume can be reduced without resorting to the latent heat. Finally, it is carried out a comparison of the performance of the two kind of tanks.

7.2.1 The base case and the variation range of the variables

Either the PCM model and the traditional tanks may be intended as commercially available products [65, 66].

A solid graphite structure had been considered in order to increase the conduction in the PCM module (this is what has been done also by Cabeza et al. [67]). A consequence of this enhancement, apart from the increase of conductivity, was to block the convective motions.

The base case, whose parameters were varied by the optimization algorithm, was a standard configuration tank without PCM having a volume of 300 liters.

To start the analysis from a simple problem the tank net height was not allowed to vary in the mono-objective optimization, and the base case tank height of 1.54 m was maintained for all the offspring solutions. For all the multi-objective optimizations the only variable modified by the algorithm affecting the water volume was the tank net height, since the tank net diameter had been considered as constant. The range in which the tank net height could vary is reported in Table 7.5. Since the base case tank height is 1.54 m and this is the central value of the range, the tanks inner volume varies from 253 to 351 liters. The DHW outlet position is automatically located 5 cm beneath the tank top. The position of the internal heat exchangers was not affected, since they were positioned below the minimum tank height. The tank gross volume is affected also by the insulation thickness, whose range of variation is reported in the same Table. Together with the energy reduction, the volume occupied by the tank inside a boiler room is a crucial aspect that has to be considered in the design phase.

In the optimization of the PCM enhanced tank, further parameters could vary. They were: the number of the cylindrical modules, their height, diameter, position from the tank bottom and phase change temperature. Also for these variables the variation interval is reported in Table 7.5. For the multi-objective analysis the only first two variables had been considered in the optimization of the traditional tank, while the others had been considered in those regarding the tank with PCM.

All these parameters were allowed to vary in a continue way, except for the number of the modules and the phase change temperature: for these parameters all the entire values included in the range had been taken into account.

Figure 7.3 reports the design of the tank, whose variables parameters depend on the type of tank: a traditional tank (a) and a PCM enhanced tank (b). The feasibility control, that in this analysis is handled by the optimization tool through constraints nodes, is described in Section 3.2.

In Table 7.5 h_t is the height of the tank, s_{ins} is the thickness [m] of the insulation, n_m is the number of the PCM module, h_m is the module height, D_m is the module diameter, $h_{m,b}$ is the height of the module from the bottom and T_{pc} is the phase change temperature of the PCM.

The water tank was subdivided in 20 layers[3], the inlet water position was fixed at 5 cm from the tank bottom. An explicit scheme for the PCM algorithm had been chosen.

[3]This discretization, compared with those used in [60], was chosen in order to keep the computational cost low.

Table 7.5: Variables and range of variation considered in the optimization processes.

PARAMETERS	RANGE	
h_t [m]	1.29	1.79
s_{ins} [m]	0.01	0.075
n_m [-]	0	30
h_m [m]	0.05	0.3
D_m [m]	0.02	0.08
$h_{m,b}$ [m]	0	1.75
T_{PC} [°C]	25	60

As reported in Sub subsection 4.2.1 a time-step of 1 minute for the plant and 12 seconds for the tank solution had been used.

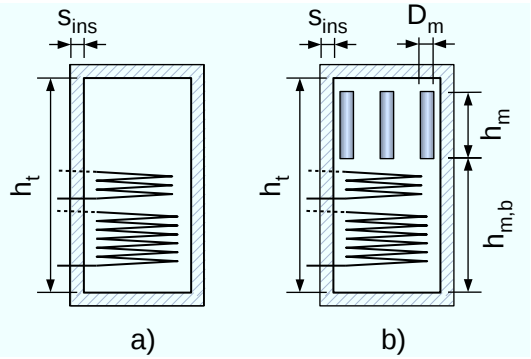

Figure 7.3: The base case: variables for the optimization of: a) the traditional tank (without PCM) and b) the PCM enhanced tank (with PCM modules).

After defining the input variables, the variation law is chosen for the problem parameters, the initial population data are collected for the first generation, few operations to be executed on the variables are established, the selected algorithm manages the processed simulations and the iterative process points out the optimal results, rejecting the unfeasible solution. Figure 7.4 shows a screen-shot of the nodes grid that had been used and linked each others. Proceeding from the top to the bottom: after the variables (or array-variable) are defined, these values are used as input data in the ESP-r files; the needed operations are executed (feasibility test, ESP-r run and results...) and the output optimized results are pointed out. Proceeding from the left towards the east, it can be read the optimization process summarized in the DoE definition and the choice of the algorithm. These two processes intersect each others and the optimal results are then pointed out.

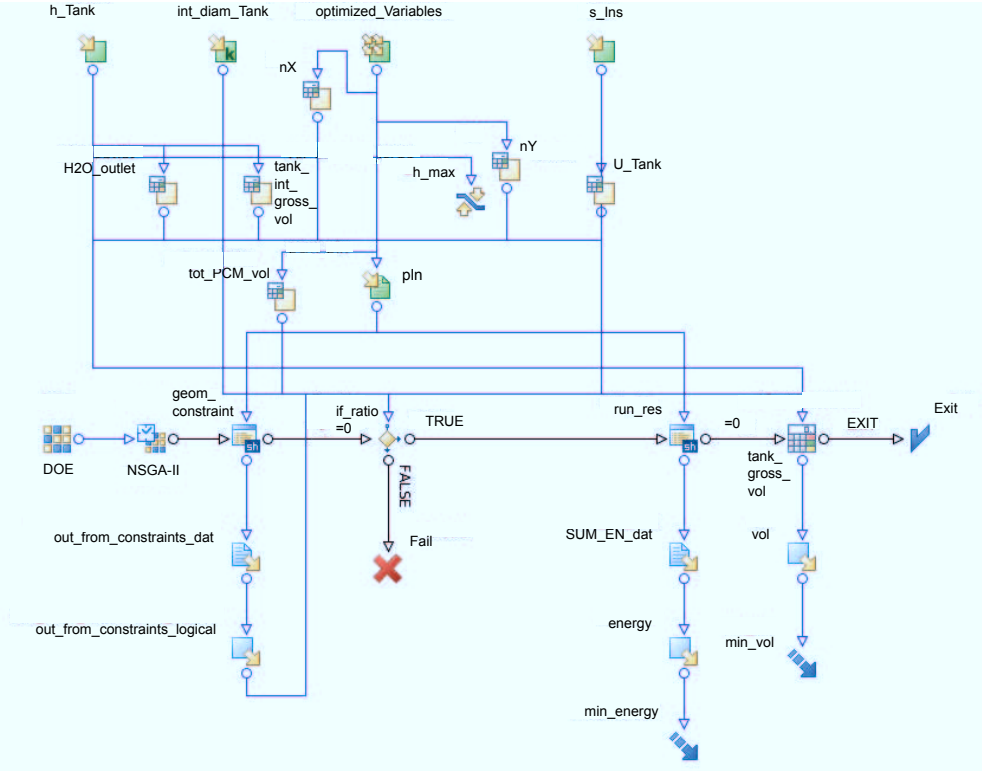

Figure 7.4: Problem scheme modeled with modeFRONTIER®.

7.2.2 The optimized traditional tanks

As already stated in Subsection 5.1.2, for an analysis that considers more than one objective, it is not possible to arrive to *one* optimal solution, but to a series of solutions that are better than other. If two best solutions are considered, it is expected that, for one objective, one of it is better than the other; for the other objective the other solution is better than the first.

The results of the multi-objective analysis on the traditional tank are reported in Figure 7.5 and Figure 7.6: they report the solutions distribution in the design space identified by the adopted algorithm. The optimal designs, pertaining to the Pareto frontier, are identified in blue. In the enlarged plot three designs are marked in red: the one set at the top right vertex of the rectangle is indicated as base case and represents the standard configuration tank with a volume of 300 liters and without PCM. In correspondence of it, the other two marks in red represent the solutions with the same occupied gross volume (1) and with the same energy consumption (2). The selected rectangle encloses therefore all the solutions dominated by the front, but better than the base case in terms of both primary energy consumption and overall volume. Since the tank net diameter is constant in all the cases and the tank net height is equal in the two selected solutions, the difference

between the two solutions depends on the tank insulation. For the same quantity of water, the difference in fuel consumption is given by the thickness of the insulation layer.

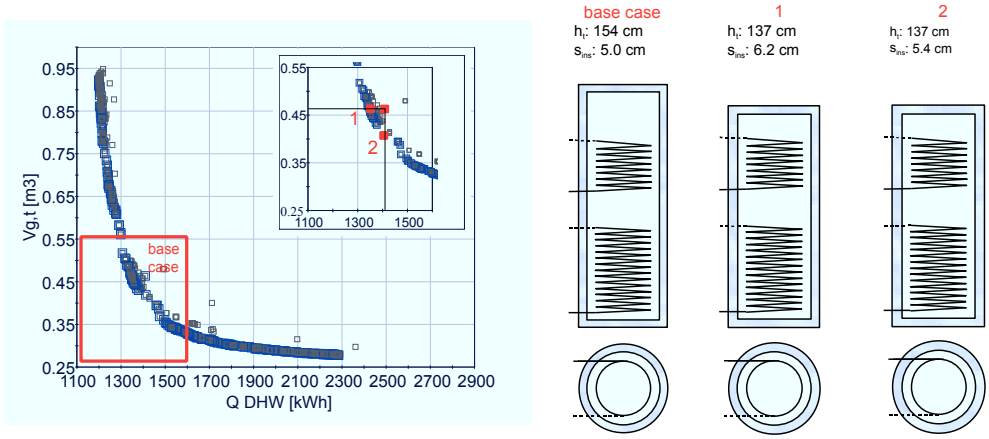

Figure 7.5: Pareto frontier for a plant in Rome, case of a tank without PCM. The geometry of the two non dominated solutions corresponding to the base case are enlighten.

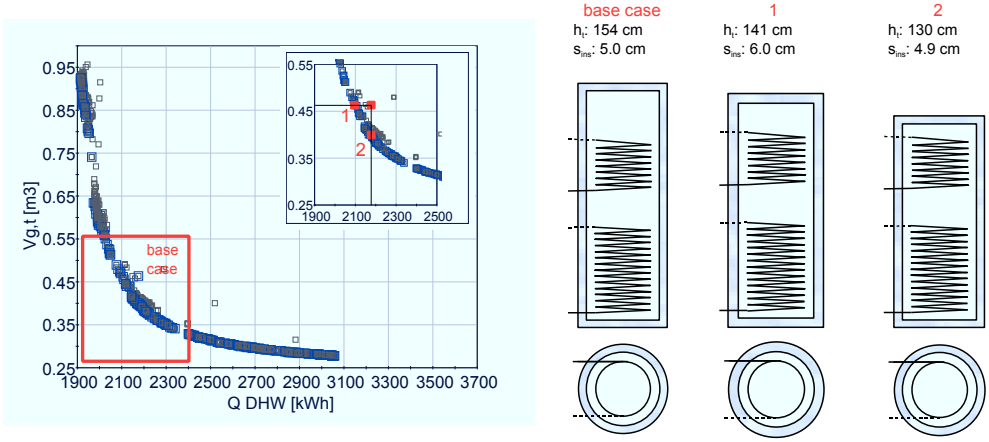

Figure 7.6: Pareto frontier for a plant in Trieste, case of a tank without PCM. The geometry of the two non dominated solutions corresponding to the base case are enlighten.

7.2.3 The optimized PCM tanks

The used PCM is a paraffin based material with the characteristics presented in Table 7.6. Such a material has been chosen in order to avoid the corrosion, as reported in [68]. The conductibility assumes values of 2 W/(mK) since a graphite-PCM compound has been considered here.

Table 7.6: PCM parameters that are fixed.

CONSTANT PARAMETERS	VALUE
ρ_s [kg/m^3]	880
ρ_l [kg/m^3]	760
c_s [J/(kgK)]	2100
c_l [J/(kgK)]	2100
L [J/kg]	1.68 E-8
k_s [kW/(mK)]	2.0
k_l [kW/(mK)]	2.0

Discretization technique

In an optimization process, when the data of the PCM-tank component are not inserted manually but automatically defined, it is worth to define an external control on the PCM module dimension and to automatically calculate the suitable grid, in order to avoid too slow simulations. The utility of such control can be clear focusing on the stability check, that points out the time step for the PCM as function of the PCM grid.

A mathematical function ($vect([\mathbf{x}], i)$), where $[\mathbf{x}]$=$[x_0, x_1, ..., x_n]$, has been adopted to locally modify the PCM grid, thus, a more suitable discretization has been found for the PCM modules. As defined in the optimization code [55], it returns the i-th element of the vector $[\mathbf{x}]$. If it were a real value, it is rounded to the closest integer, such that:

$$\begin{array}{ll} \text{if}\,(i \leq 0): & vect([x_0, x_1, ..., x_n], i) = x_0 \\ \text{if}\,(i \geq n+1): & vect([x_0, x_1, ..., x_n], i) = x_n \\ \text{if}\,(i \geq 0\,\&\,i \leq n]): & vect([x_0, x_1, ..., x_j, ..., x_n], i) = x_j \end{array}$$

where j is the closest integer to i. The mathematical function $floor(x)$ returns the largest integral value not greater than x.

The adequate number of PCM cells is calculated with two functions. The next explanation describes, for example, how nX is calculated (nX is the number of cells in the radial direction); an analogue approach has been followed for nY. Depending on the height of the PCM, values of 11, 8 or 6 cells have been chosen. The number to be chosen among these 3 values was determined by the expression:

$$\frac{h_{max,cyl} - h_{min,cyl}}{\text{selectable values}}$$

As reported in Table 7.5, if $D_{m,max} = 0.08$ and $D_{m,min} = 0.02$, and 3 were the values that could be chosen with the function $vect$, the function $floor$ gives as output the value 0.02. The complete function:

$$vect([11, 8, 6], floor((0.08 - D_{m,min})/0.02))$$

gives:

$$\begin{array}{ll} \text{for}\,D_m = 0.08: & (0.08 - 0.08)/0.02 = 0 \rightarrow nX = 11 \\ \text{for}\,D_m = 0.02: & (0.08 - 0.04)/0.02 = 2 \rightarrow nX = 8 \\ \text{for}\,D_m = 0.05: & (0.08 - 0.05)/0.02 = 3.8 \rightarrow nX = 6 \end{array}$$

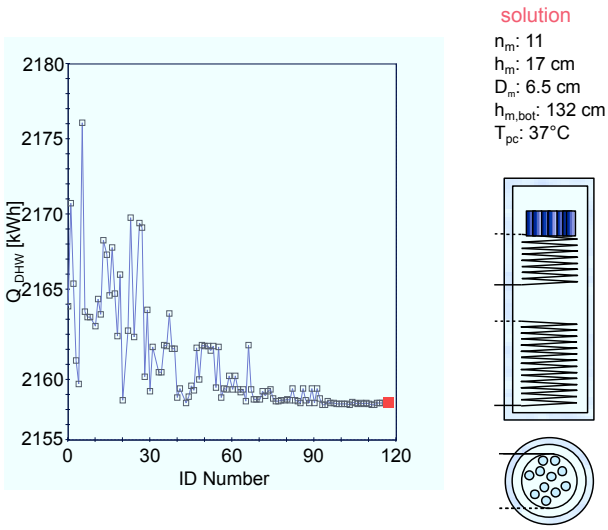

Figure 7.7: Optimization history for Trieste

The results

Mono-objective optimization

The optimization process, described by the solutions evolution towards the optimal one, can be shown through an optimization history. Figure 7.7 indicates graphically the optimization history for the location of Trieste. Even if the primary energy consumption slightly decreased, the spotted best value, that corresponded to a Q_{DHW} of 2160 kWh, was very similar to the consumption of the base case (Q_{DHW}=2164 kWh). Similar results had been obtained for Rome: for this climate, the base case consumption was attested at Q_{DHW}=1401 kWh, while the best performance corresponds to a primary energy consumption of 1390 kWh. The tank optimized design parameters identified through the optimization tool are listed at Table 7.7.

Table 7.7: Optimal solution for fixed size tank.

VARIABLE	ROME	TRIESTE
n_m [-]	15	11
h_m [m]	0.06	0.17
D_m [m]	0.05	0.065
$h_{m,b}$ [m]	0.85	1.323
T_{PC} [°C]	42	37
Q_{DHW} [kWh]	1390	2160

It can be concluded that, at least for this kind of tank/plant, it is not possible to obtain any significant reduction in energy consumption. Unless the objective of space

reduction is accounted and the boundary lines of the research are expanded, the PCM does not seem to be useful in the analyzed application. Extending the analysis on the tank volume, that is constraining the problem to point out some small tanks configurations, it is possible to obtain more satisfactory solutions.

Multi-objective optimization

In this analysis a the algorithm pointed out a series of values performing in some sense better than the others.

The distribution of 30 generations individuals are shown: the initial Sobol designs are uniformly distributed in the design space; the general dominated solutions generated through the NSGA-II algorithm moves towards the origin of the axis; the better solutions are aligned on the Pareto frontier.

Figure 7.8 explains the process to which the solutions are subjected: at the beginning of the optimizations few solutions, corresponding to the initial population, are pointed out. Then the design space is gradually filled until the best solution, corresponding to those solutions found out until the maximum number of generations created is reached. This process results in a space moving of the Pareto front. An analysis covering 30 generations solutions, generated by 31 parents, had been considered satisfactory since, in this way, about 900 possible solutions had been evaluated to find out a high performance PCM tank.

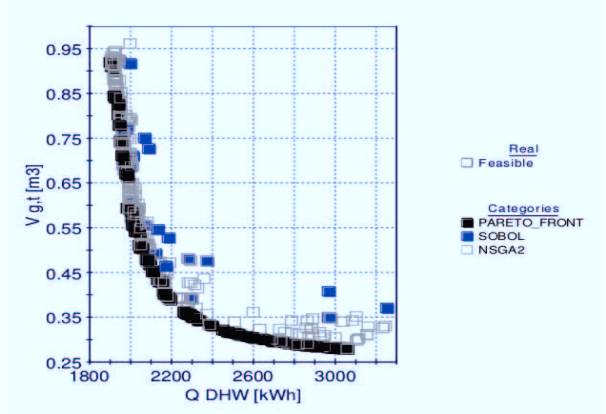

Figure 7.8: The distribution of 30 generations individuals are shown: the initial Sobol designs are uniformly distributed in the design space; the general dominated solutions move towards the origin of the axis; the better solutions are aligned on the Pareto frontier.

Figure 7.9 and Figure 7.10, that represent what had been described for the traditional tank in Sub subsection 7.2.2 for Rome and Trieste respectively, enlighten the designs with the same gross volume of the original tank, ID 873 and ID 500 and with the same primary energy absorbed, ID 826 and ID 197.

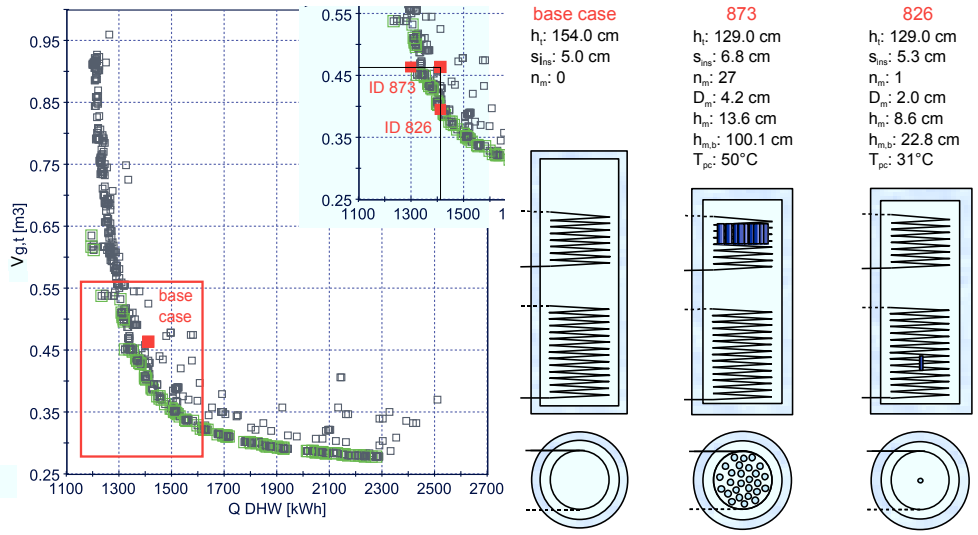

Figure 7.9: Pareto frontier for a plant in Rome, case of a tank with PCM. The geometry of the two non dominated solutions corresponding to the base case are enlighten.

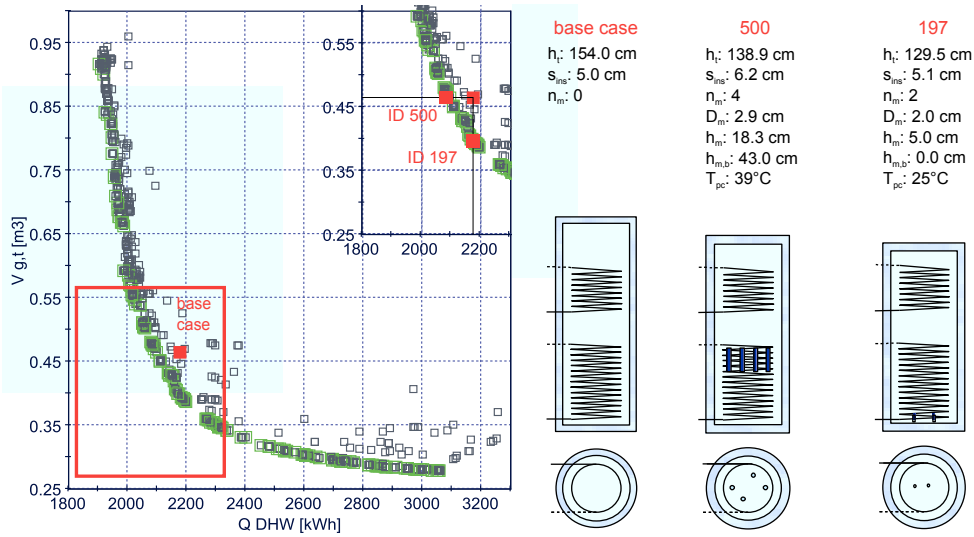

Figure 7.10: Pareto frontier for a plant in Trieste, case of a tank with PCM. The geometry of the two non dominated solutions corresponding to the base case are enlighten.

The best results can even be very similar to the base case tank. They can be seen also from the graphical representation of the tanks in Figure 7.9 and Figure 7.10. The design # 826, for example, is almost a tank without PCM. It may be supposed that the

constraints on the optimization are too severe, but this hypothesis is rejected considering that the constraint imposed on the tank is only a geometrical feasibility (see Section 3.2). Starting from an initial population of 31 individuals, the cross-over and the mutation operators are applied for 30 generations: it results that a high number of tank simulations is performed and a wide research in the design space is done. From the obtained results, a rule can be deduced: this rule is about the PCM filling in the tank. In general, a low volume tank is filled with less PCM (the order of magnitude of the PCM volume is the liter for the low energy/big tanks and the decimal of liter for high energy/small tanks). This depends on the few available space for a small tank.

Table 7.8 resumes the results for the selected designs: volume $[m^3]_{net}$ represents the tank net volume $[m^3]$, that is the volume of the water and the embedded PCM. V_g is the tank g volume, that includes both the PCM modules and the insulation layer. Inspecting this Table, it can be observed that some improvements can be obtained for both locations, if they are compared to the reference tank.

The reduction of the primary energy consumption absorbed by the plant is low: it stands at 5,85% for Rome and 3.67% for Trieste. Regarding the primary energy consumption, these outcomes confirm the results obtained for the mono-objective analysis.

The effectiveness in terms of gross volume was more sensible: a volume reduction of 10.62% for Rome and 14.01% for Trieste could be enlighten.

Table 7.8: Optimized designs parameters.

	ROME		TRIESTE	
	873	826	500	197
V_g (litre)	452	404	464	399
V_n (litre)	253	253	273	254
V_{PCM} (litre)	5.07	0.03	0.51	0.03
Q_{DHW} (kWh)	1320	1402	2100	2180
T_{PC} (°C)	50	31	39	25

The scarce impact of the PCM on the tanks storage efficiency may be ascribed to the wide temperature variation range typical for such kind of tanks.

The contribution of the solar panel does not affect much an hypothetic water stratification. The water coming from the solar panel is controlled: if the panel water temperature is too low the flow entering in the tank is avoided. Nevertheless, this water actually circulates if its temperature is *proximal* to the tank one: the chosen control permits a wider exploitation of the renewable source.

The tank water temperature variation is more significantly due to the intrinsic characteristic of the water demand. When the cold water from the grid enters the tank, the water temperature becomes almost uniform soon and the stratification effect does not affect the PCM for a long lapse of time. To be exploited at the best, the PCM should always be in the phase change, and this does not happen in the analyzed tank. If the water temperature were more constant, it might be possible that the PCM could perform better.

Taking into account the conclusion carried out from the mono-objective optimization,

the adding results presented here show that is not possible to expect substantial improvements by this technology in a solar system, unless other kind of tanks are considered. The development of a code to simulate a tank in tank with PCM is a future work.

An economic analysis

The suitability of a Thermal Energy Storages (TES) with PCM should be evaluated after an appropriate economic analysis.

The production cost of a traditional tank (500 liters) can be estimated in 400 euros (personal communication source). The prize of a PCM tank accounts also an additional production cost (the traditional tank has to be modified for the insertion of the PCM bars) and the PCM cost. A supplemental cost of 10% can be considered as the former term (440 euros), while, for the latter, the prize of the PCM depends on its characteristics. The costs of the a paraffin, for example, can vary between about 3.50 euros/kg to 6 euros/kg, depending on the quantity to be bought. The cost would rise up if devices to enhance the conductivity (such as a graphite matrix or nano-particles) should be added to the PCM.

The production costs of a PCM enhanced tank may be expensive if a non optimized solution is analyzed. Consider, for example, the "base case" described in Subsection 7.2.1 and, in particular, the maximum value for all the variables ranges, as reported in Table 7.9.

Table 7.9: Parameters considered for a PCM tank non-optimal solution.

PARAMETERS	VALUE
n_m [-]	30
h_m [m]	0.30
D_m [m]	0.08

The cost of the resulting 36 kg of paraffin can vary from 126 to 216 euros. Even if the dimension of this tank is lower than 500, a production cost of 440 euro is still accounted. The overestimation of the tank production cost can only result in a underestimation of the percent increase for the PCM addiction, estimated in $+29\% \div +49\%$. This solution does not appear to be recommendable, and confirms the necessity of optimizing the system.

If an optimal design is analyzed, where the maximal performance for the system is achieved, the production cost sounds more reasonable. Referring, for example, to the solution ID 826, described in the previous Subsection, the cost for the PCM can vary from 14 euros to 24 euros. It can be concluded that an optimized PCM tank costs about 14-15% more than a traditional tank, and much less than a non optimized solution. A solution like the former one does not seem to be viable, while the latter seems to be more convenient. This confirms that this technology can be more beneficial if fitted in the suitable plant component and plant.

Comparison of the fronts

Figure 7.11 and Figure 7.12 report the comparison of the Pareto fronts shown at Subsections 7.2.3 and 7.2.2, obtained from the traditional and PCM enhanced tank optimizations.

From these Figures it results that the Pareto frontier obtained for the optimized PCM tanks is almost the same of those carried out for the traditional tanks. This happen for both the two locations, and means that the best performance of the PCM tanks are comparable with those of the traditional tanks. The comparison is based on the same number of generations (30).

What can be concluded from this relation is that the inclusion of PCM modules in the storage tanks can not lead to sensible improvements in the storage efficiency.

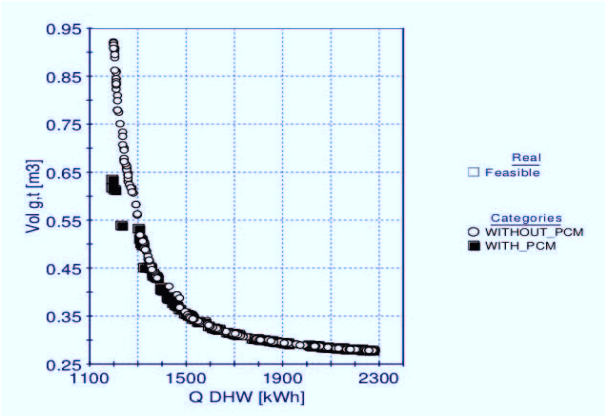

Figure 7.11: Comparison of the Pareto frontier obtained for the tank with and without PCM for a plant in Rome.

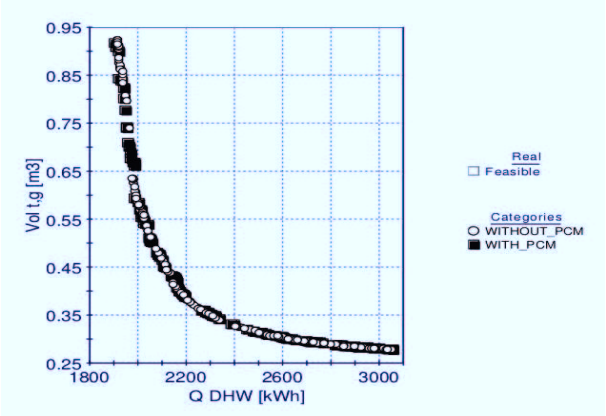

Figure 7.12: Comparison of the Pareto frontier obtained for the tank with and without PCM for a plant in Trieste.

A sensitivity analysis on the optimization variables

The tank height, the insulation thickness and the amount of the inserted PCM that characterize the objectives minimization could be analyzed together inspecting Figure 7.13 - Figure 7.16. These Figures report the scatter matrices relative to the results reported in Sub subsection 7.2.3. The reported matrices refer to both the considered cities.

The upper triangle of the matrices, at the the intersection of the i-th row and j-th column, contains the scatter charts of the variable i versus the variable j. The scatter charts represent with points all the simulated solutions and locate them in the design space on the basis of the two variables i and j. The feasible, unfeasible and optimal (Pareto) solutions are differentiated by different colors: the first are gray squares, the second red crosses and the last are enlighten with green squares.

The matrix diagonal reports the Probability Density Function chart for each variable: at the the intersection of the i-th row and i-th column it is plotted the chart for the i-th variable. The Probability Density Function represents the number of designs that fit into a fixed bin of the variable. The axis of abscissas reports the number of performed solutions, the axis of ordinates reports the variable values. So it can be read the distribution of a specific variable among the simulated design.

These matrices are symmetrical, thus the intersection of the i-th row and j-th column corresponds to the intersection of the j-th row and i-th column.

The lower triangle of the matrices does not repeat the information given in the upper triangle, but quantifies the the correlation established between the i-th variable versus the j-th variable. It represents a measure of the linear association between two variables. The numbers reported in the matrices can vary from -1 to 1: 1 represents a full positive correlation between two variables, 0 means that the two values are uncorrelated, -1 indicates a full negative correlation. As reported in the mod [55] manual, the correlation index r is calculated for all the couples of variables as:

$$r = \frac{N\Sigma xy - (\Sigma x)(\Sigma y)}{\sqrt{\left[N\Sigma x^2 - (\Sigma x)^2\right]\left[N\Sigma y^2 - (\Sigma y)^2\right]}} \tag{7.2.1}$$

where N is the number of couples and x, y the considered variables. Thanks to the intensity of the color and to the color itself, such representation gets immediately the perception of what are the parameters more incisive on the results and their weight on the optimal solutions definition. The positive correlation is indicated in red, while the negative one is in blue.

Inspecting the lower triangles of Figure 7.13 and Figure 7.15, it can be deduced that the volume of PCM has a limited effect on the primary energy consumption, since the correlation values are -0.123 and -0.234 respectively. This is also confirmed by analyzing the upper triangles: the scatter plots at the intersection between the row reporting the V_{PCM} and the column reporting the Q_{DHW}, show that the optimal designs are uniformly distributed in the design space.

This approach can be applied to all the Figures 7.13-7.16.

While most of the parameters related to the PCM seem to be almost uncorrelated with the objectives, the parameter that shows a great influence on the objectives is the

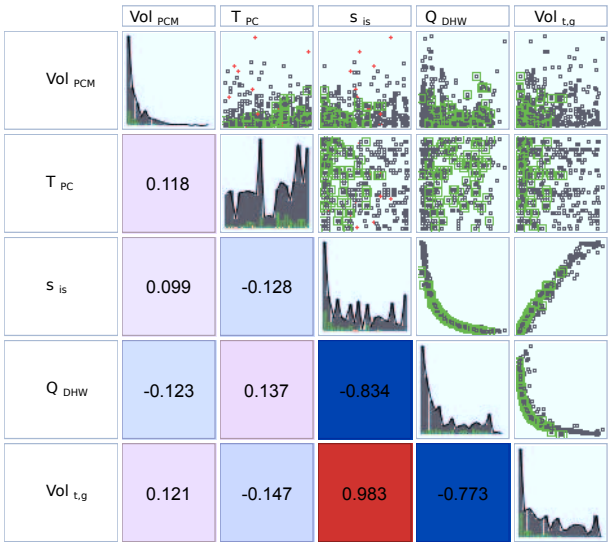

Figure 7.13: Matrix representation of the relation among optimization variables for Rome.

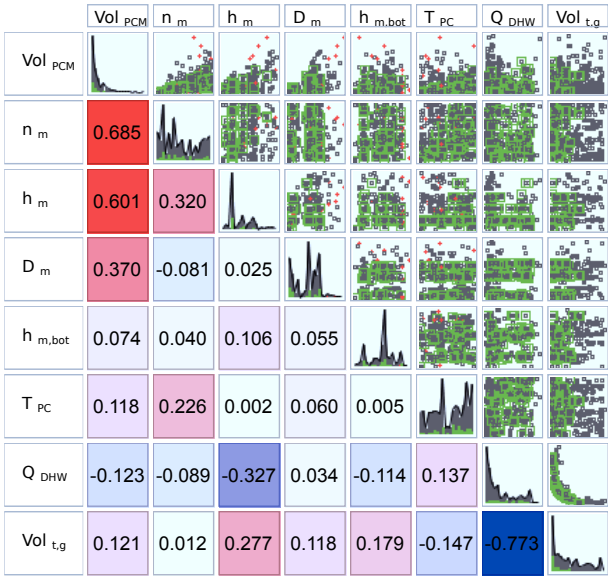

Figure 7.14: Matrix representation of the relation among optimization variables for Rome.

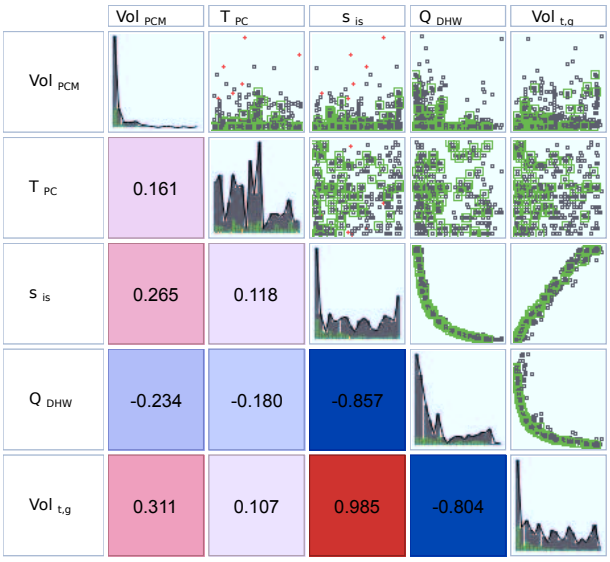

Figure 7.15: Matrix representation of the relation among optimization variables for Trieste.

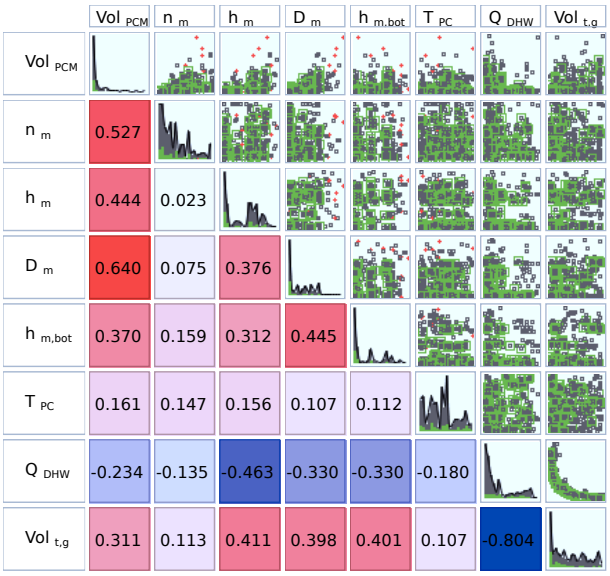

Figure 7.16: Matrix representation of the relation among optimization variables for Trieste.

insulation thickness. For this variable the correlation values is -0.834 and -0.857 for respectively Rome and Trieste; also the scatter plot shows a good correlation between row s_{ins} and column Q_{DHW}.

Figure 7.14 and Figure 7.16 enlighten that the parameters related to the PCM modules inside the tank have a marginal impact on the solution; vice-versa the parameters that have more impact in the reducing of the primary energy are the height of the module the position from bottom of the tank, with the values of -0.327 and -0.114 respectively. This indicates that the modules should be placed in an high position into the tank. The phase change temperature seems to have not a high impact on the primary energy Q_{DHW}, since the correlation values are 0.137 for Rome and -0.18 for Trieste.

It can be concluded that a general scarce impact and low correlation is established among all the variables referred to the PCM and the objective functions.

Review and concluding remarks

The thesis describes the analysis that had been carried on a tank for the domestic hot water storage in solar plants. A performing storage system is an essential requisite of an efficient DHW plant. The aim of the carried out analysis was to inspect a strategy to enhance the storage potentiality. The possibility of enhancing the storage capacity through the embedding of PCM modules into the tank had been described in the literature as a promising technology, that needed further optimization analyses.

A tool that let analyze the dynamic performance of a PCM enhanced tank had been identified in the ESP-r code. The idea of basing the study of the PCM tank on a plant component was due to the possibility of prototyping the components in a rapid way that could be easily automatized, in order to simulate smartly a wide range of designs.

Resuming, the achievement of the objective of the thesis had been possible dividing the problem into several steps:

- the writing of a phase change model to simulate the PCM-water exchanged heat flux. The enthalpic method had been chosen and adapted to a cylindrical geometry; the routines had been compacted such that both the implemented methods, Euler explicit and implicit, use the same coefficients.
- the connection of the phase change algorithm to the existing ESP-r tanks routines: this phase included the initialization and the continuous upgrade of the temperature and the heat flux between the water and the PCM. This phase permitted the simulation of the enhanced tank together with several different conditions, controls, and all the facilities offered by the simulation tool;
- the validation, based on experimental data obtained from the literature, to confirm that the performance of the PCM corresponds to the real behavior;
- the simulation of initial test models, to test the effectiveness of the technology;
- the refinement of the model, that consisted in the enhancement from the mono-dimensional to a bi-dimensional one, passing from a concentrated parameters tank to a stratified one. Moreover, the simulation of some aspects, that had been neglected in the initial phases, had been added, for example the convection in the liquid phase of the PCM, implemented throughout a correlation, and the presence of a containment for the PCM, modeled through an additive resistance.
- the optimization of the PCM tank and the analysis of the design variables that affect the performance of the tank, to find out the solutions able to perform at the best level.

The problem had been studied and contextualized also through further analysis based on the performance of traditional tanks:

- a CFD test to reproduce the experimental data of the cooling down of a traditional tank and to be used as comparison term for the results obtained with ESP-r;
- an optimization test, to let the optimization tool individuate the correct value of tank parameters.

As further work it might be considered the comparison between the simulations results and the experimental data (this step had been just outlined) and the refinement of the phase change model, for example with implementation of a model to take into account the sub-cooling. A useful refinement of the work could be identified in the modelization of a component, based on the phase change model implemented for the 2 stratified storage tanks. A new PCM component allows also to differentiate the PCM modules in a single tank, in terms of technical data and geometry: since the high storage of the PCM happens in a small temperature range, it might be possible that dividing this interval into smaller ones, and assigning each of them to different PCM may be beneficial. An other interesting analysis could be carried on different tank models: the reason of this choice is discussed in the next paragraphs.

The conclusion that may be carried on at the end of this analysis is that the performance of the PCM tanks are similar to those obtainable by the traditional tanks, thus the energy and size improvements, that are reached optimizing the model, can be attained by changing tank geometry only. The conclusion drawn in this thesis seems to be reasonable if some results reported in the literature are considered, in particular those that doubt the effectiveness of the PCM and the need of an optimization analysis.

The subtraction of water volume due the presence of the PCM modules reduces the sensible heat absorbed. For other kind of tanks, for example tank in-tank models, the presence of PCM may be more effective, since the temperature of the water in the external tank does not vary as much as in the tank adopted in this thesis. This is also considered a future work. For this optimization the used PCM was paraffin. Other materials that perform better than the paraffin, like Hydrated Salts, show other kind of drawbacks, like the high corrosion: this material could not had been used in such tank since the modules are in direct contact with the DHW. From the obtained results it appears that the PCM enhanced stratified tank for solar systems can be a viable solution to reduce the volume of the tanks. Vice-versa the impact of the PCM on the energy consumption reduction is not significant. The tuning of this technology, that depends also on the used PCM and the internal and external geometry, demands a big effort: a large number of variables can affect its performance.

Appendix

Coefficients definition

The coefficients a_P^0 and a_P used in Chapter 2 for both the explicit and implicit formulation are defined as follows:

$$a_P^0 = \frac{V_P}{\Delta t}$$

and

$$a_P = a_{nb} = \frac{k_i A_i}{\Delta s_{PI}}$$

with i=e, w, s, n referred to the interface areas among cells and I=E,W,S,N referred to the neighboring cells nodes. P is the index referred to the considered node. t stands for time, s is the general spatial coordinate, V is the cell volume, k is the material conductivity and A is the cell interface area between two cells. The normals at the cells faces are towards outside, so the thermal flux entering the cells becomes negative. In the implemented code all the terms was explicited and referred to a bi-dimensional cylindrical geometry, shown at Figure 2.4. Taken for example the explicit method, the complete implemented formulation for the general cell becomes:

$$\rho V \frac{H_P - H_P^0}{\Delta t} = -\sum_i \frac{k_i A_i}{\Delta s_{PI}} (T_P - T_I)$$

where ρ is the node density, H is the node enthalpy and T is the node temperature. Note that for the implicit notation the coefficients $a_P = a_{nb}$ are expressed later as $-A_I$, that are the coefficient characterizing the solving system (see the Appendix Section "Equation system coefficients").

For the general k cell the variables multiplying the temperature difference can be joined into a general coefficient, that can be called by different routines.

$$A_{I,k} = -\frac{k_i A_i}{\Delta s_{PI}} \tag{7.2.2}$$

was similar to the following Equation (7.2.3), written again with reference to the explicit scheme, corresponding to the complete formulation for the general cell:

$$\begin{aligned} \frac{\rho V_P}{\Delta t} H_P = \frac{\rho V_P}{\Delta t} H_P^0 + \frac{k_e A_e}{\Delta r_{PE}} T_E^0 + \frac{k_w A_w}{\Delta r_{PW}} T_W^0 + \frac{k_n A_n}{\Delta l_{PN}} T_N^0 + \frac{k_s A_s}{\Delta l_{PS}} T_S^0 + \\ - \left(\frac{k_e A_e}{\Delta r_{PE}} + \frac{k_w A_w}{\Delta r_{PW}} + \frac{k_n A_n}{\Delta l_{PN}} + \frac{k_s A_s}{\Delta l_{PS}} \right) T_P^0 \end{aligned} \tag{7.2.3}$$

Here Δs, the general distance among cells nodes, is replaced by Δr and Δl, that are the distance among nodes in the radial and axial direction. The formulation for the border cells differs from it because the heat flux deriving from the surrounding water is taken into account, while for the axis cells the only contribution to the heat flux component in the radial direction comes from the west cell (see Figure 2.4).

Equation system coefficients

In the code the solving system referring to the implicit method had been written by recursing to coefficients usually adopted to join the equation terms. The equations compounding the solving system, for the general cell, can be reshaped and written in the form reported in the Appendix "Coefficients definition". The accumulation and diffusive term can be enlighten:

$$\underbrace{\left[\underbrace{\frac{\rho c^A V}{\Delta t}}_{A_P^a} + \left(\underbrace{\frac{k_w A_w}{\Delta r} + \frac{k_e A_e}{\Delta r} + \frac{k_s A_s}{\Delta l} + \frac{k_n A_n}{\Delta l}}_{A_P^d}\right)\right]}_{A_{P,k}} \cdot T_P^n + \underbrace{-\frac{k_w A_w}{\Delta r}}_{A_{W,k}} \cdot T_W^n \underbrace{-\frac{k_e A_e}{\Delta r}}_{A_{E,k}} \cdot T_E^n \underbrace{-\frac{k_s A_s}{\Delta l}}_{A_{S,k}} \cdot T_S^n \underbrace{-\frac{k_n A_n}{\Delta l}}_{A_{N,k}} \cdot T_N^n = \underbrace{\frac{\rho c^A V}{\Delta t} \cdot T_P^{n-1} + \frac{\rho V}{\Delta t} \cdot \left(H_P^0 - H_P^{n-1}\right)}_{S_{P,k}} \tag{7.2.4}$$

The A and S coefficients, written for each k-cell, are implemented in the code as follows:

$$A_{P,k} = \frac{\rho c^A V}{\Delta t} + \frac{k_w A_w}{\Delta r} + \frac{k_e A_e}{\Delta r} + \frac{k_s A_s}{\Delta z} + \frac{k_n A_n}{\Delta l}$$

$$A_{W,k} = -\frac{k_w A_w}{\Delta r}$$

$$A_{E,k} = -\frac{k_e A_e}{\Delta r}$$

$$A_{S,k} = -\frac{k_s A_s}{\Delta l}$$

$$A_{N,k} = -\frac{k_n A_n}{\Delta l}$$

$$S_{P,k} = \frac{\rho c^A V}{\Delta t} T_{P,k}^{n-1} + \frac{\rho V}{\Delta t}\left(H_{P,k}^0 - H_{P,k}^{n-1}\right)$$

so the equation for the general cell is:

$$\frac{\rho c^A V}{\Delta t} T_P^n + \frac{k_w A_w}{\Delta r}\left(T_P^n - T_W^n\right) + \frac{k_e A_e}{\Delta r}\left(T_P^n - T_E^n\right) + \frac{k_s A_s}{\Delta l}\left(T_P^n - T_S^n\right) + \frac{k_n A_n}{\Delta l}\left(T_P^n - T_N^n\right) = \frac{\rho c^A V}{\Delta t} T_P^{n-1} + \frac{\rho V}{\Delta t}\left(H_P^0 - H_P^{n-1}\right)$$

The routine calculating the coefficients is called either from the routine that solves the problem with the implicit approach and from the one using the explicit method.

Glossary

Acronyms

CFD	Computational Fluid Dynamic. 6, 65, 66, 68, 69, 71, 72
CHP	Combined Heat and Power system. vi
CNR	Consiglio Nazionale delle Ricerche. 65, 66
CV	Control Volume. 14, 15, 17, 18, 20, 25, 31, 65
DHW	Domestic Hot Water. v, 2, 9, 42, 55, 56, 92, 108
DoE	Design of Experiments. 61, 63, 93
ESP-r	Environmental Systems Performance - research. vi, 4, 10, 13, 15, 20, 22, 25, 31, 37–39, 43, 44, 48, 52, 55, 64–75, 90, 93, 107, 108
ESRU	Energy Systems Research Unit. 37
GA	Genetic Algorithm. 61–63
GHG	Greenhouse Gas. iii, iv, 10
HTF	Heat Transfer Fluid. 7
HVAC	Heating, Ventilation, and Air Conditioning. 41, 58
IGDG	Italian Gianni De Giorgio. 58
IPCC	Intergovernmental Panel on Climate Change. iii
LHS	Left Hand Side. 22, 41
LHSU	Latent Heat Storage Unit. 3, 7, 8, 91
NSGA	Nondominated Sorting Genetic Algorithm. 61, 62, 64, 91
PCM	Phase Change Material. v–vii, 1–10, 12, 13, 15–21, 25–35, 43, 44, 46–48, 52, 56, 64, 75–81, 83–85, 87–96, 98–103, 106–108
PV	Photovoltaic. vi
RHS	Right Hand Side. 22, 41
SDHW	Solar Domestic Hot Water. v–vii, 3, 9, 10, 32, 43, 44, 52, 57, 64, 77, 87, 89, 90
TES	Thermal Energy Storages. 101

Symbols

A	area [m^2]. 14, 40, 44, 52, 53, 109
D	diameter [m]. 29, 75, 92
G	solar radiation incident upon the collector [-]. 52
H_0	gas heating value at STP [J/m^3]. 54, 57
H	total enthalpy [J/kg]. 14, 109
L	characteristic length [m]. 2
L	latent heat [J/kg]. 12, 80, 87
M	mass [kg]. 40, 52, 54
Nu	Nusselt number [-]. 30
Pr	Prandtl number [-]. 2

Q	primary energy [kWh]. 57, 89, 97
Ra	Rayleigh number [-]. 30
Re	Reynolds number [-]. 2, 30
R	resistance [(K/W)]. 11, 12
R	mass diversion ratio [-]. 40, 52
S	thickness [m]. 5, 11, 12, 15, 67, 80, 92
T	temperature [C]. 11, 12, 14, 17, 19, 20, 24, 25, 52, 54, 56, 75, 80, 90, 92, 109
U	U-value [W/(m^{2}K)]. 40, 44, 65
V	volume [m^3]. 14, 29, 100, 109
ΔV	thermal expansion coefficient [%]. 80
Δl	distance among nodes in axial direction [m]. 28, 110
Δr	distance among nodes in radial direction [m]. 28, 110
Δs	general distance [m]. 110
$\bar{c}$	mass weighted average specific heat capacity [J/(kg K)]. 40, 52
$\dot{V}$	boiler full load gas firing rate [m^3/s]. 54, 57
$\dot{m}$	mass flow rate [m^3/s]. 45, 52, 54, 56
$\mathbf{v}$	velocity [m/s]. 14
a	boiler coefficients. 55
c	specific heat capacity [J/(kg K)]. 2, 18, 19, 21, 22, 24, 25, 40, 52, 75, 80, 87
f	boiler fractional load factor [%]. 54, 55
g	liquid volume fraction [-]. 1, 24, 25
h	height [m]. 1, 75, 80, 92
k	conductivity [W/(mK)]. 2, 7, 11, 18, 19, 25, 45, 67, 75, 80, 87, 109
n	number, quantity [-]. 80, 92
r	correlation index. 103
r	radius, distance axis-node [m]. 28
s	general spatial coordinate. 17, 109
t	time [s]. 5, 11, 12, 52, 109
u	velocity component in the vertical direction [m/s]. 1

Symbols - Greeks

Γ	solid-liquid interface. 14, 15, 25
α	convection heat transfer coefficient [W/(m^{2}K)]. 11, 21, 31, 33, 67
β	elevation from horizontal [°]. 54
δ	azimuth [°]. 54
η_0	constant coeff. of solar collector [-]. 53
η_1	linear coeff. of efficiency solar collector [W/(m^{2}K)]. 53
η_2	quadratic coeff. of solar collector [W/(m^{2}K^2)]. 53
μ	mass fraction [%]. 54
ν	kinematic viscosity [mm^2/s]. 80
ϕ	thermal flux [W]. 11, 40
ρ	density[kg/m^3]. 2, 12, 16, 18, 19, 75, 80, 87, 109
ε	small temperature interval[K]. 14, 21, 24, 25

Symbols - Subscripts

E	East, referred to the east node. 17, 25, 109

I	index referred to the neighboring node (North, East, South, West). 17, 109
N	North, referred to the north node. 17, 109
P	index referred to the considered node. 15, 16, 20, 109
S	South, referred to the south node. 17, 109
W	West, referred to the west node. 17, 109
α	convective. 12
a	air. 11, 40, 52
bc	border cell. 31
b	border. 29
b	bottom. 75, 80, 92
b	boiler. 55
$coll$	collector. 54
cyl	cylinder. 29
env	environment. 40, 44
ext	external. 67
e	east, referred to the east interface. 17, 25, 109
f	fluid. 11
f	forced. 30
gas	gas. 55
gly	glycol. 54
g	gross. 100
ins	insulation. 80, 92
int	internal. 67
in	inlet. 53
i	counter referred to the axial direction, counter referred to the tank node, index referred to the neighboring interface area (north, east, south, west). 17, 44, 109
l	liquid. 13, 14, 80, 87
m	PCM module. 75, 80, 92
nb	neighboring. 16, 20, 109
net	net. 100
n	natural. 30
n	north, referred to the north interface. 17, 109
obj	objective. 60
out	outlet. 52
pc	phase change. 11, 12, 14, 15, 19, 20, 24, 25, 90, 92
r	return. 54
st	state. 18
s	solid. 13, 14, 80, 87
s	south, referred to the south interface. 17, 109
t	tank. 56, 80, 92
v	vapor. 40
w	water. 31
w	west, referred to the west interface. 17, 109
x	east, west, normal to the radial direction. 11, 12, 22, 28

y north, south, normal plane to the axial direction. 22, 28

Symbols - Superscripts

0 initial, previous. 11, 16, 20, 21, 41

A apparent. 21, 22, 24, 25

n iteration. 21

Bibliography

[1] K. Kelly. *Quello che vuole la tecnologia*. Codice, 1st edition, 2011.

[2] Report of the world commission on environment and development: Our common future, 1987. `http://www.un-documents.net/our-common-future.pdf`.

[3] D.P. van Vuuren, M.G.J. den Elzen, P.L. Lucas, B. Eickhout, B.J. Strengers, B. van Ruijven, S. Wonink, and R. van Houdt. Stabilizing greenhouse gas concentrations at low levels: an assessment of reduction strategies and costs. *Climatic Change*, 81: 119–159, 2007.

[4] R. Moss, M. Babiker, S. Brinkman, E. Calvo, T. Carter, J. Edmonds, I. Elgizouli, S. Emori, L. Erda, K. Hibbard, R. Jones, M. Kainuma, J. Kelleher, J.F. Lamarque, M. Manning, B. Matthews, J. Meehl, L. Meyer, J. Mitchell, N. Nakicenovic, B. O'Neill, R. Pichs, K. Riahi, S. Rose, P. Runci, R. Stouffer, D. van Vuuren, J. Weyant, T. Wilbanks, J. P. van Ypersele, and M. Zurek. *Towards New Scenarios for Analysis of Emissions, Climate Change, Impacts, and Response Strategies. Technical Summary. Intergovernmental Panel on Climate Change*, 2008.

[5] Directive 2012/27/eu on energy efficiency, . `http://eur-lex.europa.eu/LexUriServ` visited 05-11-2013.

[6] Directive 2010/31/eu on the energy performance of buildings, . `http://eur-lex.europa.eu/LexUriServ` visited 05-11-2013.

[7] L.F. Cabeza. *Thermal Energy Storage*. Reference Module in Earth Systems and Environmental Sciences. Elsevier Ltd, 2012.

[8] Y.M. Han, R.Z. Wang, and Y.J. Dai. Thermal stratification within the water tank. *Renewable and Sustainable Energy Reviews*, 13(5):1014–1026, 2009.

[9] J.A. Clarke. *Energy Simulation in Building Design*. Butterworth Heinmann, 2nd edition, 2001.

[10] Z. Lavan and J. Thompson. Experimental study of thermally stratified hot water storage tanks. *Solar Energy*, 19(5):519–524, 1977.

[11] E. Hahne and Y. Chen. Numerical study of flow and heat transfer characteristics in hot water stores. *Solar Energy*, 64(1–3):9–18, 1998.

[12] N. Altuntop, M. Arslan, V. Ozceyhan, and M. Kanoglu. Effect of obstacles on thermal stratification in hot water storage tanks. *Applied Thermal Engineering*, 25: 2285–2298, 2005.

[13] H. Mehling, L.F. Cabeza, S. Hippeli, and S. Hiebler. PCM-module to improve hot water heat stores with stratification. *Renewable Energy*, 28:699–711, 2003.

[14] J. Bony, S. Citherlet, A. Heinz, P. Puschnig, H. Schranzhofer, and J.M. Schultz. *Simulation Models of PCM Storage Units – A Report of IEA Solar Heating and Cooling programme - Task 32, "Advanced storage concepts for solar and low energy buildings"*, Subtask C(Report C5), 2008.

[15] M.M. Farid and R. M. Hussian. An electrical storage heater using the phase-change method of heat storage. *Energy Convers. Mgmt*, 30(3):219–230, 1990.

[16] B. Zivkovic and I. Fujii. An analysis of isothermal phase change of phase change material within rectangular and cylindrical containers. *Solar Energy*, 70(1):51–61, 2001.

[17] R. Padovan. Modelization of a stratified storage tank with PCM using ESP-r. *67° Congresso Nazionale ATI, Trieste, 11-14 September*, 2012.

[18] J.L.M. Hensen and M.J.H. Hamelinck. Energy simulation of displacement ventilation in offices. *Building Services Engineering Research and Technology*, 16(2):77–81, 1995.

[19] S. Hoffmann. *Numerische und experimentelle Untersuchung von Phasen Übergangsmaterialien zur Reduktion hoher sommerlicher Raumtemperaturen.* Ph.D. thesis, Bauhaus-Universität Weimar, 2006.

[20] A.L. Hashem. *Thermal Energy Storage for Building-Integrated Photovoltaic Components – Energy Simulation in Building Design.* Ph.D. thesis, Energy Systems Research Unit, Strathclyde University, 2011.

[21] Y. Dutil, D. R. Rousse, N. Ben Salah, S. Lassue, and L. Zalewski. A review on phase-change materials: Mathematical modeling and simulations. *Renewable and Sustainable Energy reviews*, 15(1):112–130, January 2011.

[22] V.R. Voller. *An Overview of Numerical Methods for Phase Change Problems.* Pineridge, r.w. lewis edition, 1996.

[23] A.A. Ghoneim. Comparison of theoretical models of phase change and sensible heat storage for air and water-based solar heating systems. *Solar Energy*, 42(3):209–220, 1989.

[24] J. Bony and S. Citherlet. Numerical model and experimental validation of heat storage with phase change materials. *Energy and Buildings*, 39(10):1065–1072, 2007.

[25] M. Lacroix. Numerical simulation of a shell-and-tube latent heat thermal energy storage unit. *Solar Energy*, 50(4):357–367, 1993.

[26] V.R. Voller and M. Cross. *Applications of control volume enthalpy methods in the solution of Stefan problems.* Pineridge, r.w. lewis edition, 1985.

[27] E.M. Sparrow, E.D. Larson, and J.W. Ramsey. Numerical investigation of a PCM-based heat sink with internal fins: Constant heat flux. *International Journal of Heat and Mass Transfer*, 24:213–284, 1981.

[28] V.R. Voller, M. Cross, and N.C. Markatos. An enthalpy method for convection/diffusion phase change. *International Journal For Numerical Methods In Engineering*, 24:271–284, 1987.

[29] E.M. Sparrow, J.W. Ramsey, and R.G. Kemink. Freezing ontrolled by natural convection. *Transactions of the ASME*, 101:578–584, 1979.

[30] S.E. Hibbert, N.C. Markatos, and V.R. Voller. Computer simulation of moving-interface, convective, phase-change processes. *International Journal of Heat and Mass Transfer*, 31(9):1785–1795, 1988.

[31] O. Bertrand B. Binetb, H. Combeau S. Couturier, Y. Delannoy, D. Gobin, M. Lacroix, P. Le Quéré, M. Médale, J. Mencinger, H. Sadat, and G. Vieira. Melting driven by natural convection - A comparison exercise: first results. *International Journal of Thermal Sciences*, 38:5–26, 1999.

[32] H. Schranzhofer, P. Pusching, A. Heinz, and W. Streicher. 2006. `ftp://ftp.grenoble.cstb.fr/Public/MESSIB-CSTB/TASK`.

[33] H.A. Adine and H. El Qarnia. Numerical analysis of the thermal behaviour of a shell-and-tube heat storage unit using phase change materials. *Applied Mathematical Modelling*, 33:2132–2144, 2009.

[34] A. Laouadi and M. Lacroix. Thermal performance of a latent heat energy storage ventilated panel for electric load management. *International Journal of Heat and Mass Transfer*, 42:164–175, 1999.

[35] V. Shatikian, G. Ziskind, and R. Letan. Numerical investigation of a PCM-based heat sink with internal fins: Constant heat flux. *International Journal of Heat and Mass Transfer*, 51:1488–1493, 2008.

[36] T. Kousksou, P. Bruel, G. Cherreau, V. Leoussoff, and T. El Rhafiki. PCM storage for solar DHW: From an unfulfilled promise to a real benefit. *Solar Energy*, 85(9): 2033–2040, 2011.

[37] M. Esen and A. Durmus. Geometric design of solar aided latent heat store depending on various parameters and phase change materials. *Solar Energy*, 62(10):19–28, January 1998.

[38] M. Rostamizadeh, M. Khanlarkhani, and S.M. Sadrameli. Numerical investigation of a PCM-based heat sink with internal fins: Constant heat flux. *Energy and Buildings*, 49:419–422, 2012.

[39] E. Talmatsky and A. Kribus. PCM storage for solar DHW: An unfulfilled promise? *Solar Energy*, 82:861–869, 2008.

[40] M. Ibáñez, L. F. Cabeza, C. Solé, J. Roca, and M. Nogués. Modelization of a water tank including a PCM module. *Applied Thermal Engineering*, 26(11–12):1328–1333, 2006.

[41] H. Mehling and L. Cabeza. *Heat and cold storage with PCM*. Springer, 1st edition, 2007.

[42] G.E. Bell. On theperfonnance of the enthalpy method. *International Journal of Heat and Mass Transfer*, 25(4):587–589.

[43] V.R. Voller and C.R. Swaminathan. Treatment of discontinuous thermal conductivity in control-volume solutions of phase-change problems. *Numerical Heat Transfer*, 24 (B):161–180, 1993.

[44] I. Dincer and M. Rosen. *Thermal energy storage systems and applications*. John Wiley & Sons Ltd, 2nd edition, 2011.

[45] F.P. Incropera, D.P. De Witt, T.L. Bergman, and A.S. Lavine. *Fundamentals of Heat and Mass Transfer*. John Wiley & Sons Ltd, 6th edition, 2007.

[46] R.L. Graham, B.D. Lubachevsky, K.J. Nurmela, and P.R.J. Östergård. Dense packings of congruent circles in a circle. *Discrete Mathematics*, 181(1–3):139–154, 1998.

[47] B. Collins-Sussman, B. W. Fitzpatrick, and C. M. Pilato. *Branching and Merging*. 2011.

[48] J.W. Hand. Esp-r developers guide, 2012. `http://www.esru.strath.ac.uk` visited 2012-03-20.

[49] J.L.M. Hensen. *On the thermal interaction of building structure and heating and ventilating system*. Ph.D. thesis, Energy Systems Research Unit, Strathclyde University, 1991.

[50] D. Thevenard and K. Haddad. Development of a stratified tank model with immersed heat exchangers in ESP-r. *The 6th IBPSA Canada conference, Winnipeg, May 19-20*, 2010.

[51] D. Thevenard, K. Haddad, and J. Purdy. Development of a new solar collector model in ESP-r. *Canadian Solar Buildings Conference, Montreal, August 20-24*, 2004.

[52] Ashrae. `https://www.ashrae.org/` visited 2012-03-20.

[53] G. de Giorgio. Dati climatici g.de giorgio. `http://apps1.eere.energy.gov/buildings/energyplus/pdfs/italia_dati_climatici_g_de_giorgio.pdf` visited 2012-03-20.

[54] B. Y.Liu and R. C. Jordan. The Interrelationship and Characteristic Distribution of Direct, Diffuse and Total Solar Radiation. *Solar Energy*, 4(3):1–19, 1960.

[55] modefrontier version 4.4.2 documentation, 2013. `http://www.esteco.com`.

[56] P. Ranut. *Optimization and inverse problems in heat transfer*. Ph.D. thesis, University of Udine, 2012.

[57] K. Deb, A. Pratap, S. Agarwal, and T. Meyarivan. A fast and elitist multi-objective genetic algorithm: NSGA-II. *IEEE Transactions on Evolutionary Computation*, 6 (2):182–197, 2002. `http://www.iitk.ac.in/kangal/reports.shtml`.

[58] Ansys cfx and ansys icem cfd version 14 user manual, 2012. `http://www.ansys.com`.

[59] R. Padovan and M. Manzan. Development of a tank storage component for ESP-r with embedded PCM modules. *on CD-ROM*, The 2nd International Conference on Microgeneration and Related Technologies, Glasgow, 4-6 April, 2011.

[60] R. Padovan and M. Manzan. Development of a stratified tank storage component for ESP-r with embedded phase change material modules. *Proc IMechE Part A: J Power and Energy*, 0(Special Issue):1–9, 2013.

[61] H. Heimrat and M. Haller. The Reference Heating System. *The Template Solar System – Report A2, of IEA Solar Heating and Cooling programme - Task 32, "Advanced storage concepts for solar and low energy buildings"*, (Report A2), 2008.

[62] R. Padovan and M. Manzan. L'Ottimizzazione per il risparmio energetico negli edifici. *Analisi & Calcolo*, 55:42–51, 2013.

[63] M. Manzan R. Padovan. Optimisation of a stratified storage tank for a Solar Domestic Hot Water plant. *68° Congresso Nazionale ATI, Bologna, 11-13 September. Atti*, 2013.

[64] R. Padovan and M. Manzan. Enhanced Storage Tank for Solar Domestic Hot Water Systems. *on USB*, The 3rd International Conference on Microgeneration and Related Technologies, Naples, 15-17 April, 2013.

[65] Riello. `http://www.riello.it` visited 2013-03-20.

[66] Pcm products. `http://www.pcmproducts.net/Phase_Change_Material_Products.htm` visited 2012-03-20.

[67] L.F. Cabeza, M. Ibáñez, and C. Solé. Experimentation with a water tank including a PCM module. *Solar Energy Materials and Solar Cells*, 90:1273–1282, 2006.

[68] B. Zalba, J.M. Marín, L.F. Cabeza, and H. Mehling. Review on thermal energy storage with phase change: materials, heat transfer analysis and applications. *Applied Thermal Engineering*, 23:251–283, 2003.

[69] A. Castell, C Solé, M. Medrano, J. Roca, L.F. Cabeza, and D Garc'ıa. Natural convection heat transfer coefficients in phase change material (PCM) modules with external vertical fins. *Applied Thermal Engineering*, 28:1676–1686, 2008.

[70] J.W. Hand. The esp-r cookbook - strategies for deploying virtual representations of the built environment, 2011. `http://www.esru.strath.ac.uk`.

[71] G. Comini, G. Croce, and E. Nobile. *Fondamenti di termofluidodinamica computazionale*. SGEditoriali, 3rd edition, 2008.

[72] M. Esen and T. Ayhan. Development of a model compatible with solar assisted cylindrical energy storage tank and variation of stored energy with time for different phase change materials. *Energy Convers. Mgmt*, 37(12):1775–1785, December 1996.

[73] M. Kenisarin and M. Mahkamov. Solar energy storage using phase change materials. *Renewable and Sustainable Energy Reviews*, 11(9):1913–1965, 2007.

[74] R. Padovan. *Materiali innovativi nell'edilizia e nell'impiantistica residenziale: studio dell'utilizzo di materiali a cambiamento di fase per il risparmio energetico e per il miglioramento del benessere termico*. ME. thesis, University of Trieste, 2010.

[75] D.J. Morrison and S.I. Abdel Khalik. Effect on phase-change energy storage on the performance of air-based and liquid-based solar heating systems. *Solar Energy*, 20: 57–67, 1978.

[76] A. Santoro. *Tecniche numeriche per problemi di cambio fase solido liquido*. BE. thesis, University of Trieste, 2009.

[77] H.K. Versteeg and W. Malalasekera. . Longman Group, john wiley & sons ltd edition, 1995.

[78] V.R. Voller and M. Cross. Estimating the solidification/melting times of cylindrically symmetric regions. *Int Journal Heat Mass Transfer*, 24:1457–1462, 1981.